Gene targeting in human pluripotent cell-derived neural stem cells for the study and treatment of neurological disorders

Dissertation

zur

Erlangung des Doktorgrades (Dr. rer. nat.)

der

Mathematisch-Naturwissenschaftlichen Fakultät

der

Rheinischen Friedrich-Wilhelms-Universität Bonn

vorgelegt von

Daniel Poppe

aus Ulm

Bonn, 2015

Angefertigt mit Genehmigung der Mathematisch-Naturwissenschaftlichen Fakultät der
Rheinischen Friedrich-Wilhelms-Universität Bonn

1. Gutachter: Prof. Dr. Oliver Brüstle

2. Gutachter: Prof. Dr. Walter Witke

Tag der mündlichen Prüfung: 26.10.2015

Erscheinungsjahr: 2015

Table of contents

1 Introduction

1.1 Stem cells

Stem cells have the remarkable potential to differentiate into specialized cells and thereby are key factors for the development of the whole organism. All types of stem cells share their unique ability for self-renewal while maintaining their undifferentiated state and the potential to undergo differentiation into diverse and more restricted progeny. All tissues and organs of the body are derived from cascades of stem cells, which become more and more restricted in differentiation potential the further through development they arise. A new organism starts as a totipotent fertilized egg, which starts to divide, forming after several divisions the blastocyst. The outer layer consists of the trophoblast, giving rise to the placenta, while the inner cell mass forms all three germ layers of the embryo. The cells of the inner cell mass, known as embryonic stem cells, can be extracted and cultured in vitro, and are able to generate any cell type of the mature organism *in vitro* (Smith, 2001; Thomson et al., 1998). For this reason, embryonic stem cells are termed pluripotent, while unipotent stem cells can only form a single lineage (Weissman, 2000). During embryonic development, a program called neurogenesis, composed of complex patterns of sequential cycles of symmetrical and asymmetrical division of neural stem cells, establishes the complex structure of the brain (Breunig et al., 2011; Kriegstein and Alvarez-Buylla, 2009; Noctor et al., 2001; Rakic, 1988; Reynolds and Weiss, 1992; Urbach et al., 2004). Neural stem cells of this process can give rise to neurons and glia, the two lineages most cells of the central nervous system belong to, and are therefore called multipotent. In the adult human brain, the hippocampus and the subventricular zone (SVZ) are the only brain areas with residual neural stem cell populations (Eriksson et al., 1998; Gage, 2000). This might suggest that most parts of the human brain cannot be regenerated after neurogenesis is completed, with fatal consequences for patients in case of disease or injury.

The ability to generate all cell populations of the human body by harnessing human pluripotent stem (hPS) cells to reconstruct diseased or injured tissue has become a major focus in regenerative medicine (Lovell-Badge, 2001). Moreover, the development of human stem cell-based disease models represents a newly born research area and has received much attention (Colman and Dreesen, 2009; Han et al., 2011). Neuronal tissue from patients is not readily available, and most cells in the central nervous system are post-mitotic, which renders them unsuitable for genetic modifications. However, the use of patient-derived stem cell populations offers an unlimited source of cells and the potential to derive the cell type of interest together with the possibility to enrich for genetic modifications during the dividing stem cell state.

1.1.1 Human pluripotent stem cells

Landmark discoveries of the young field of human stem cell science were the isolation and culture of inner cell mass from human blastocysts by Bongso in 1994 and in the derivation of the first hES cell lines reported by Thomson and coworkers in 1998 (Bongso et al., 1994; Thomson et al., 1998). These achievements opened the field, which has seen constant improvements in the derivation and maintenance of hES cells since then (Kim et al., 2005; Marteyn et al., 2011; Strelchenko et al., 2004). In classical protocols, hES cells are cultured as colonies in a coculture system with growth-inhibited mouse embryonic feeder cells in medium containing FGF2 and fetal bovine serum, while newer protocols have improved towards chemically defined media and synthetic xeno-free substrates that meet GMP requirements, a prerequisite if cells are to be used for therapeutical application (Chen et al., 2011b; Klimanskaya et al., 2005; Rodin et al., 2010). Analysis of the molecular characteristics of hES cells helped to decipher the mechanisms of pluripotency (Cartwright, 2005; Chambers et al., 2003; Li, 2005; Niwa et al., 1998; Rodda et al., 2005; Takasugi et al., 2003). In 2006 these efforts culminated in the discovery of induced pluripotency (iP) by Takahashi and Yamanaka, who demonstrated that adult somatic cells can be directly reprogrammed into pluripotent stem cells by retroviral overexpression of only four transcription factors that were previously discovered as key regulators of the embryonic stem cell state (Takahashi et al., 2007; Takahashi and Yamanaka, 2006). The resulting induced pluripotent stem, or iPS, cells appear to have the same characteristics of self-renewal and differentiation potential as hES cells (Gore et al., 2011; Hussein et al., 2011; Lister et al., 2011). Since the discovery of induced pluripotency, reprogramming technology developed rapidly towards safer methods such as using integration-free techniques like direct protein transduction, mRNA, or the use of Sendaivirus and mature microRNA transfection as well as by reducing the number of transcription factors and even replacing them with chemical compounds (Anokye-Danso et al., 2011; Ban et al., 2011; Kim et al., 2009; Miyoshi et al., 2011; Nakagawa et al., 2008; Warren et al., 2010; Zhu et al., 2010). The emergence of iPS cell technology revolutionized the stem cell field as it not only avoids the ethical and legal issues connected to hES cell research, but also implies the generation of any cell type from any individual in unlimited quantities. For regenerative medicine approaches and the investigation of disease mechanisms, the key challenge for stem cell research will be to find protocols for efficient differentiation of pluripotent cells *in vitro* into authentic somatic cell types.

1.1.2 *In vitro* differentiation potential of human pluripotent and neural stem cells

By translating knowledge from developmental neurobiology, protocols to generate distinct neural cell types from pluripotent cells have been established. Pluripotent stem cells represent the most immature stem cell population that is capable of neurogenic differentiation. In the earliest protocols that were established, the founding pluripotent cells were sequentially exposed to a cocktail of morphogens to directly guide them into a mature neural cell type. When the self-renewal promoting environment of pluripotent stem cells is withdrawn, a large portion of them ultimately form neurons and glia, which led to the impression of a 'neuro-by-default' mechanism (Carpenter et al., 2001; Muotri et al., 2005; Reubinoff et al., 2001; Thomson et al., 1998; Tropepe et al., 2001). Drawbacks of these early protocols are the relatively long time spans required, especially with slowly dividing human cells, as well as batch-to-batch variations, which may result in a different outcome for each single experiment. Distinct from such so-called ‚run-through' protocols are those using an emerging stable neural stem cell population as a well-defined intermediate. A variety of multipotent neural stem cells from human pluripotent cells with differing potential have been reported and can be aligned to specific stages of human neurodevelopment (Conti and Cattaneo, 2010).

Early neuroepithelium precursor cells spontaneously convert into metastable rosette neuroepithelial stem (r-NES) cells that depend on SHH and Notch agonists when kept in culture for a few passages (Elkabetz et al., 2008). These cells express the transcription-factors PLZF and Dach1, form characteristic rosette structures with apical ZO1 expression and show interkinetic nuclear migration qualifying them as an in vitro reflection of early neural tube forming cells (Abranches et al., 2009; Elkabetz et al., 2008; Zhang et al., 2001). When exposed to the mitogens FGF2 and EGF in addition to B27 supplement mix, a homogenous and stable rosette-type long-term self-renewing neuroepithelial stem cell population (lt-NES cells) can be generated (Koch et al., 2009; Nemati et al., 2010). Caudalizing morphogenic activity of FGF2 (Cox and Hemmati-Brivanlou, 1995; Mason, 1996) and retinoic acid from the B27 mixture might explain the observed anterior hindbrain phenotype of lt-NES cells, which is, however, responsive to other instructive morphogens (Cox and Hemmati-Brivanlou, 1995; Glaser et al., 2005; Koch et al., 2009; Mason, 1996). This cell population may overcome many of the limitations described for hES cells, also because they can be extensively propagated for at least 150 passages and display a stable neurogenic differentiation pattern over the passages. In comparison to hESC, these cells exhibit significantly shorter doubling times (38 vs. 51-81 hours) and a higher clonogenicity. Moreover, lt-NES cells have been shown to be readily amenable to genetic manipulation, e.g. by electroporation or viral transduction (Koch et al., 2009; Ladewig et al., 2008).

1.2 Candidate diseases for therapeutic intervention

Organic diseases can roughly be divided into two groups: those of genetic origin and those of idiopathic origin. A genetic disease itself can be based on a single mutation, which disrupts the function of a protein, or on the combination of many different alterations, which alone may never result in a phenotype, but in interplay with other contributors can lead to a disease state. The advent of stem cell technology offers new possibilities on the one hand in understanding the reasons for disease, for example by generating *in vitro* the affected tissue from patient-derived pluripotent cells and using it in disease studies. On the other hand, it also opens the field for possible therapeutic applications by correcting a known disease-associated phenotype in cell culture and bringing the healthy cells back to its donor. If a disease is based on a known genotype like a mutation in a specific gene, a correction of the affected sequence into a physiological version should effect in a cure. More complicated is the cure of diseases that are either linked to a very complex genotype with several involved loci, or without a known genetic reason at all. In this case, the understanding of physiological processes within the biochemical network affected allows the deduction which enzymes could be modified to positively influence the disease. Hence, genetic modification can be beneficial in both cases of genetic and idiopathic diseases. For the application of genetically modified lt-NES cells, candidate diseases for both kinds of disorders were evaluated. In the following section, two neurological disorders are described: First the monogenetic disorder Machado-Joseph-Disease and second the large group of idiopathic epilepsies. Additionally, possible points of genetic interactions are shown.

1.2.1 Machado-Joseph-Disease or Ataxia type 3

Machado-Joseph-Disease (MJD) is an autosomal dominant neurodegenerative disease of late onset and the most frequent form of ataxia in humans (Schöls et al., 2004; Schöls et al., 1995). Originally described in and named after two families of emigrants from the Azorean islands based on the clinical phenotype (Nakano et al., 1972; Rosenberg et al., 1976), genetic testing later showed that MJD and the spinocerebellar ataxia of type 3 (SCA3) are based on the same gene defect (Haberhausen et al., 1995). It originates from an expansion of CAG repeats in exon 10 of the *ATXN3* gene, which leads to an elongated polyglutamine (polyQ) tract of its gene product ataxin-3 in its c-terminus (Kawaguchi et al., 1994). Length of the CAG tract is negatively correlated with disease onset (Maciel et al., 1995; van de Warrenburg et al., 2002), which affects predominantly cerebellar, pyramidal, extrapyramidal, motor neurons and oculomotor systems (Coutinho and Andrade, 1978; Rosenberg, 1992). Although the central nervous system is the place of all pathological processes in MJD,

ataxin-3 is not only expressed in neural tissue, but ubiquitously all over the body (Ichikawa et al., 2001). Several genetic studies found the physiological range of CAG repeats in the *ATXN3* gene to be up to 47 and the expanded repeat size in patients to be at least 45 (Dürr et al., 1996; Matilla et al., 1995; Padiath et al., 2005). As repeat length in both populations overlap, the number of CAG repeats alone does not always indicate susceptibility to the disease, a phenomenon that has also been shown for other polyQ diseases like Huntington (Brinkman et al., 1997).

1.2.1.1 The functional role of ataxin-3

Ataxin-3 is composed of a globular N-terminal Josephin domain (JD) followed by a flexible C-terminal tail (Masino et al., 2003). The JD bears ubiquitin protease activity while the tail has two ubiquitin interaction motifs, followed by the polyQ region. Inhibiting the deubiquitinating activity results in an increase of polyubiquitinated proteins similar to the result of proteasome inhibition (Berke et al., 2005). Functional analysis has shown interaction with proteins of the proteosomal protein degradation pathway like Rag23 and VCP (Doss-Pepe et al., 2003; Wang et al., 2000b). Rag23 itself interacts with the proteasomal subunit S5a (Hiyama et al., 1999; Ryu et al., 2003) suggesting a role in the shuttling of proteins into the proteasome for degradation. This system is especially responsible for the degradation of misfolded proteins labeled by ubiquitination, and called ERAD (endoplasmatic reticulum-associated degradation), leading to the export into the cytosol for degradation by the proteasome (Burnett et al., 2003; Wang et al., 2006; Wang et al., 2004)). It is not yet clear if ataxin-3 promotes or decreases degradation via this pathway and it could function either as a modulator via ubiquitin-modification to ensure degradation or associate with the proteasome for substrate recognition (Boeddrich et al., 2006; Wang et al., 2008). Another likely role for ataxin-3 is in quality control, as it is reported to be involved in aggresome formation. These structures are formed from misfolded proteins at the microtubule-organizing center (MTOC) when the proteasome itself cannot use them, leading to their transfer into lysosomes. Ataxin-3 seems to be involved in the regulation and formation of aggresomes as it co-localizes with pro-aggresomes (Burnett and Pittman, 2005; Markossian and Kurganov, 2004). It has been further proposed that ataxin-3 is responsible for the transport and stabilization of misfolded proteins to the MTOC as it interacts with parts of the cytoskeleton and transport proteins (Mazzucchelli et al., 2009; Rodrigues et al., 2010). It is very likely that interaction with cytoskeletal proteins is not only restricted to aggresome formation as there is evidence for a role of ataxin-3 in morphology and adhesion of the cell (Rodrigues et al., 2010). For example, absence prevents cytoskeletal maturation needed for myogenesis (do Carmo Costa et al.,

2010). Through its C-terminal domain, ataxin-3 does interact with several transcription factors and histones, influencing gene expression (Evert et al., 2006; Li et al., 2002). So far, it is not clear if this is a direct interaction or if ataxin-3 modifies the turnover rate and thus duration of action of the affected transcription factors. The different roles of ataxin-3 and its consequently wide distribution in the cell are depicted in Fig 1.1.

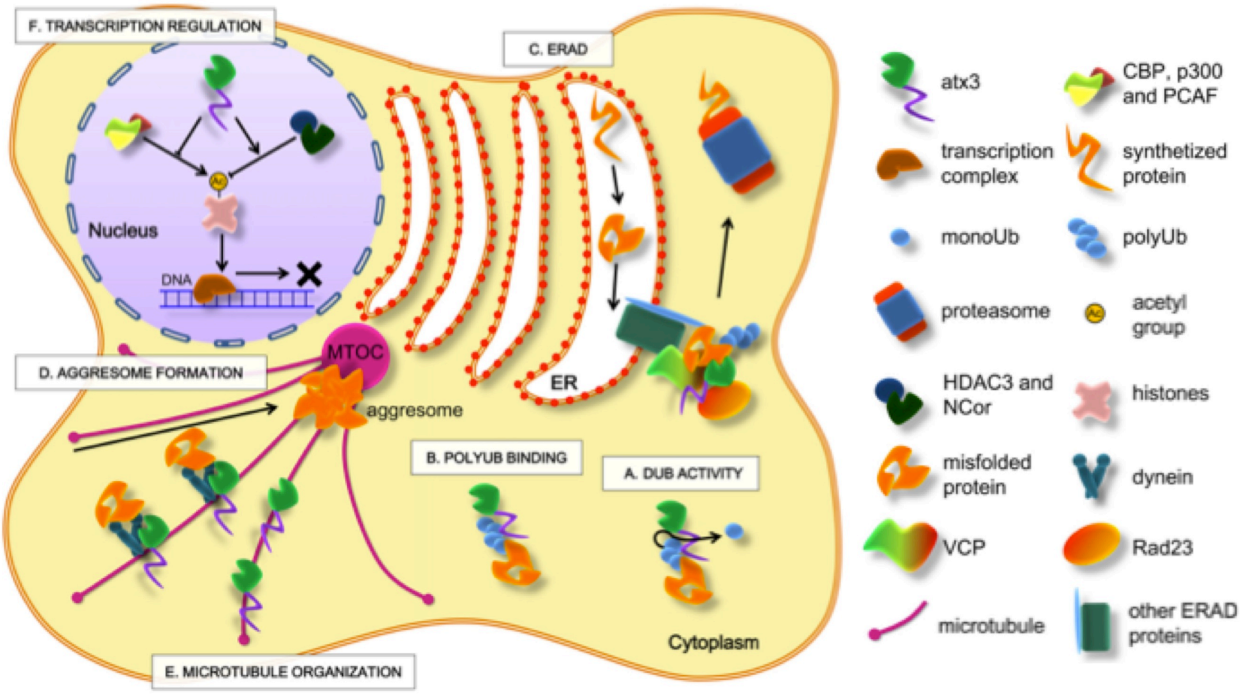

Figure 1.1: Physiological roles of ataxin-3.
Activity, interactions and roles of ataxin-3 proposed to date. It displays deubiquitinating (DUB) activity (A), and interacts with polyUB chains (B). Ataxin-3 was also shown to participate in protein homeostasis via ERAD (C). Additionally, roles in formation of aggresomes (D) and cytoskeletal interactions have been described (E) as well as regulation of histone acetylation and transcriptional regulation (F). Taken from Matos et al. (2011).

1.2.1.2 Biochemical properties of aberrant-elongated ataxin-3

Ataxin-3 has a normal molecular weight of 42 kD, but with enlarged CAG repeats can become significantly larger, which confirms that the repeat is translated into a polyQ stretch. An important histological hallmark of MJD is intranuclear inclusion bodies in neuronal cells (Fig. 1.2b) (Zoghbi and Orr, 2000). These inclusions are large protein aggregates containing ataxin-3 along with many other proteins such as proteasomal subunits and transcription factors. Recent evidence supports the idea that these aggregates result from cellular protective mechanisms against the toxicity of the expanded protein oligomers (Arrasate et al., 2004; Ross and Poirier, 2004; Shao and Diamond, 2007; Slow et al., 2005). Additionally,

toxicity of the expanded CAG repeat of the mRNA transcript has been shown (Li et al., 2008). PolyQ-elongated ataxin-3 influences many cellular processes by hindering transcription (McCampbell et al., 2000), disturbing the quality control system (Ferrigno and Silver, 2000), impairing axonal transport (Gunawardena et al., 2003) and facilitating aggregation of several ubiquitinated proteins (Donaldson et al., 2003) due to the loss of proper physiological ataxin-3 function or blocking of interaction partners (Fig. 1.2a). PolyQ proteins generally tend to form aggregates and due to their histological visibility and their predisposition to involve other protein species as well in these complexes, investigation has focused on understanding how ataxin-3 can aggregate. Overexpression of polyQ-elongated ataxin-3 causes amyloid-like fibrils (Bevivino and Loll, 2001), but in overexpression models, the non-expanded variant and the JD alone can also form aggregates (Chow et al., 2004; Gales et al., 2005; Masino et al., 2004). Additionally, mouse models overexpressing expanded human ataxin-3 did not show any phenotype, while a strong pathology similar to human patients could be seen in models overexpressing only the expanded CAG fragment of human protein (Ikeda et al., 1996). Aggregation kinetics in the normal variant seems to be very slow and when interacting with different binding partners, ataxin-3 is unlikely to form these complexes. In contrast, the expanded variant seems to form more quickly and the resulting aggregates are more stable, leading, over decades, to the disease in patients. One important question is, as ataxin-3 is present in all tissues, why does its elongation specifically lead to a neuronal disease?

The development of new cellular models of MJD is crucial for the understanding of how the described biochemical alterations finally lead to the incurable loss of neurons. By using MJD-patient-specific induced pluripotent stem cell-derived neural stem cells, our group found a possible mechanism for aggregate formation and why neurons are the cell population of disease action (Koch et al., 2011). Proteolytic cleavage of highly aggregation-prone polyQ fragments of ataxin-3 has been proposed to trigger the formation of aggregates. The formation of early aggregation intermediates is thought to have a critical role in disease initiation, but the precise pathogenic mechanism operating in MJD has remained elusive. It was found that glutamate-induced excitation of patient-derived neurons initiates Ca^{2+}-dependent proteolysis of ataxin-3 followed by the formation of SDS-insoluble aggregates. This phenotype could be abolished by calpain inhibition, confirming a key role of this protease in ataxin-3 aggregation (Fig. 1.2c). Aggregate formation was further dependent on functional Na^{+} and K^{+} channels as well as ionotropic and voltage-gated Ca^{2+} channels, and was not observed in the founding stem cells, fibroblasts or glia, thereby providing an explanation for the neuron-specific phenotype of the disease. This data also illustrates that neural stem cells enable the study of aberrant protein processing associated with late-onset neurodegenerative disorders in patient-specific neurons.

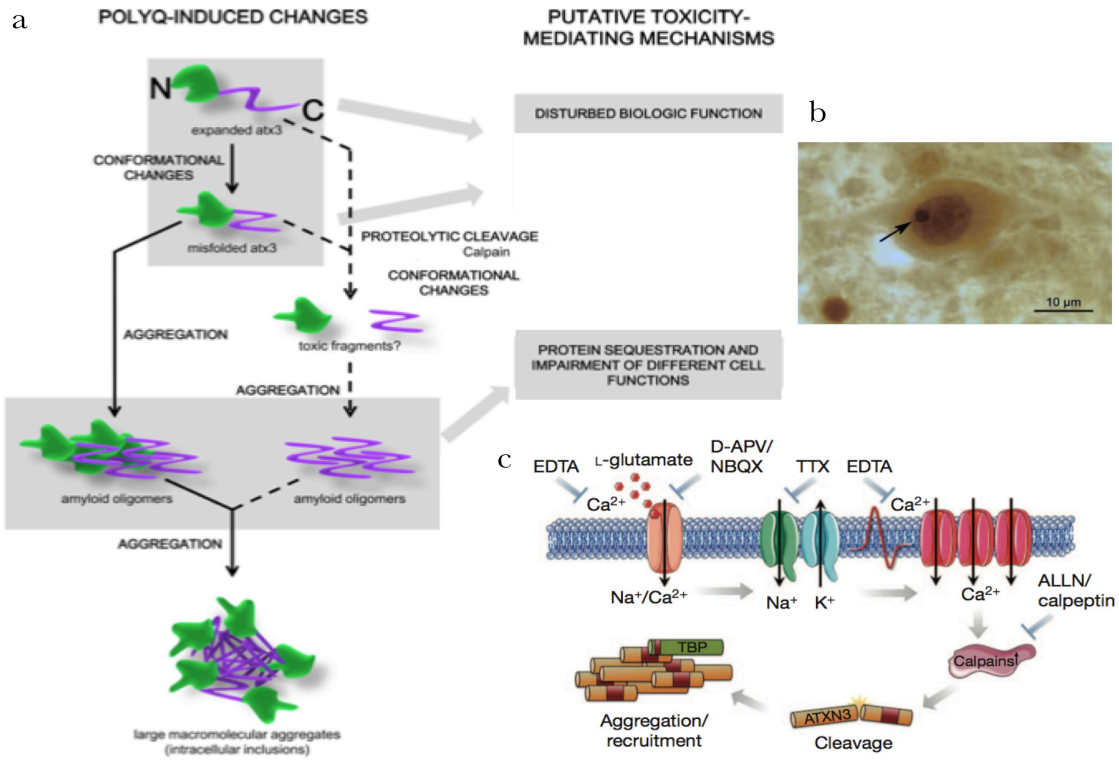

Figure 1.2: Mechanisms of ataxin-3 toxicity.
a. *PolyQ-expanded ataxin-3 leads to MJD but the responsible mechanisms are still under debate. The conformational changes causes by the polyQ stretch may disturb the biologic function of ataxin-3, thereby compromising the protein homeostasis system, the cytoskeleton or hindering transcription. Aggregation of whole protein or toxic fragments of proteolytic cleavage by calpains can lead to membrane destabilization and the impairment of protein sequestration mechanisms. All this interference with cell function finally leads to cell death. Adapted from Matos et al. (2011).* ***b.*** *Ataxin-3 immunoreactive neuronal intranuclear inclusion bodies are a result of the aggregate forming process. Adopted from Riess et al. (2008).* ***c.*** *Proposed model of excitation-induced aggregate formation in neurons involving activation-dependent Ca^{2+} influx via voltage-gated Ca^{2+} channels and subsequent calpain-mediated ataxin-3 cleavage. Taken from Koch et al. (2011).*

1.2.2 Epilepsy associated with different neurological disorders

Epilepsy is a common set of chronic neurological disorders affecting ~1% of the population, and characterized by seizures (Jallon, 1997). It is characterized by changes in the equilibrium between excitatory (glutamatergic) and inhibitory (GABA-ergic) neurotransmission. Dysfunction of anticonvulsant or neuroprotective regulatory systems have also been reported (DeLorenzo et al., 2007). The process that transforms a healthy brain into an epileptic brain, such as status epilepticus or traumatic brain injury, is called epileptogenesis, and is triggered by initial precipitating injuries (Delorenzo et al., 2005; Prince et al., 2012). Although some monogenetic epilepsies are known, most of which are based on ion channel defects, most cases are idiopathic. Often a cause cannot be identified despite several potential causative factors such as trauma, strokes, cancer or drug misuse (Chang and Lowenstein, 2003).

Currently used antiepileptic drugs largely act on targets involved in neurotransmission to suppress seizures, but do not suppress the process of epileptogenesis (Löscher and Schmidt, 2006). Surgical interventions also act only symptomatically (Engel, 1996). So far, no effective prophylaxis or pharmacotherapeutic cure is available. Additionally, the progression to chronic epilepsy often leads to pharmacoresistance and intractable seizures, by which up to 30% of all patients with epilepsy are affected (Jallon, 1997). These patients are often severely disabled and have an increased risk of sudden death. Thus, new therapeutic strategies are needed. A prerequisite for the development of new therapies is the understanding of mechanisms underlying epilepsy.

1.2.2.1 Adenosine balance in the central nervous system

Epilepsy can be seen either as an increased activation or a decreased inhibition of neuronal circuits. Therefore, the basal mechanism of activation and inhibition should be examined to understand which kind of deregulation leads to seizures. Adenosine acts as a neurotransmitter in the brain through the activation of four distinct G-protein-coupled receptors that mediate neuroprotection and a general down-regulation of neuronal activity (Lombardo et al., 2007). Hence, adenosine itself is thought to act as an endogenous anticonvulsant (Beutler, 1993; Fredholm et al., 2005a; Roberts et al., 1994). So far, four adenosine receptors have been identified: high-affinity inhibitory A_1 and excitatory A_{2A} receptors and low-affinity A_{2B} and A_3 receptors. Different affinities of these receptors to adenosine and variable distribution within the brain form a highly complex system of adenosine action (Dunwiddie and Masino, 2001; Fredholm et al., 2005b). The anticonvulsant functions of adenosine are thought to base largely upon the activation of A_1 receptors coupled to inhibitory G proteins leading to an inhibition of the release of neurotransmitters, in particular glutamate. The excitatory A_{2A} receptors appear to be restricted to active synapses and modulate the action of other neurotransmitters (Ferré et al., 2005). The role of the low affinity receptors is not completely understood so far, but all four adenosine receptors can form heterodimers with other G-protein coupled receptors, thereby influencing a large regulatory network (Sebastião and Ribeiro, 2009).

Adenosine acts as a fast endogenous response during events of overshooting activity, as its release is upregulated during seizures in human patients and during pharmacologically induced seizures in rats (Berman et al., 2000; During and Spencer, 1992). Mimicking this response by administrating adenosine can moderate epilepsy, but despite optimal drug treatment, seizures persist in ~35% of patients with partial epilepsy (Devinsky, 1999). When administered systemically, adenosine and its analogues cause strong effects ranging from

sedation to suppression of cardiovascular functions and cessation of spontaneous motor activity (Dunwiddie, 1999). A local administration of adenosine only in the affected brain region would be favored.

1.2.2.2 The role of adenosine kinase

The enzyme adenosine kinase (also known as ATP:adenosine 5'-phosphotransferase, ADK; EC 2.7.1.20) catalyzes the phosphorylation of adenosine to adenosine monophosphate (AMP) (Irion et al., 2007) (Fig. 1.3a) and thus plays a key role in the regulation of intra- and extracellular adenosine levels. Adenosine is also metabolized by adenosine deaminase, but ADK is considered to be the key enzyme due to its lower K_m value. This has been further validated by inhibition of the ADK, resulting in an increase in synaptic adenosine, which in turn suppresses glutamatergic excitatory synaptic transmission (Etherington et al., 2009; Lee et al., 1984). Astrogliosis, a pathological hallmark in several epilepsies in patients, is often accompanied by overexpression of ADK and resulting adenosine deficiency (Li et al., 2007a). Also, in chemically induced spontaneous seizures in animal models, an increase in the enzymatic activity of ADK has been detected (Gouder et al., 2004). Thereby deregulated ADK provides a molecular link between astrogliosis and neuronal dysfunction in epilepsy. In line with this, the viral overexpression of ADK in the hippocampus alone was sufficient to trigger seizures (Theofilas et al., 2011).

The importance of ADK for adenosine levels in the brain has led to a strong interest in using this enzyme as a therapeutic target. Local administration of adenosine was assessed by implantation of an adenosine releasing synthetic polymer that released low adenosine concentrations and protected against electrically induced seizures with no detectable side effects in animals (Boison et al., 1999). Such low concentrations should also be producible by biological sources. The Boison group developed a system of adenosine-releasing fibroblasts with inactivated adenosine kinase and adenosine deaminase. These cells were transplanted into brain ventricles in a rat epilepsy model and were shown to efficiently suppress seizures (Huber et al., 2001).

The study of Huber and colleagues used cells engineered by undirected mutagenesis comprising a high risk of oncogenic potential. Also, fibroblasts are not a natural population of the brain, so a neural cell type with a specifically altered genotype was demanded. This was achieved by engineering murine embryonic stem cells by genetic disruption of both alleles of the ADK and subsequent differentiation into neural precursor cells by the laboratories of Brüstle and Boison (Fedele et al., 2004; Li et al., 2007b). These cells were transplanted into rats where they differentiated *in vivo* into neurons and integrated into the host tissue. This

population efficiently suppressed epileptogenesis through adenosine release, while a control cell population of baby hamster kidney cells with the same destruction of the ADK gene did not show similar benefits after transplantation, underlining the importance of functional integration of cells for cell therapy purposes.

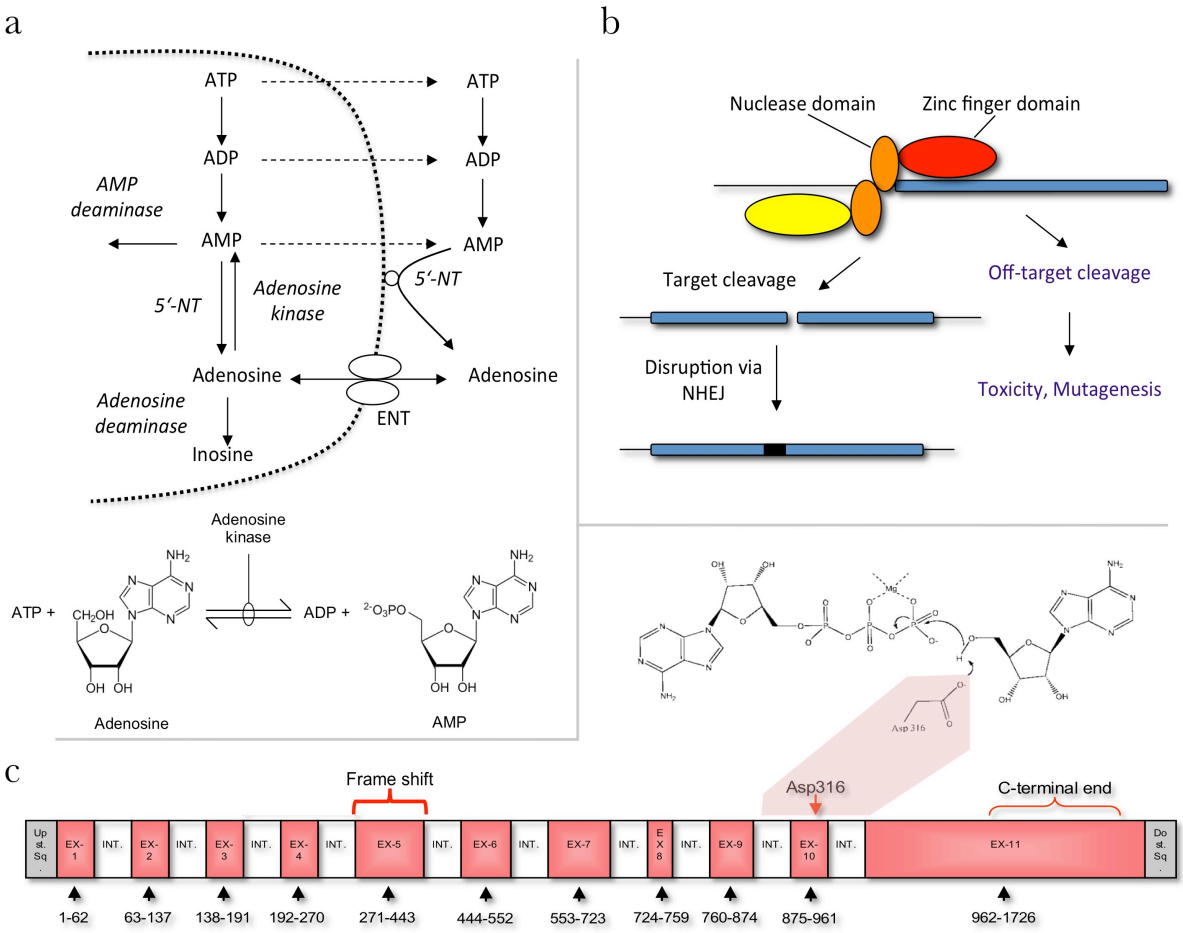

Figure 1.3: Adenosine kinase function and locus.
a. *The most important metabolizing enzymes of adenosine are adenosine kinase (ADK) and adenosine deaminase (ADA). Exchange of intracellular adenosine with extracellular compartments is performed via equilibrative nucleoside transporter (ENT).* ***b.*** *Zinc finger nucleases (ZFN) are synthetic fusion proteins of a DNA-binding zinc finger domain and a double strand break-inducing nuclease domain. Dimerization of nuclease domains is necessary for target cleavage. The cellular machinery for non-homologous end joining (NHEJ) is involved in repairing the double strand break, a mechanism that is error-prone and can thus result in disruption of the target gene.* ***c.*** *Locus of the ADK gene with exons in red and introns in white. The catalytic core around Asp316 is situated at the C-terminal end of the protein. Introduction of frame shifts within a coding exon of the gene prior to the catalytic part leads to destruction of all enzymatic activity. Also shown is the reaction in which Arg316 attacks adenosine to form the phosphate bond.*

This study investigates the use of site-specific disruption of the ADK gene using zinc finger nucleases (ZFN, Fig. 1.3b) on a human multipotent neural stem cell population. For the targeting approach, the constitution of the gene locus is of importance. Essential for the enzyme function is its active site: Asparagine 316 acts as a catalytic base that deprotonates the 5'-hydroxyl of adenosine to initiate the transfer of phosphate from ATP to form AMP (Fig. 1.3c). Substitution of this residue inactivates the enzyme. The C-terminus forms local secondary structures constituting the adenosine-binding site (Schumacher et al., 2000), and its disruption is accompanied by loss of ADK activity. The gene consists of 11 exons with lengths of 36 to 765 bp, the majority having a length below 100 bp (Fig. 1.3c). The collaboration partner Sangamo® provided three different ZFNs for targeting exon 5 of the ADK gene. Induction of a double-strand break and subsequent frame shifting would result in a disrupted gene, whose protein product would be without all enzymatic activities.

1.3 Gene targeting in human cells

Genetic techniques that specifically change endogenous genes are called gene targeting (Thomas and Capecchi, 1987). The term is normally used for modifications that are achieved by homologous recombination, and allows removal or addition of whole genes or the modification of exons or introduction of point mutations. Targeting implies its specificity to target uniquely in the genome, in contrast to random integration of genetic material, e.g. for overexpression studies. In model organisms, gene targeting is often achieved by altering the germ line to raise whole animals with a modified genome. For the creation of such animals, Mario Capecchi, Martin Evans and Oliver Smithies were awarded the Nobel Prize in medicine in 2007. Pluripotent stem cells are the major cell source for targeting approaches.

Although a huge knowledge was accumulated by the use of model organisms, which are often susceptible to transformation into the corresponding genes in humans, the limited extrapolation potential to other species or cell types constrains such studies. This applies especially to the study of higher brain functions and its disorders in humans due to its significantly higher complexity, other metabolism or protein composition. However, in mammalian cells, non-homologous recombination is more frequent (Waldman, 1992). Although there are several methods for enrichment available, such as positive-negative selection, where antibiotic resistance is combined with a suicide-enzyme like HSV-TK only integrating at off-target-sites (Mansour et al., 1988), or promoterless vectors (Hanson and Sedivy, 1995), which in theory are fail-safe, many of them improve the specificity at surprisingly low rates in practice (Bunz, 2002).

Targeting efficacy is of particular importance for human cells because, unlike in the mouse system where a heterozygous targeting event can be bred to homozygosity, the generation of homozygously altered human cell lines requires the targeting of both alleles. For a homologous recombination with acceptable efficiencies, plasmid lengths of several kb are needed (Rubnitz and Subramani, 1984). Because of the high number of single-nucleotide polymorphisms in the human genome (Wang et al., 1998) isogenic DNA should be used, which would necessitate a customization for each cell line used.

Transformed tumor cell lines are readily available and easy to handle but offer a very artificial model to study the natural function of human genes, while primary cell lines are themselves limited to a definite number of passages in cell culture, leaving only a small time window and a small population for experiments. Established human embryonic stem (ES) cell lines that can be kept in culture theoretically for an unlimited number of passages, offer the possibility to establish stable, genetically modified human cell lines. The widespread arrival of induced pluripotent (iPS) cells free of ethical controversies now offer the generation of patient-specific stem cells that can be differentiated into affected cell types. This will greatly facilitate the understanding of biochemistry and physiology of disease-associated genes.

So far gene manipulation in human cells remains inefficient which aggravates the development of disease models or therapeutic applications. Homologous recombination-mediated genome modification has been used experimentally for decades in yeast while its use in mammalian cells was limited by its low spontaneous rate (Porteus and Baltimore, 2003; Sedivy and Sharp, 1989). Nonetheless, gene targeting has been used as an extremely important tool in murine embryonic stem cells. Pioneers in this field were the groups of Capecchi and Smithies (Doetschman et al., 1988; Thomas and Capecchi, 1987), which were awarded the Nobel Prize in physiology in 2007 for the generation of transgenic mice by transferring such modified ES cells into blastocysts. By using this strategy, thousands of mouse models have been derived.

Up to now, only few approaches for genetic modification of human ES cells have been reported. Zwaka and co-workers were the first to achieve a homologous recombination in the HRPT1 locus in human ES cells using a reporter construct for clone selection (Zwaka and Thomson, 2003). However, the reported efficiencies are low compared to standard efficiencies in the mouse system. This may be due to the fact that human ES cells are much more sensitive to physical manipulations resulting in low survival and clonogenicity. A few months later, Urbach and co-workers targeted the same locus to introduce a mutation found in Lesch-Nyhan disease into the HRPT1 gene, which for the first time established a model for a human-specific disorder in a hES cell-derived culture system (Urbach et al., 2004).

The fact that since the first description of human embryonic stem cell lines in 1998 (Thomson et al., 1998) only few groups were able to report homologous recombination in the human system emphasizes limitations and difficulties of classical gene targeting approaches. Other approaches to overcome technical limitations have been developed in the past years. These include viral systems like adeno-associated virus (AAV) (Khan et al., 2010) and helper-dependent adenoviral vectors (HDAdV) (Suzuki et al., 2008) as well as BACs (Song et al., 2010) or synthetic fusion proteins of nucleases with zinc finger or TALEN domains (Cermak et al., 2011; Lombardo et al., 2007) and the recently discovered, RNA-guided Crispr/Cas9-system (Mali et al., 2013).

1.3.1 Viral systems for gene delivery

One possibility to enhance the poor rate of homologous recombination events in human cells is to use tools optimized by nature for gene delivery: viruses. The direct application of viral vectors always bears the danger of unwanted random integration into the genome, which can lead to a transformation of single cells into a malignant state (Hackett et al., 2007). One single transformed cell already has the potential to form a tumor and up to now, no integrative viral system is known that would lack this attribute. Therefore, efforts switched to use monoclonal cell populations simplifying screening procedures used to detect unwanted alterations (Noda et al., 1986).

First attempts to repair mutations in genes with retroviral vectors showed high frequencies of correction and thus successful targeting, but was also associated with unwanted gene conversion in other regions and random integration typical for retroviruses (Ellis and Bernstein, 1989). Other studies used modified adenoviral vectors with large homologous portions, which deliver their genome with high efficacy and at preferred ratios of correct targeting to random insertion, i.e. 1:2.5 (Mitani et al., 1995). They offer a genetic size of over 30 kb, which allows a flexible selection of homologous parts and the integration of a large amount of genetic information, but making the design of targeting vectors difficult. Also, new helper-dependent vectors no longer contain toxic viral elements responsible for immune responses and their side effects reported for adenoviruses (Christ et al., 1997; Nunes et al., 1999). Much easier to engineer due its smaller vector size but also with high integration efficiencies are Adeno-associated viral (AAV) particles.

1.3.2 Recombinant adeno-associated virus type 2 for site-specific targeting

The adeno-associated virus (AAV) is a member of the parvovirus family, the only human virus family with a linear single-stranded DNA genome identified so far. They belong to the smallest viruses known and bear a relatively small genome of around 5000 bases (Chapman and Rossmann, 1993) Nine subtypes (AAV 1-9) are known, for which humans are the primary host, subtype 2 being the most common. While 80% of the human population are seropositive, no pathology is associated with the virus (Vasileva and Jessberger, 2005).

The genome of AAV-2 contains two open reading frames (ORFs), called cap (3 transcripts) and rep (4 transcripts) (Srivastava et al., 1983) These coding sequences are flanked on both sides by palindromic inverted terminal repeats (ITRs) that form hairpin loops. The rep ORF encodes proteins that are involved in viral replication and integration, while the cap genes are responsible for packaging and cell infection. Heparan sulphate proteoglycan (HSPG) has been shown to act as the primary receptor (Summerford and Samulski, 1998) while $\alpha V\beta 5$ integrin and human fibroblast growth factor receptor 1 have been proposed as co-receptors (Qing et al., 1999; Summerford et al., 1999). This enables AAV-2 to infect a large variety of cell types including epithelial cells, skeletal muscle, neurons and mesenchymal stem cells (Flotte et al., 1992; Kaplitt et al., 1994; Stender et al., 2007; Wang et al., 2000a).

A lytic infection with production of new AAV particles by the infected cells is dependent on a co-infection with an adeno virus, which acts as a helper virus for the AAV due to the presence of the immediate early genes E1, E2A, E3 and E4 of adeno virus in the affected cells (Richardson and Westphal, 1981). Without these gene products, AAV-2 enters a lysogenic cycle, i.e. without the production of virus particles, and stably integrates in the human genome. This integration is random, but with a high prevalence for a specific region on chromosome 19q13.3, called AAVS1 (Kotin et al., 1992). Presumably, homology in the ITRs with this locus is responsible for the preference. For stable integration, the rep transcripts are essential. After infection with the suitable helper virus, AAV can again enter the lytic cycle.

Due to its defective replication, the non-pathogenicity and its ability for site-specific integration in chromosome 19, AAV2 was considered potentially useful for gene therapy approaches that used the addition of functional genes into a “safe harbour” (Linden et al., 1996). The sequences between the ITRs could be replaced by desired genes and so integrated into a passive site of the genome without the danger to impede active genes. Soon, vector systems were established, which supplied the rep and cap ORFs needed for vector production as well as helper-virus elements in trans.

Because of its small genome of only 4.8 kb, this vector system is not suitable for large genes. Also the danger of a randomized insertion persists, and even when inserted into the main

locus at chromosome 19, an influence on cellular genes lying nearby, like the MBS85, was reported (Tan et al., 2001). Insertions were observed mainly at transcriptionally active sites (Nakai et al., 2003) which can also bear oncogenic potential (Miller et al., 2002). These problems seemed to restrict the use of AAV2 as a tool for adding genes to the genome. Nevertheless, AAVs were used in attempts to treat Duchenne muscular dystrophy (Athanasopoulos et al., 2004) or beta-thalassemia (Tan et al., 2001) where non-dominant negative mutations could be compensated by the integration of wild-type genes into the AAVS1 locus. The use of AAVs was further simplified by the arrival of commercially available systems.

Following the hypothesis that homology of the ITRs with the AAVS1 locus is responsible for preferred respective insertion of AAV genomes, Russell and colleagues used a recombinant AAV containing genomic sequences to establish an area of homology in the vector for directing the site of integration (Russell and Hirata, 1998). They disrupted the human HPRT gene by introducing a mutation of a few base pairs while the total length of homology between the substrate and the targeting vector was 2.7 kb. This was about four times less than the length required for efficient targeting with conventional systems. Correct integrations were about two orders of magnitude higher than observed with adenoviral or retroviral vectors (Ellis and Bernstein, 1989). It has been shown that the cellular homologous recombination machinery is required for this site-specific gene targeting (Vasileva et al., 2006).

As the HPRT gene is situated on the X-chromosome and male cells were used, a selection marker was not required and instead a suicide metabolite could be applied. For normal biallelic genes another targeting design was necessary. By reducing the homology to 900 bp on both sites flanking the target sequence, the system has also been shown to work efficiently by disrupting a gene in a human colon cancer cell line (Kohli et al., 2004). This system used rAAVs with homology arms laying directly inwards from both ITRs to direct the insertion to a specific site. The gained space in the vector of 2.5 kb was employed to incorporate a selection marker. From there onwards, two AAV based vector systems were established that have to be clearly distinguished. First, the gene adding system for integration into the AAVS1 locus on chromosome 19, for which commercial systems are available. This system only requires the ITRs in the targeting vector and bears a capacity of ~4.5 kb. Second, a site-specific system that relies on homology arms inside the ITRs of together 1.8 kb length, reducing the available space for a selection cassette to ~2.5 kb.

The Russell group showed the functionality of this new system for the first time *in vivo* by correcting a mutant lacZ gene at the ROSA26 locus in mouse (Miller et al., 2006). Gene correction and gene deletion are possible with the AAV system, each shown in cell culture on

transformed cells and *in vivo* with somatic cells, respectively. However, until now this system has not been used on human somatic cells in a cell culture system. For neurons and glia, AAV application was reported to be stable and non-toxic when insertion into AAVS1 locus was used for gene addition (Howard et al., 2008). These observations suggest that human neural stem cells (lt-NES cells), being precursors of glia und neurons were also suitable candidates for transduction.

1.3.3 Alternative systems for genetic modifications of human cells

Besides the already listed viral and electroporation systems, other methods for genetic manipulations, or corrections have been described. These include homologous integration, which was reported for short double- or single-stranded DNAs (Colosimo et al., 2001), and also for DNA/RNA chimeras (Kmiec, 1999) and triplex forming oligos (Fox, 2000). These approaches work well and very efficiently for the substitution of only a few base pairs, but are not applicable to larger portions of the genome. Therefore they could be used for gene correction purposes, but presumably not delivery of whole genes. Also, AAV vectors have size limitations, albeit showing a high targeting efficiency. A completely different approach is the use of bacterial artificial chromosomes or BACs, which are large circular DNA elements up to several megabases in size that can bear several genes and also show a high specificity for site-directed targeting due to the large amount of homology they provide. One of the major drawbacks is the difficulty to produce and engineer such large constructs, and special techniques are needed. For the investigation of disease models, as well as for a possible therapeutic application, a system is required that is highly efficient in targeting the desired locus, easy to engineer so that it can be used for different approaches, and applicable to human stem cells. For the application of patient-specific cells, as well as for use with different cell lines, a targeting vector with a relatively short homology region is preferable, so that a once constructed vector can be used with cells other than those of isogenic origin.

1.3.4 Zinc finger nuclease targeting

A relatively new method showing high specificity for the desired locus on the one hand and only needing a relatively small recognition sequence on the other hand, are zinc finger nucleases (ZFN). Chandrasegaran and coworkers developed the first of these by fusing the nonsequence-specific cleavage domain of the FokI restriction endonuclease domain to a new DNA-binding domain (Kim et al., 1996). The first DNA-binding domain used was a fruit fly homeobox domain, followed by zinc-finger DNA binding domain and yeast Gal4 DNA-binding

domain (Kim and Chandrasegaran, 1994; Kim et al., 1998). Further optimization was performed by Bibikova et al. (2001), finding cleavage was most efficient when binding sites were inversely oriented, separated by six nucleotides and without a peptide linker between DNA-binding and nuclease domain. Additionally, these experiments were the first using living cells of *Xenopus laevis* and proved activation of the ZFN substrate for homologous recombination by cellular mechanisms. Until then, all DNA-binding domains used were of natural origin and thus targeted their known recognition site. The special appeal of ZFN however is the possibility to modify the DNA-binding domain to bind specifically chosen target sequences, allowing an induced double strand break at a defined position.

Zinc finger modules are part of the DNA-binding domain of one of the largest families of transcription factors in eukaryotic genomes (Diakun et al., 1986). Already in the human genome there are more then 4000 different modules in 700 proteins present (Jantz et al., 2004; Notarangelo et al., 2000). Each module forms a finger of 30 amino acids size binding to a 3 bp sequence of DNA and each finger binds its target site independently (Pavletich and Pabo, 1991). Combining individual fingers with different triplet targets changes the overall binding specificity of the zinc finger protein. The naturally occurring fingers with known binding preference were disassembled to find fingers for all 64 different target triplets to enable the generation of zinc finger domains binding to any target sequence possible (Pabo et al., 2001; Segal and Barbas, 2001; Segal et al., 2003; Wolfe et al., 2000). Despite modules for specific sequence blocks being known, there is no general assembly code for the generation of consistently high affinity binding of zinc fingers. This makes screening of zinc finger domain libraries necessary to optimize their specificity.

A double strand break per se cannot be termed gene targeting, because it is defined as the exchange of DNA in a specific locus by homologous recombination. However, if a frame shift resulting in a gene knockout is induced, the outcome is of the same quality; a specific gene modified in a very small range without interference with other loci.

1.4 Aim of this study

Apart from the substantial progress made in the last years using human stem cell populations for the study of disease mechanism- and progression or their application in cell therapeutic paradigms, the majority of studies still focuses on pluripotent populations that require time-consuming run-through protocols resulting in populations with a bias for batch-to-batch variations. As viable alternatives, intermediate stem cell populations, which are closer to the cell type of interest but still have the advantages of unlimited self-renewal in culture, like the lt-NES cells used in this study could be employed.

To test the proficiency of lt-NES cells for different applications aiming for disease-modeling or therapeutic approaches, straightforward genetic manipulation is essential. This study employs different methods exhibiting site-specific genetic intervention to overcome common problems of overexpression of proteins or microRNAs. Using gene-editing methods to modify endogenous genes in a specific, site-directed manner should have great benefits compared to aforementioned techniques, where random integration can lead to genomic instability or tumorigenesis, while gene knockdowns by microRNA may be incomplete.

The present study combines the advantages of a stable somatic intermediate stem cell population with multiple approaches of site-specific genetic manipulation. Two examples were chosen to address the question: First, exchange of elongated polyQ alleles in the *ATXN3* gene for disease modeling *in vitro* to permit comparison of effects and mechanisms using isogenic cell lines. Second, the disruption of the adenosine kinase (ADK) gene as a basis for cell-mediated activity-dependent adenosine delivery.

In Machado-Joseph-Disease-patient derived neural stem cells, the polyQ-elongated protein variant is causative for the disease and its depletion/deletion or genetic correction should result in a cell population with normalized biochemical characteristics. For the site-specific exchange of the pathogenic allele of ataxin-3 against its wildtype variant an approach using the ability of adeno-associated viruses for site-specific targeting was designed. The resulting isogenic populations only differing in one specific locus should offer a better control population for elucidating disease mechanism than studies using controls generated from relatives.

Adenosine kinase is a key enzyme for the metabolization of adenosine in the brain and its depletion increases adenosine efflux of affected cells. By application of zinc-finger nucleases specific for the human adenosine kinase gene, a biallelic knockout to generate an adenosine-releasing cell population for cell therapeutic approaches is intended. Adenosine itself acts as a suppressor of neuronal activity and was shown to moderate epilepsy. Cells with homozygous knockout of the ADK gene might be useful in a cell therapy model of epilepsy.

2 Material

2.1 Technical equipment

Appliance	Name	Manufacturer	Registered office
Autoclave	D-150	Systec	Wettenberg, Germany
Balance	BL610	Sartorius	Göttingen, Germany
Balance	LA310S	Sartorius	Göttingen, Germany
Block heater	Thermomixer compact	Eppendorf	Hamburg, Germany
Bone drill 0.7 mm burrs	Micro Drill	Fine Science Tools	Hamburg, Germany
Centrifuge (large)	Megafuge 1.0R	Kendro	Hanau, Germany
Centrifuge (table top)	5415D	Eppendorf	Hamburg, Germany
Concentrator	Speed Vac 5301	Eppendorf	Hamburg, Germany
Counting chamber	Fuchs-Rosenthal	Faust	Halle, Germany
Cryostat	CL6000	Leica	Dresden, Germany
Digital camera	C 5050 Zoom	Olympus Optical	Hamburg, Germany
Digital camera	Powershot G5	Canon	Krefeld, Germany
Electroporator	Nucleofector 2b	Lonza	Basel, Switzerland
Fluorescence lamp	HAL100	Carl Zeiss	Jena, Germany
Fluorescence microscope	Axioskop 2	Carl Zeiss	Jena, Germany
Freezer -80°C	HERAfreeze	Kendro	Hanau, Germany
Gel electrophoresis chamber	Agagel	Biometra	Göttingen, Germany
Glass-Microelectrode puller	PE-21	Tritech Research	Los Angeles, USA
Imaging system	Chemidoc 2000	Bio-Rad	München, Germany
Imaging system	Geldoc EZ	Bio-Rad	München, Germany

Appliance	Name	Manufacturer	Registered office
Incubator	HERAcell	Kendro	Hanau, Germany
Inverse light microscope	Axiovert 25	Carl Zeiss	Jena, Germany
LED light source	Colibri 2	Carl Zeiss	Jena, Germany
Liquid nitrogen store	MVE 611	Chart Industries	Burnsville, USA
Microliter pipet	1710N	Hamilton	Bonaduz, Switzerland
Microscope	Axiovert 40 CFL	Carl Zeiss	Jena, Germany
Microscope	Axiovert 200M	Carl Zeiss	Jena,Germany
Microscope camera	Axiocam MRM	Carl Zeiss	Jena, Germany
Micro-Spectrophotometer	Nanodrop ND-1000	Thermo Fisher Scientific	Wilmington, USA
Micropipettes	Labmate L2, L10, L20, L100, L1000	Labmate	Langenfeld, Germany
PAGE/Blot equipment	Mini-Protean 3	Bio-Rad	München, Germany
pH-meter	CG840	Schott	Mainz, Germany
Pipette-boy	Accu-Jet	Brand	Wertheim, Germany
Power supply for electrophoresis	Standard Power Pack P25	Biometra	Göttingen, Germany
Refrigerators 4°C /-20°C	G 2013 Comfort	Liebherr	Lindau, Germany
Shaker	Bühler WS10	Johanna Otto	Hechingen, Germany
Secure horizontal flow hood	HERAsecure	Kendro	Hanau, Germany
Southern blotter	Turbo Blotter	Carl Roth	Karlsruhe, Germany
Sterile laminar flow hood	HERAsafe	Kendro	Hanau, Germany
Stereo microscope	STEMI 2000-C	Carl Zeiss	Göttingen, Germany
Stereotactic Frame	Stereotactic Frame	Stoelting	Illinois, USA
Sterilizer	Hot Bead Sterilizer	Fine Science Tools	Heidelberg, Germany

Appliance	Name	Manufacturer	Registered office
Table centrifuge	Centrifuge 5415R	Eppendorf	Hamburg, Germany
Thermocycler	T3 Thermocycler	Biometra	Göttingen, Germany
Transplantation instruments	Transplantation Tool Set	Fine Science Tools	Heidelberg, Germany
Vacuum pump	Vacuubrand	Brand	Wertheim, Germany
Vortex mixer	Vortex Genie 2	Scientific Industries	New York, USA
Water bath	1008	GFL	Burgwedel, Germany
Water filter	Millipak 40	Millipore	Eschborn, Germany

2.2 Plastic ware

Consumables	Manufacturer	Registered Office
6-well culture dishes Nunclon surface	Nunc	Wiesbaden, Germany
12-well culture dishes Nunclon surface	Nunc	Wiesbaden, Germany
24-well culture dishes Costar	Corning Life Sciences	Schiphol-Rijk, The Netherlands
48-well culture dishes Costar	Corning Life Sciences	Schiphol-Rijk, The Netherlands
Cell Strainer 40 μm Nylon	BD Falcon	Bedford, USA
Cryovials 1 ml	Nunc	Wiesbaden, Germany
Cryovials 1.8 ml	Nunc	Wiesbaden, Germany
PCR strip tubes 0.2 ml	peqLab	Erlangen, Germany
Petri dishes ∅ 3.5 cm	BD Biosciences	Heidelberg, Germany
Petri dishes ∅ 6 cm	BD Biosciences	Heidelberg, Germany
Petri dishes ∅ 10 cm	PAA	Pasching, Austria
Round bottom tubes - 12x75 mm	BD Biosciences	Heidelberg, Germany
Serological pipettes 1 ml	BD Falcon	Bedford, USA
Serological pipettes 2ml	Corning Life Sciences	Schiphol-Rijk, The Netherlands
Serological pipettes 5 ml	Corning Life Sciences	Schiphol-Rijk, The Netherlands
Serological pipettes 10 ml	Corning Life Sciences	Schiphol-Rijk, The Netherlands
Serological pipettes 25 ml	BD Biosciences	Heidelberg, Germany
Syringes 20 ml	BD Biosciences	Heidelberg, Germany
Syringe filter 0.2 μm	Pall	Dreieich, Germany
Syringe filter 0.2 μm	PALL	Dreieich, Germany
TC dishes ∅ 3.5 cm	PAA	Pasching, Austria
TC dishes ∅ 6 cm	PAA	Pasching, Austria

Consumables	Manufacturer	Registered Office
TC dishes ∅ 10 cm	PAA	Pasching, Austria
Tubes 0.5 ml	Greiner Bio-One	Solingen, Germany
Tubes 1.5 ml	Greiner Bio-One	Solingen, Germany
Tubes 15 ml	Greiner Bio-One	Solingen, Germany
Tubes 50 ml	Greiner Bio-One	Solingen, Germany

2.3 Chemicals

Chemicals	Manufacturer	Registered office
2-Mercaptoethanol	Invitrogen	Karlsruhe, Germany
30% Bis/Acrylamide	Carl Roth	Karlsruhe, Germany
8-Chloroadenosine	Enzo	Lörrach, Germany
8-Cl-cAMP	Enzo	Lörrach, Germany
Agar	Sigma	Deisenhofen, Germany
Agarose	PeqLab	Erlangen, Germany
Ampiciline	Sigma	Deisenhofen, Germany
APS, 10%	Sigma	Deisenhofen, Germany
Atipamezol	Pfizer	Berlin, Germany
Azide	Sigma	Deisenhofen, Germany
B-27 supplement	Invitrogen	Karlsruhe, Germany
Bone wax	Fine Scientific Tools	Heidelberg, Germany
Bromphenol blue	Sigma	Deisenhofen, Germany
BSA solution (7.5%)	Sigma	Deisenhofen, Germany
$CaCl_2$	Sigma Aldrich	Deisenhofen, Germany

Chemicals	Manufacturer	Registered office
cAMP	Sigma Aldrich	Deisenhofen, Germany
Carprofen	Pfizer	Berlin, Germany
Chemiluminescent Substrates	Thermo Scientific	Frankfurt, Germany
Chloroform	Sigma	Deisenhofen, Germany
Chloroquin	Sigma Aldrich	Deisenhofen, Germany
Collagenase IV	Sigma Aldrich	Deisenhofen, Germany
Complete ULTRA™ tablets	Roche Diagnostics	Basel, Swizerland
CytocoonTM Buffer II	Evotec Technologies	Hamburg, Germany
Cytoseal	Microm	Walldorf, Germany
DABCO	Sigma Aldrich	Deisenhofen, Germany
DAPI	Sigma	Deisenhofen, Germany
DAPT	Sigma Aldrich	Deisenhofen, Germany
Diazepam	Roche	Basel, Switzerland
Direct PCR Lysis Reagent	PeqLab	Erlangen, Germany
DMEM/F12 (1:1)	Invitrogen	Karlsruhe, Germany
DMEM high glucose	Invitrogen	Karlsruhe, Germany
DMSO	Sigma	Deisenhofen, Germany
DNA ladder (100bp)	PeqLab	Erlangen, Germany
DNA ladder (1kb)	PeqLab	Erlangen, Germany
dNTPs	PeqLab	Erlangen, Germany
Doxycycline	Sigma Aldrich	Deisenhofen, Germany
EDTA	Sigma	Deisenhofen, Germany
EGF	R&D Systems	Wiesbaden, Germany

Chemicals	Manufacturer	Registered office
EHNA	Sigma	Deisenhofen, Germany
Eosin Y solution	Sigma-Aldrich	Deisenhofen, Germany
Ethanol	Merck	Darmstadt, Germany
Ethidium bromide	Sigma	Deisenhofen, Germany
FCS	Invitrogen	Karlsruhe, Germany
Fentanyl	Roche	Basel, Switzerland
FGF2	R&D systems	Wiesbaden, Germany
Ficoll-400 DL	Sigma	Deisenhofen, Germany
Flumazenil	Roche	Basel, Switzerland
Formic acid	Sigma	Deisenhofen, Germany
G418 solution	Sigma	Deisenhofen, Germany
Gelatine	Invitrogen	Karlsruhe, Germany
Glucose	Sigma	Deisenhofen, Germany
L-Glutamate	Sigma	Deisenhofen, Germany
L-Glutamine	Invitrogen	Karlsruhe, Germany
Glycerol	Sigma	Deisenhofen, Germany
HCl	Sigma Aldrich	Deisenhofen, Germany
Hematoxylin solution Mayer's	Sigma Aldrich	Deisenhofen, Germany
HEPES	Sigma Aldrich	Deisenhofen, Germany
Insulin	Sigma	Deisenhofen, Germany
Isopropanol	Sigma Aldrich	Deisenhofen, Germany
Kainic acid	Sigma	Deisenhofen, Germany
Ketamine	Pfizer	Berlin, Germany

Chemicals	Manufacturer	Registered office
Laminin	Sigma	Deisenhofen, Germany
Matrigel (MG)	BD Biosciences	Heidelberg, Germany
Meditomidin	Novartis	Nürnberg, Germany
Methylscopolamine	Sigma	Deisenhofen, Germany
Midazolam	Roche	Basel, Switzerland
Moviol	Sigma Aldrich	Deisenhofen, Germany
N2 supplement (100x)	Invitrogen	Karlsruhe, Germany
NaCl	Sigma Aldrich	Deisenhofen, Germany
$NaHCO_3$	Sigma	Deisenhofen, Germany
Naloxon	Roche	Basel, Switzerland
NaOH	Sigma Aldrich	Deisenhofen, Germany
Neurobasal medium	Invitrogen	Karlsruhe, Germany
Non-essential amino acids	Invitrogen	Karlsruhe, Germany
Opti-MEM basal media	Invitrogen	Karlsruhe, Germany
PBS	Invitrogen	Karlsruhe, Germany
PFA	Sigma	Deisenhofen, Germany
Phenol	Sigma	Deisenhofen, Germany
PhosSTOP™ tablets	Roche Diagnostics	Basel, Swizerland
Pilocarpine	Sigma	Deisenhofen, Germany
Poly-L-ornithine	Sigma	Deisenhofen, Germany
RIPA buffer	Sigma Aldrich	Deisenhofen, Germany
RNAiMAX	Invitrogen	Karlsruhe, Germany
Roti-Block 10%	Carl Roth	Karlsruhe, Germany

Chemicals	Manufacturer	Registered office
SDS	Sigma Aldrich	Deisenhofen, Germany
Serum Replacement	Invitrogen	Karlsruhe, Germany
Sodium pyruvate	Invitrogen	Karlsruhe, Germany
Sucrose (60%)	Carl Roth	Karlsruhe, Germany
TEMED	Sigma Aldrich	Deisenhofen, Germany
Tissue-Tek	Weckert Labortechnik	Kitzingen, Germany
Tris	Merck	Darmstadt, Germany
Triton-X-100	Sigma Aldrich	Deisenhofen, Germany
Trypane Blue	Invitrogen	Karlsruhe, Germany
Trypsin inhibitor (TI)	Invitrogen	Karlsruhe, Germany
Trypsin-EDTA (10x)	Invitrogen	Karlsruhe, Germany
Tryptone	Sigma	Deisenhofen, Germany
VectaShield mounting medium	Axxora	Loerrach, Germany
Xylene Cyanole FF	Bio-Rad	München, Germany
Yeast extract	Sigma	Deisenhofen, Germany

2.4 Enzymes

Enzyme name	Manufacturer	Registered office
Alkaline Phosphatase, Shrimp	Roche Diagnostics	Penzberg, Germany
DNase (cell culture)	Cell Systems	Troisdorf, Germany
DnaseI (mol. Bio.)	Invitrogen	Karlsruhe, Germany
Phusion High Fidelity Polymerase	Finnzymes	Heidelberg, Germany
Platinum Taq DNA Polymerase High Fidelity	Invitrogen	Karlsruhe, Germany

Enzyme name	Manufacturer	Registered office
T4 DNA Ligase	New England Biolabs	Frankfurt, Germany
Taq DNA Polymerase, recombinant	Invitrogen	Karlsruhe, Germany

2.5 Restriction endonucleases

Enzyme name	Restriction site	Manufacturer	Registered office
KpnI	5'…GGTAC^C…3' 3'…C^CATGG…5'	New England Biolabs	Frankfurt, Germany
NdeI	5'…CA^TATG…3' 3'…GTAT^AC…5'	New England Biolabs	Frankfurt, Germany
NotI	5'…GC^GGCCGC…3' 3'…CGCCGG^CG…5'	New England Biolabs	Frankfurt, Germany
PstI	5'…CTGCA^A…3' 3'…G^ACGTC…5'	New England Biolabs	Frankfurt, Germany
SpeI	5'…A^CTAGT…3' 3'…TGATC^A…5'	New England Biolabs	Frankfurt, Germany

2.6 Cell lines and animals

Cell line or mouse strain	**Source**
E. coli DH5a	Invitrogen, Karlsruhe, Germany
HEK-293AAV	Stratagene, La Jolla, USA,
hES cell line I3	Haifa, Israel (Amit et al., 2000)
iPS cell line iPS-1	Bonn, Germany (Koch et al., 2011)
iPS cell line MJD	Bonn, Germany (Koch et al., 2011)
Mouse strain C57/BL/6	Charles River, Wilmington, USA
Mouse strain Fox Scid/Beige (CB17/Icr-Prkdc scid/Crl)	Charles River, Wilmington, USA
Mouse strain C57BL/6 Rag2 conditional knock out	Taconic, Cologne, Germany

2.7 Plasmids

Plasmid name	Portions used	Producer
pAAV-MCS	Backbone	Stratagene, La Jolla, USA
pAAV-RC	Unaltered for AAV production	Stratagene, La Jolla, USA
pcDNA3.1	Backbone	Invitrogen, Karlsruhe, Germany
pHelper	Unaltered for AAV production	Stratagene, La Jolla, USA
pWPXL	EF1alpha-eGFP	Lausanne, Switzerland (Trono, 2000)
ZFN18337	Transient expression of upstream ZFN for *ATXN3*	Sangamo, Richmond, USA
ZFN18339	Transient expression of downstream ZFN for *ATXN3*	Sangamo, Richmond, USA
ZFN18781	Transient expression of upstream ZFN for *ATXN3*	Sangamo, Richmond, USA

2.8 Bacterial solutions

	LB agar
10 g	Tryptone
5 g	Yeast extract
5 g	NaCl
7 g	Agar
H_2O was added to 1 l and the mixture was autoclaved and stored at 4 °C	

	LB medium
10 g	Tryptone
5 g	Yeast extract
5 g	NaCl
1 ml	1 M NaOH
H_2O was added to 1 l and the mixture was autoclaved and stored at 4 °C	

	SOB medium
20 g	Tryptone
5 g	Yeast extract
0.5 g	NaCl
0.19 g	KCl
5 ml	2 M MgCl2
H_2O was added to 1 l, pH adjusted to 7.0 with 5 M NaOH, then the mixture was autoclaved and stored at 4°C	

2.9 Cell culture media

All basal media were ordered from Invitrogen (Karlsruhe). All compounds were mixed and sterile-filtered (0.2 µm filter), stored at 4°C and used within 4 weeks.

%	MEF (mouse embryonic feeder)
86	DMEM-high-glucose
10	FCS
1	Sodium pyruvate
1	L-Glutamine
1	Non-essential amino acids
1	Pen / Strep

%	Neural stem cell (N2) medium
97.5	DMEM/F12
1	N2 Supplements
1	Pen/Strep
0.5	Insulin
	D-Glucose (1.5 mg/ml)

%	Neuronal generation (NGMC) medium
50	Neural stem cell (N2) medium
48	Neurobasal medium
2	B27 supplement
	cAMP (100 ng/ml)

%	hPS cell medium
78	Knockout-DMEM
18.6	Serum replacement
1	Non-essential amino acids
1	L-glutamine
1	Penicilin-Streptomycin
0.4	2-Mercaptoethanol
	FGF2 (4 ng/ml)

%	Embryoid body (EB) medium
78	Knockout-DMEM
19	Serum replacement
1	Non-essential amino acids
1	L-glutamine
1	Penicillin Streptomycin

%	Neural stem cell freezing medium
70	Serum replacement
20	Cytocoon™ Buffer II
10	DMSO

%	FCS-based freezing medium
90	FCS, heat inactivated
10	DMSO

2.10 Cell culture solutions

%	1xTrypsin/EDTA (TE)
90	PBS
10	Trypsin-EDTA (10x)

%	Trypsin inhibitor (TI)
100	PBS
	Trypsin inhibitor (0.25 mg/ml ≡ 700 units/mg)
mixed, sterile-filtered and stored at 4°C	

%	Poly-L-ornithine (PO)
99	H_2O
1	Poly-L-ornithine (1.5 mg/ml stock)
mixed, sterile-filtered and stored at 4°C	

%	Laminin (Ln) coating solution
100	H_2O
	Laminin (1 μg/ml)

%	0.1% Gelatine
99.9	H_2O
0.1	Gelatine
mixed, autoclaved and stored at 4°C	

%	Matrigel (MG) coating solution
97	H_2O
3	Matrigel (MG) in DMEM:F12 (1:1)

	2x HBS buffer
8 g	NaCl
0.38 g	KCl
0.1 g	Na_2HPO_4
5 g	Hepes
1 g	Glucose
H_2O was added to 500 ml, the pH was adjusted to 7.05, the mixture was sterile-filtered and stored at -20°C	

2.11 Cell culture stock solutions

Reagent	Concentration	Solvent
B27	Used directly from Invitrogen	
EGF	10 µg/ml	0.1 M Acetic acid + 0.1% BSA
FGF2	10 µg/ml	PBS + 0.1% BSA
G418	50 mg/ml	H_2O
Hyg B	100 mg/ml	H_2O
Insulin	5 mg/ml	10 mM NaOH
Laminin	Used directly from Sigma	

2.12 Molecular biology reagents

50x	Tris-acetate-EDTA-buffer (TAE)
242 g	Tris
100 ml	0.5 M EDTA (pH 8)
57.1 ml	Water-free acetic acid
Total volume of 1 l was adjusted with H_2O For use 50x TAE was diluted with H_2O 1:50	

6x	DNA loading buffer
2 ml	0.5 M EDTA (pH 8)
6 g	Sucrose
0,2 ml	2% Bromphenol-blue-solution
0,2 ml	2% Xylene-cyanol-solution
0,2 g	Ficoll
3,8 ml	Aqua bidest.
The solution was mixed well, prepared in 1 ml aliquots and stored at 4°C	

	PFA fixation solution (4%)
40 g	PFA
1000 ml	H_2O
The solution was heated until PFA dissolved completely, pH adjusted to 7.4 and sterile filtered.	

%	Immuno-blocking solution
89.9	PBS
10	FCS
0.1	Triton X100 (only for intracellular epitopes)

	Moviol / DABCO
12 ml	Tris solution (0.2 M; pH 8.5)
6 ml	H_2O
6 g	Glycerol
2.6 g	Moviol
0.1 g	DABCO

	SDS-PAGE resolving gel buffer
99.6%	1.5 M Tris solution (pH 8.8)
0.4%	SDS

	SDS-PAGE stacking gel buffer
99.6%	1.5 M Tris solution (pH 6.8)
0.4%	SDS

	SDS-PAGE running buffer
3 g	Tris
14.4 g	Glycin
1 g	SDS
add	H_2O to 1000 ml (pH 8.8)

	Western blotting buffer
3 g	Tris
14.4 g	Glycin
add	H_2O to 800 ml (pH 8.8)
Add 200 ml Methanol prior to use.	

10x	TBST
121 g	Tris
87 g	NaCl
10 ml	Tween-20
add	H_2O to 1000 ml

%	Protein loading buffer
75.75	Tris solution (0.1 M; pH 6.8)
20	Glycerol
4	SDS
0.25	Bromphenol blue

	Southern denaturing buffer
20 g	NaOH
87.66 g	NaCl
add	H_2O to 1000 ml
Adjust pH to 7.0	

	Southern neutralizing buffer
60.56 g	Tris-HCl
87.66 g	NaCl
add	H_2O to 800 ml
Adjust pH to 7.0 with concentrated HCl, then add H_2O to 1000 ml.	

20x	SSC Transfer Buffer
175.5 g	NaCl
88.2 g	Na citrate
add	H_2O to 800 ml
Adjust pH to 7.0 with concentrated HCl, then add H_2O to 1000 ml.	

	Southern washing buffer
11.6 g	Maleic acid
8.77 g	NaCl
300 μl	Tween-20
add	H_2O to 1000 ml
Adjust pH to 7.5 with solid NaOH.	

	Maleic acid buffer
11.6 g	Maleic acid
8.77 g	NaCl
add	H_2O to 1000 ml
Adjust pH to 7.5 with solid NaOH.	

	Southern detection buffer
15.76 g	Tris-HCl
5.84 g	NaCl
add	H_2O to 1000 ml
Adjust pH to 9.5 with solid NaOH.	

	TE-buffer
1.58 g	Tris-HCl
0.29 g	EDTA
add	H_2O to 1000 ml
Adjust pH to 8 with solid NaOH.	

2.13 Software

Name	Application	Producer
ApE – A plasmid Editor v2.0.7	Cloning strategies	M. Wayne Davis
AxioVision 4.5	Fluorescence microscopy	Carl Zeiss MicroImaging
Chromas v2.31	DNA sequence analysis	Technelysium
ClustalW v1.83	Sequence alignment	EMBL-EBI (Thompson et al., 1994)
Illumina BeadStudio	SNP analysis	Illumina
Microsoft Office 2008	Figures and text processing	Microsoft
Primer3 v0.4.0	Primer picking	Rozen and Skaletsky (2000)
Quantity One	Electrophoresis gel documentation	Bio-Rad
RepeatMasker	Gene locus analysis	Arian Smit, Gustavo Glusman, Robert Hubley
USCS Genome Browser	Genome database and in silico PCR	Human genome consortium

2.14 Kits

Name	Producer	Office
DIG High Prime DNA Labeling and Detection Starter Kit II	Roche Applied Science	Basel, Switzerland
DNeasy Blood Tissue Kit	Qiagen	Hilden, Germany
iScript cDNA Synthesis Kit	Bio-Rad	München, Germany
MEGAscript T7 Kit	Ambion	Austin, USA
PCR DIG Probe Synthesis Kit	Roche Aplied Science	Basel, Switzerland
peqGOLD CyclePure Kit	Peqlab Biotechnologie	Erlangen, Germany
peqGOLD Gel Extraction Kit	Peqlab Biotechnologie	Erlangen, Germany
peqGOLD Plasmid Miniprep Kit I	Peqlab Biotechnologie	Erlangen, Germany

Name	Producer	Office
PureYield Plasmid Maxiprep System	Promega	Mannheim, Germany
QuikChange Lightning Site-Directed Mutagenesis Kit	Stratagene	Waldbronn, Germany
RNeasy Kit	Qiagen	Hilden, Germany
ScriptCap m7G Capping System	CellScript	Madison, USA

2.15 Primer

Name		Primer sequence (5'-3')
P1	upstream HA fw	GGGTTCCTGC^GGCCGCCGTTTCTGCTTTTTAAAGCTCATGT NotI
P2	upstream HA rv	TATGGATCCA^CTAGTTATGTAAATACAAACACAGAAAACCAA SpeI
P3	downstream HA fw	ACCACTGTGCA^TATGGGTTATTTTGTGATGAAAATACCTACC NdeI
P4	downstream HA rv	GGGTTCCTGC^GGCCGCCTACTACTAATTGGCCAAAGTTTAA GA NotI
P5	Sca3 fw	AGCACTTCCATATTTTAAAGTAATCTG
P6	Sca3 rv	TGCTCCTTAATCCAGGGAAA
P7	ADK fw	TTGCAGATGATTTTGCACCT
P8	ADK rv	GACCCCTTTGGGGTATCTGT
P9	Neo fw	GCTTGGGTGGAGAGGCTATT
P10	Neo rv	GCGATACCGTAAAGCACGAG
P11	QuikChange fw	GCAGCAGGGGGACCTGTCAGGACAGAGTT
P12	QuikChange rv	AACTCTGTCCTGACAGGTCCCCCTGCTGC

In case of cloning primers, restriction sites in the overhanging ends are indicated in red, while the genome binding sequence is indicated by yellow background.

2.16 Antibodies

Primary antibody	Dilution	Source
Actin	1:2000	Sigma Aldrich, Deisenhofen, Germany
ADK	1:500	Abcam, Cambridge, United Kingdom
Ataxin-3	1:100	ProteinTech, Chicago, USA
DACH1	1:50	ProteinTech, Chicago, USA
EGFP (rb)	1:3000	Abcam, Cambridge, United Kingdom
GABA	1:500	Sigma Aldrich, Deisenhofen, Germany
GFAP	1:1000	DAKO, Glostrup, Danemark
Map2ab	1:500	Chemicon, Temecula, USA
Nestin	1:500	R&D Systems, Minneapolis, USA
NeuN	1:100	Millipore, Billerica, USA
Neurofilament (HO14)	1:100	gift from Virginia Lee, Philadelphia, USA

Secondary antibody	Dilution	Source
Cy3 gt-anti-ms	1:1000	Jackson , West Grove, USA
Cy3-gt-anti-rb	1:1000	Jackson , West Grove, USA
Cy3-dk-anti-gt	1:1000	Jackson , West Grove, USA
Cy3-gt-anti-rat	1:1000	Jackson , West Grove, USA
FITC-gt-anti-ms	1:1000	Jackson , West Grove, USA
FITC-gt-anti-rb	1:1000	Jackson , West Grove, USA
HRP-gt-anti-ms	1:10000	Thermo Scientific, Waltham, USA
HRP-gt-anti-rb	1:10000	Thermo Scientific, Waltham, USA

ms = mouse; rb = rabbit; gt = goadt; dk = donkey

3 Methods

3.1 In vitro differentiation of hPS cells into lt-NES cells

All cell culture experiments were performed in a sterile laminar flow hood using sterile media, glass and plastic instruments. Cells were cultivated in an incubator at 37°C, 5% CO_2 and saturated air humidity. *In vitro* differentiation of hPS cells (hES and iPS cells) into long term proliferating pluripotent stem cell-derived neuroepithelial stem (lt-NES) cells was performed as described previously (Koch et al., 2009).

HPS cells were cultivated on a layer of irradiated mouse fibroblasts and grown in hPS cell medium. Medium was changed daily and passaging was performed using collagenase IV (1 mg/ml). To induce differentiation, embryoid bodies (EBs) were generated by cultivating hPS cell colonies in EB medium as floating aggregates. After four days, EBs were transferred to poly-l-ornithine (PO) coated tissue culture dishes and propagated in N2 (Invitrogen) medium containing FGF2 (10 ng/ml; R&D Systems). Neural tube-like structures developed within 10 days in the EB outgrowth and were mechanically isolated and propagated as free-floating neurospheres in N2 medium containing FGF2 (10 ng/ml). After three days, neurospheres were incubated with trypsin/EDTA (TE; Invitrogen) and trypsin inhibitor (TI; Invitrogen), mechanically triturated into single cells and plated on poly-l-ornithine/laminin (PO/Ln; both Sigma Aldrich) coated plastic dishes. Obtained lt-NES cell lines were cultivated in N2 medium containing FGF2, EGF (both 10 ng/ml; R&D Systems) and 1 µl/ml B27 supplement (Invitrogen) on PO/Ln cell culture dishes and passaged using TE/TI. Seeding densities were 5 - 8 $x10^5$ cells/cm^2. Lt-NES cell lines can be passaged up to >100 passages and were monitored daily regarding proliferation ability and morphological integrity. For storage, trypsinized lt-NES cells were resuspended in neural stem cell freezing medium and directly transferred to –80°C or liquid nitrogen storage tanks.

For the generation of an adenosine kinase knock out cell line, lt-NES cells derived from the parental human embryonic stem cell line I_3 were used, while gene correction of the *ATXN3* gene locus was performed in MJD-lt-NES cells gained from patient-derived induced pluripotent stem (iPS) cells.

3.2 Differentiation of lt-NES cells into neuronal and astrocytic cultures

Lt-NES cells represent a standardized multipotent stem cell population that constantly retains its capability to generate defined cultures of neurons and glial cells over long-term culture. To initiate terminal differentiation, lt-NES cells were transferred to matrigel (MG)-coated cell

culture dishes. Upon reaching confluence, culture medium was changed to NGMC medium, which was exchanged every second day. To generate astrocytes-enriched cultures, 10% FCS was added to culture media, while neuronal enrichment was achieved by adding 10 μM DAPT (Sigma) for the first 5 days of differentiation.

3.3 Immunocytochemical analysis

Cells were fixed in 4% PFA for 5 min at room temperature, washed twice with PBS and blocked with 10% FCS and 0.1% Triton-X-100 in PBS for 30 min at room temperature. The respective primary antibodies (listed) were applied overnight at 4°C in blocking solution. Cells were washed twice with PBS before secondary antibodies (listed) were applied for 2 h at room temperature. Cell nuclei were counterstained with DAPI and finally cells were rinsed with PBS, mounted with Moviol and covered with a glass coverslip.

3.4 SNP analysis and sequencing

Genomic DNA was prepared using the DNeasy Blood & Tissue Kit (Qiagen). Whole genome single nucleotide polymorphism (SNP) genotyping was performed at the Institute of Human Genetics at the University of Bonn. Genomic DNA at a concentration of 50 ng/µl was used for whole genome amplification. Afterwards, the amplified DNA was fragmented and hybridized to sequence-specific oligomers bound to beads on an Illumina Human 660W Quad chip. Data was analyzed using Illumina BeadStudio.

3.5 Western immunoblotting

Cells were scraped from the dishes and incubated in RIPA buffer (1 hr; 4°C; Sigma Aldrich) containing protease inhibitors (Roche cOmplete ULTRA). Lysates were clarified by centrifugation (16000 rcf; 15 min; 4°C) and run on a SDS-PAGE using standard gels. Briefly, 10% SDS-PAGE gels contained resolving and stacking gels and were cast using 30% Acrylamid/Bisacrylamid (37.5:1; Carl Roth), TEMED, 10% APS, and the respective gel buffers. Protein lysates were loaded on SDS-PAGE gels and run in MINI-Protean chambers (Biorad). Seperated proteins were blotted on MeOH-activated PVDF membranes, blocked with 10% Roti-Block (Carl Roth) in TBST for 20 min and incubated with an appropriate primary antibody (listed) over-night at 4°C. Washed membranes were incubated with an HRP-linked secondary antibody (1 h) and visualized by chemoluminescence (Thermo Scientific SuperSignal West Chemiluminescent Substrates).

3.6 Design of AAV virus for the targeting of *ATXN3* gene in human lt-NES cells

The general composition of an AAV targeting vector is illustrated in Fig. 3.1. Two homology arms (HAs) flanking the selection cassette are necessary for site-specific targeting and were amplified from genomic DNA of the same cell line that was later targeted. For primer design and in-silico genome analysis, the Ensembl databases (http://www.ensembl.org) and Primer3 (http://frodo.wi.mit.edu/) were used. For selection, a promoterless cassette bearing neomycin resistance was chosen and cloned into the commercially pAAV-MCS vector (Stratagene).

3.6.1 Generation of homology arms

The *ATXN3* gene consists of 12 exons, of which exon 10 contains the polyglutamine encoding CAG repeat motif. Based on an *in silico* analysis with RepeatMasker, exon 10 and the surrounding intronic sequences did not contain any repetitive motifs beside the CAG repeat and thus was found to be suitable for our targeting strategy. The AAV vector system allows the incorporation of around 2 kb for HA usage, which should be evenly distributed between the two HAs lying upstream and downstream of the selection cassette. With a size of 405 bp, Exon 10 of the *ATXN3* gene is small enough for the complete incorporation into the downstream HA. Primers were picked using the Primer3 algorithm (Rozen and Skaletsky, 2000) on the intronic sequences surrounding the exon, generating a downstream HA of 1165 bp length (Fig. 3.1). The upstream HA was chosen to contain only intronic sequences found between exons 9 and 10 with a length of 814 bp.

For the amplification of the two homology arms, genomic DNA was isolated from MJD-lt-NES cells using the Qiagen DNeasy Blood and Tissue DNA isolation kit according to the manufacturer's instructions. The homology arms were amplified from genomic DNA by PCR using primers with overhanging ends containing restriction sites for NotI, SpeI or NdeI (Tab. 2.14). Primer sequences encompassed 26-27 nucleotides of target binding, the restriction enzyme recognition site and additional nucleotides homologous to the selection cassettes resulting in an overall-length of 41-43 nucleotides.

2 μM of each forward and reverse primers, 0.025 U/μl Taq-Polymerase, 2 mM of Mg^{2+} and 0.2 mM dNTPS were added to 1 μg of DNA in a total volume of 50 μl PCR buffer. The cycling conditions were the following: 1 cycle of 94°C for 5 min; 20 cycles of 94°C for 30 s, 53°C for 30 s and 72°C for 90 s; 1 cycle of 72°C for 10 min. The primers were removed using the peqLab PCR cycle pure kit. The extracted DNA was digested with NotI (20 units) and SpeI (10 units) in 20 μl NEB buffer 2 or with NotI (10 units) and NdeI (15 units) in 20 μl NEB buffer 3 for 90 min at 37°C. Electrophoresis on a 0.8% agarose gel yielded strong bands of correct

sizes, in case of the downstream HA products of both alleles were gained, of which the shorter variant was excised and gel-extracted using the peqLab gel extraction kit.

3.6.2 Cloning of targeting vector

The contents of the targeting vector are depicted in Fig. 3.1. Besides a classical backbone with Amp resistance for bacterial amplification it contains the targeting cassette flanked on both sides by the ITRs that give rise to the hairpin shaped termini of the viral genome. Between the ITRs the homology arms are situated and in between them, lays the selection cassette containing a synthetic exon promoter trap (SEPT) (Topaloglu et al., 2005) that allows neomycin resistance only if integrated into an actively transcribed gene locus, thus massively increasing the amount of positive resistant clones. The ITRs and the backbone are derived from the pAAV-MCS vector, which is part of the commercial helper-free AAV-system from Stratagene.

The creation of the targeting vector is a multi-step-process: first the upstream HA was ligated into a pWpXL-backbone containing the SEPT cassette, then this larger fragment was excised and, together with the downstream HA, ligated into the pAAV-MCS backbone. The excision and ligation process is shown in Fig. 3.1.

The pWpXL vector contained the whole SEPT cassette directly downstream of its multiple cloning site, bearing restriction sites for NotI and SpeI. To open the plasmid and insert the upstream HA in front of the SEPT cassette, both were digested with NotI (20 units) and SpeI (10 units) in 20 µl NEB buffer 2 for 90 min at 37°C, and purified from a 0.8 % agarose gel using the peqLab gel extraction kit according to the manufacturer's instructions. The linearized backbone (50 ng) was then combined with the digested homology arm (150 ng) so that the insert was in 20 fold molar excess of backbone. Ligation was performed using T4 ligase (400 units) in 20 µl NEB T4 ligation buffer for 30 min at 22°C. The ligated vector was transformed into competent E. coli cells. 100 µl of frozen competent bacteria were thawed on ice, all 20 µl of the DNA solution were added, and the reaction tube chilled on ice for 30 min. Then, heat shock was performed for 90 sec at 42°C and the sample again chilled for 5 min. To allow the cells to gain antibiotic resistance, 500 µl SOB medium was added and the tube shaken in an incubator at 37°C for 90 min. Cells were then plated on LB agar plates containing 100 mg/l ampicillin and incubated over night (o/n) at 37°C.

The next morning, plates were put into the fridge to pick colonies in the evening. Each colony was grown o/n at 37°C on a shaker in 3 ml LB medium containing ampicillin. The DNA was isolated using the peqLab DNA mini prep kit according to the manufacturer's instructions. 1 µl of the preparations were further analyzed by electrophoresis on a 1 % agarose gel after

digestion with NotI (10 units) and NdeI (15 units) in 20 µl NEB buffer 3 for 90 min at 37°C. Clones showing two bands (backbone and fusion of upper HA with selection cassette) of the correct sizes were considered positive. One of these clones was selected and grown o/n in shaking incubator at 37°C in 200 ml LB medium containing 100 mg/l ampicillin. DNA purification was performed using the Promega PureYield Plasmid Maxiprep System kit according to the manufacturer's instructions.

The next ligation step combined to downstream HA with adjacent SEPT cassette with the PCR-amplified upstream HA into the pAAV-MCS backbone to gain the functional targeting vector. The pAAV-MCS plasmid was digested with 10 units of NotI in 20 µl of NEB buffer 3 for 90 min. at 37°C and the larger fragment (2887 bp) was purified from a 0.8 % agarose gel using the PeqLab gel extraction kit. To prevent unwanted circularization, the linearized fragment was dephosphorylated using 10 units of alkaline phosphatase in 10 µl of dephosphorylation buffer. After an incubation of 30 min. at 37°C the alkaline phosphatase was inactivated for 15 min. at 65°C. The downstream HA–PCR product and the fusion-construct of upstream HA with selection cassette was digested with NotI and NdeI as described above. Ligation was performed with 50 ng of pAAV-MCS-backbone, 350 ng of downstream HA and 50 ng of upper-HA-selection cassette-fusion-construct in 20 µl NEB T4 ligation buffer with 400 units of T4 ligase for 30 min at 22°C. This time, the HA was used in 200 fold excess of the other segments to ensure efficient incorporation. Transformation of competent cells and clone picking were performed as described above. Positive clones were chosen on the results of digestions with either NotI or SpeI or the combination of both (each 10 units in 20 µl NEB buffer 3) following agarose gel electrophoresis. Again, PCR was conducted to verify integration of the homology arms.

3.6.3 Mutation of targeting vector

To easily discriminate between the original wild type allele and the gene-corrected allele, a 1-bp-mutation was inserted in the targeting vector. This mutation is a silent one, which would not affect the translated protein. For modification of the plasmid, the QuikChange Lightning Site-Directed Mutagenesis Kit (Stratagene) was used following the manufacturers' instructions. The used primers P11 and P12 were designed with Stratagene' webpage tool.

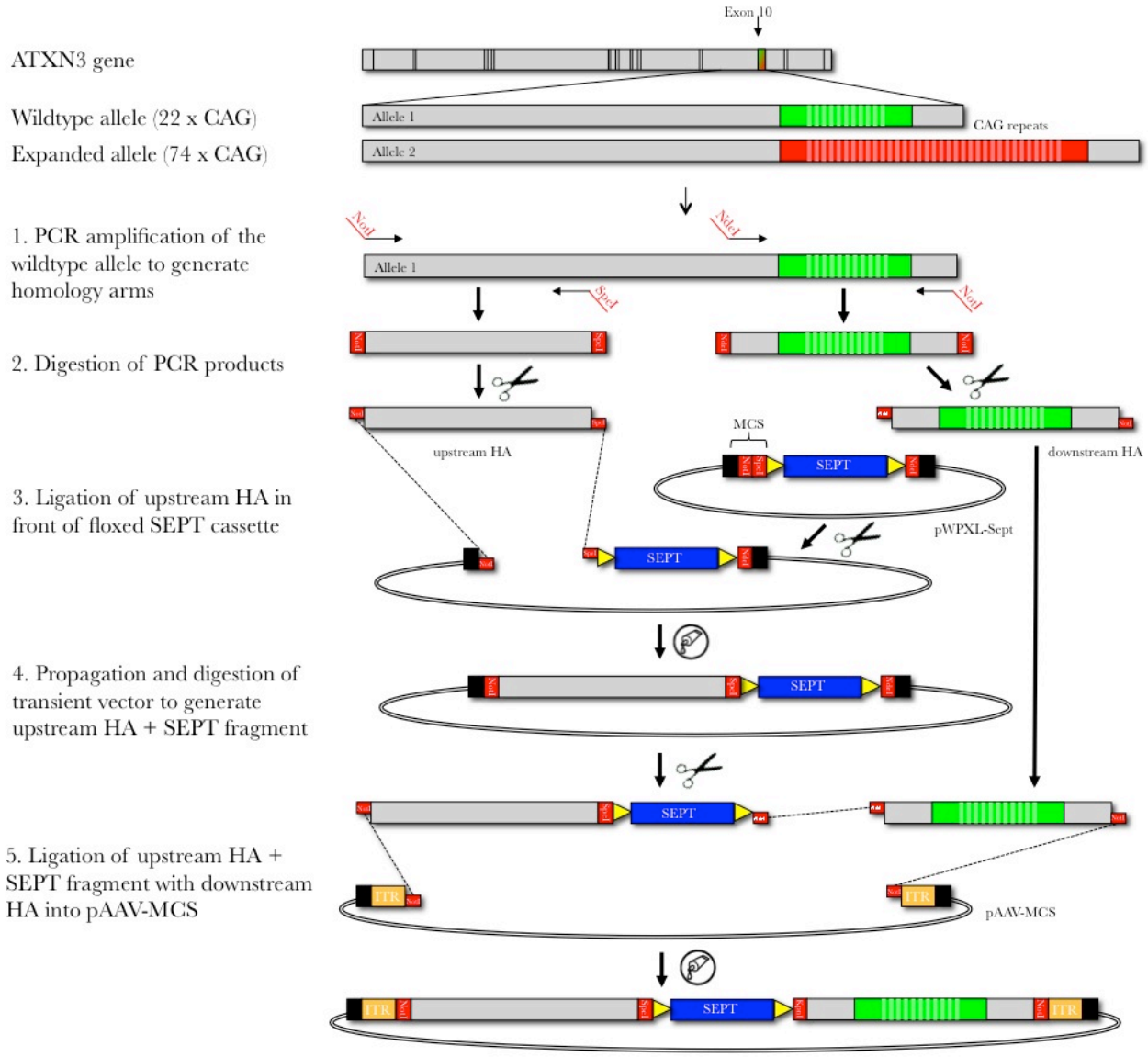

Figure 3.1: Cloning strategy for* ATXN3*-AAV targeting vector for site-specific integration.
Upstream and downstream homology arms (HAs) were PCR-amplified from the shorter allele of exon 10 of the ATXN3 *gene of MJD-patient derived lt-NES cells. Primers used also carried restriction nuclease recognition sequences for cloning purposes. The upstream HA was first ligated directly in front of the SEPT cassette, which was already present in a pWPXL vector, using its multiple cloning site (MCS). The new construct was expanded and used to excise an upstream HA+ SEPT fragment for the next ligation step. Together with the downstream HA; it was ligated in a dephosphorylated pAAV-MCS backbone to gain the complete targeting vector composed of a SEPT cassette flanked by homology arms for site directed integration, nested between inverted tandem repeat (ITR) sequences of the viral backbone.*

3.7 Preparation of competent E. coli and glycerol stocks

Competent cells were prepared and transformed according to the Inoue method for ultra competent cells (Inoue et al., 1990). Of every plasmid-producing clone, glycerol stocks were prepared allowing an easy and quick access to the desired DNA. From the culture flask used for maxi preparation of its plasmid DNA, 800 µl of bacterial solution were thoroughly mixed with 200 µl of glycerol, transferred into a cryovial and frozen at -80°C. The bacterial cells can be stored like this for at least one year. To raise a new culture from the stock, a small amount of frozen cells was scratched with a pipette tip and dripped into fresh LB medium with ampicillin. The stock did not have to be thawed for this purpose.

3.8 Generation of AAV particles

The HEK-293 cell line is of human embryonic kidney origin and has been transformed by the adenoviral E1A gene product. Hence it already brings along one of the needed components to produce adenoviral-associated viruses. The missing parts of the adenoviral genome are brought into the cells by helper plasmids, so that the targeting vector can be used for structural design of the AAV genome. Transient transfection into HEK-293 cells is a common way to produce and harvest both proteins and viral particles. These cells are known to be highly transfectable by the calcium phosphate method and are used to produce large amounts of AAV particles after triple transfection of the three viral plasmids.

AAV-293 cells (Stratagene) that are further optimized for AAV particle generation were used. Cells were propagated as monolayer culture until confluency reached 80% and then passaged with TE.

3.8.1 Triple transfection using the calcium phosphate method

To initiate viral particle production, AAV-293 cells were transfected with the three plasmids pAAV-RC, pHelper (both from Stratagene) and the targeting vector.

AAV-293 cells were grown on 15 cm gelatine coated dishes until a confluence of 90% was reached. 30 min prior to transfection, medium was changed to fresh MEF containing 25 µM chloroquine which helps stabilizing DNA for better uptake. The targeting vector (15 µg) was mixed with pAAV-RC and pHelper plasmids (10 µg each) in 700 µl of water. This solution was well mixed with 89 µl of 2.5 M $CaCl_2$. In a 15 ml Falcon tube, 700 µl of 2xHBS were prepared. A 2 ml plastic pipette was put into this falcon while the DNA-solution was taken with a 1 ml micropipette to be dropped carefully onto the outside of the plastic pipette while a pipette boy was used to blow air into the 2xHBS. The DNA-solution now floated into the

2xHBS and was thoroughly mixed by ascending bubbles. This transfection reagent was incubated for 30 min. at room temperature and then added dropwise to the cell dish. After 6 h, the medium was replaced.

3.8.2 Harvesting and freezing of AAV particles

48 h after transfection, cells were detached from the dish with a cell scraper, pelleted and washed with PBS. The cells of one 15 cm dish were resuspended in 1 ml of PBS and subjected to five cycles of freezing and thawing and finally centrifuged for 3 min at 12 000 g to remove cell debris. The supernatant was frozen at -80°C and could be directly used for treatment of target cells.

3.9 Gene targeting of MJD-lt-NES cells

Compared to lentiviral vectors, the transduction efficiency of AAV particles is relatively low. As the aim was to generate monoclonal cell lines, this low efficiency was an advantage that allowed single clones to grow at distances, which prevented any unwanted mixing.

3.9.1 Transduction of AAV particles

For viral transduction, MJD-lt-NES cells were seeded on 12-well-plates and infected with 50 µl of viral stock-solution per well. After 24 h at 37 °C, the media was aspirated from the cells and substituted by fresh medium. After three days of propagation, cells were split onto 6 well-plates and from the following day on taken under antibiotic selection with G418 (100 µg/ml.) Within one week of selection, all non-targeted cells were dying.

As resistant colonies emerged, selection was removed to not further stress the cells and to let the existing colonies grow. As soon as colonies began to form spherical bulges, they were picked with a 10 µl micropipette by scratching and soaking, and then plated onto 48 well-plates. The clones were again taken under selection and expanded. Whenever enough cells were available to form a monolayer on a 12-well, they were dissociated with trypsin and separated. As soon as enough cells of a clone were present to secure the propagation, genomic DNA was isolated for screening purposes.

3.9.2 Screening for targeting events

Exchange of the expanded allele against its wildtype variant should be easily detected in a PCR screen for exon 10 of *ATXN3*. Therefore, genomic DNA was extracted using the

DNeasy Blood & Tissue Kit (Qiagen). PCR amplification of Exon 10 of the *ATXN3* gene was performed using Phusion Polymerase (Finnzymes) with primers P4 and P5 (Table 2.4). PCR included a preincubation at 98 °C for 30 s followed by 35 cycles of denaturation at 98°C for 10 s, annealing at 60°C for 30 s and extension at 72°C for 60 s with a final extension step at 72°C for 10 min. Fragments were extracted from the gel and subsequently sequenced. Sequencing was performed by Seqlab Laboratories. Positive clones and controls were further expanded and used for analysis of ataxin-3 by SDS-PAGE and Western Blotting.

3.9.3 Cre-mediated excision of selection cassette

After the selection process, the SEPT cassette had to be removed to again derive a functional expression of ataxin-3 protein from the targeted allele. The incorporated loxP sequences at both ends of the cassette allowed its excision with Cre protein. To transiently express Cre in the targeted MJD-lt-NES cells, transfection of mRNA coding for Cre protein was chosen.

RNA was synthesized with the MEGAscript T7 kit (Ambion), with 0.5 µg of Cre sequence containing plasmid to template a 40 µL reaction. The T7 capping system ScriptCap (Ambion) with a ribonucleoside mix of adenosine triphosphate (2 mM), guanosine triphosphate (2 mM), cytidine triphosphate (1.5 mM), uridine triphosphate (1.5 mM), 5-methylcytidine triphosphate (375 μM) and pseudouridine triphosphate (375 μM, all from Ambion) was used. Reactions were incubated 4 hr at 37°C and DNAse treated. RNA was purified with Quick Spin RNA columns (Roche), followed by treatment with antarctic phosphatase (New England Biolabs) for 20 min at 37°C to remove residual 5′-triphosphates. The resulting modified RNA was repurified, quantitated by Nanodrop (Thermo Scientific), and adjusted to 100 ng/µL working concentration by addition of H_2O.

RNA transfections were performed with RNAiMAX (Invitrogen) cationic lipid delivery vehicles. RNA and reagent were first diluted in Opti-MEM basal media (Invitrogen). 100 ng/µL RNA was diluted 5× and 5 µL of RNAiMAX per microgram of RNA was diluted 10×, then these components were pooled and incubated 15 min at room temperature (RT) before being added dropwise to culture media. RNA transfections were performed in Opti-MEM plus 2% FBS. After 6 hrs, media was replaced by fresh N2. After 2 days, another RNA transfection was applied and the cells analyzed for successful excision of selection cassette via PCR and western blot analysis.

3.10 Southern blot analysis

10 µg of genomic DNA isolated with DNeasy Blood & Tissue Kit (Qiagen) was digested with 3 units of PstI restriction enzyme per µg DNA at 37°C over night in a total volume of 400 µl. Digested DNA was loaded onto 0.8% agarose gel and electrophoresed at 40 volts, 35 mA for 8 hours.

Blotting on Nytran SuPerCharge® Nylon membranes (Whatman) was performed using a TurboBlotter system (Whatman). Agarose gel was denatured for 30 min at room temperature in denaturing buffer, afterwards rinsed in distilled water and transferred to neutralizing buffer. After 30 min of slow shaking, gel was soaked in 20x SSC transfer buffer for 30 min. Nylon membrane was wetted in distilled water and then soaked in 20x SSC transfer buffer for 5 min. TurboBlotter was put together following manufacturer's instructions. The nylon membrane was placed on the blotting paper stack followed by the agerose gel and additional sheets of blotting paper. Transfer was carried out overnight with 20x SSC transfer buffer. Following transfer, the transfer membrane was washed in 2x SSC for 5 min and dried with blotting paper. Immobilization of DNA onto the membrane was done by baking the membrane for 2 hrs at 80°C.

For the generation of southern probes, PCR DIG Probe Synthesis Kit (Roche) was used according to the manufacturer's instructions with a PCR template cycled from the neomycin resistance gene within the SEPT cassette with primers P9 and P10. Hybridization and detection of southern blots was carried out with the DIG High Prime DNA Labeling and Detection Starter Kit II (Roche). Southern blot membranes were hybridized with 30 ng/ml of denatured DIG-labeled DNA probe in 10 ml of DIG Easy Hub solution, sealed in plastic foil, over night at 40°C. The next day, membranes were washed twice for 5 min in ample 2 x SSC, 0.1% SDS at room temperature followed by two washing steps in 0.5 x SSC, 0.1% SDS at 68°C. Immunological detection was performed according to guidelines from the DIG High Prime Kit in a Chemidoc imaging system (Bio-Rad).

3.11 Transcript analysis of gene corrected MJD-lt-NES cells

To verify the functional transcription from both alleles, wildtype and gene-corrected, *ATXN3* mRNAs were sequenced and checked for the integrated 1-bp-mutation. Total RNA from cells was purified (Quiagen RNeasy kit) and reversely transcribed into cDNAs (Biorad iScript cDNA synthesis kit). PCR was performed using standard protocols (Invitrogen Taq DNA Polymerase) with primers P5 and P6.

3.12 Glutamate treatment and microaggregate formation analysis

Stimulation experiments were conducted in neuronal cultures 6-8 weeks after growth factor withdrawal. MJD-neurons or Ctrl-neurons cultured in 3,5 cm dishes were washed 3 times with 2 ml BSS (balanced salt solution) containing 25 mM Tris, 120 mM NaCl, 15 mM glucose, 5.4 mM KCl, 1.8 mM CaCl2, 0.8 mM MgCl2, pH 7.4. After treatment with 100 μM L-glutamate (Sigma G8415) in BSS for 30 min cells were washed again 3 times and either immediately frozen in liquid N2 followed by lysis in RIPA-buffer (50 mM Tris, 150 mM NaCl, 0.2 % Triton X100) containing 25 mM EDTA or left to recover for 30 min in differentiation media followed by a second 30 min L-glutamate treatment in BSS, and subsequently cultured in differentiation media until analyzed 24 h later.

For analysis of fragmentation and aggregation of ataxin-3 by SDS-PAGE and Western Blotting, extracts were analyzed either immediately after lysis or after fractionation. For fractionation, lysates were centrifuged at 22,000 x g for 20 min at 4°C. The pellet fractions were separated from supernatants (Triton-X 100-soluble fraction) and homogenized in RIPA buffer containing 2% SDS followed by a second centrifugation step. The supernatants (SDS-soluble fraction) were removed, and the remaining pellets were incubated for 16 h in 100 % formic acid at 37°C (Haacke et al., 2007; Hazeki et al., 2000). After evaporation in a Speed Vac concentrator (Thermo Scientific), the pellet was dissolved in Laemmli-buffer (SDS-insoluble fraction) followed by pH-adjustment with 2 M Tris-base for SDS-PAGE analysis.

3.13 Transfection of Zinc-Finger-Nucleases and clone selection

For the delivery of Zinc finger nucleases (ZFN) into cell nuclei, coding plasmids for its transient expression were nucleofected into lt-NES cells. Three different plasmids bearing ZFNs developed by Sangamo were used, ZFN18339 coding for downstream binding, ZFN18337 and ZFN18781 coding for upstream binding of target sequence. Pairs of either -39 and -37 or -39 and -81 were used to target the adenosine kinase while the combination of -37 and -81 served as control.

For nucleofection, the Nucleofector system (Lonza) was used with Solution V and program B23. Each reaction used 1 μg of each ZFN plasmid, making a total of 2 μg of DNA. 1 x 10^6 lt-NES cells were pelleted and resuspended in 100 μl of supplemented Nucleofector Solution V and immediately mixed with the DNA into a nucleofection cuvette. The suspension was nucleofected with program B23 and directly plated into one well of a sixwell plate already covered with N2F media. After 6 hrs, media was exchanged.

Being an enzyme, the disruption of adenosine kinase could be selected for with two chemical compounds that are metabolized by ADK into toxic species. Two passages after nucleofection, chemoselection of cells started with 10 μM 8-Cl-cAMP (8-Chloroadenosine

3',5'-cyclic monophosphate; Enzo) and 10 μM 8-Cl-Ado (8-Chloroadenosine; Enzo). After 20 days of selection, resistant colonies emerged which where further expanded and analyzed via sequencing of the ZFN recognition site with primers P7 and P8.

3.14 Measurements of adenosine levels in cell culture supernatants

To decipher to what extent the disruption of adenosine kinase leads to a higher level of adenosine secretion by cells in culture, adenosine levels were measured using high-pressure liquid chromatography (HPLC). These analyses were performed by the group of Christa E. Müller at the Department of Pharmacy at the University of Bonn.

Normal cell culture media could not be used with the detection method, and therefore a cell buffer with reduced organic compounds was used (140 mM NaCl, 4 mM KCl, 1.8 mM $CaCl_2$, 2.2 mM $MgSO_4$, 0.48 mM NaH_2PO_4, 2 mM Na-Pyruvate, 5.5 mM D(+)-Glucose, 10 mM HEPES, pH 7.4) To prevent adenosine breakdown, addition of 100 μM of the deaminase-inhibitor EHNA (erythro-9-2-hydroxy-3-nonyl-adenine, Sigma) was necessary. Supernatants of lt-NES cells, neuronal- or astrocytic-enriched cultures were collected at distinct time points after switch to cell buffer and lyophilized. The resulting pellets were dissolved in methanol/acidic acid using sonification. After precipitation of inorganic salts by centrifugation for 1 h at 10,000 g, supernatants were directly used for mass spectrometric analysis. Samples were injected into a HPLC Dionex Ultimate 3000 system (Thermo Scientific) coupled to a micrOTOF-Q mass spectrometer (Bruker) with an electrospray ionization source. Chromatographic separation was performed on a hydrophobic ether-bonded phenyl-phase column. It was started with 100% H_2O containing 0.1% acetic acid followed by a gradient to 100% acetonitrile containing 0.1% acetic acid. Positive scan MS was observed from 50-1000 m/z optimized to peak 268.1038. For quantifying the extract ion counts 268.1038 ± 0.01 was used. Calibration curves were determined by dissolution of a broad range of adenosine concentrations in acetonitrile : water (1:1), and the cell buffer used. The limit of detection of the method was below 1 ng/ml for adenosine dissolved in the acetonitrile-water mixture while in cell bufferthe detection limit was about 10-fold higher.

3.15 Mouse experiments

In pilot experiments, mouse strains C57Bl/6 and SCID/beige were used. For all cell transplantation experiments, immunodeficient Rag2 constitutive knock out mice with C57Bl/6 background (Taconic) were used. All animals were treated according to guidelines approved by the European Ethics Committee (decree 86/609/EEC). The animals were kept under

environmentally controlled conditions (12 h normal light/dark cycles, 20–23°C and 50% relative humidity) with food and water ad libitum.

3.15.1 Stereotactic transplantation into the mouse brain

Cell transplantation into the mouse brain was performed by standard procedures of the Institute of Reconstructive Neurobiology. Cells for transplantation were trypsinized and re-suspended in CytoconTMBuffer II containing 0.1% DNAse (200.000 cells/μl). Mice were anesthetized with Fentanyl (0.05 mg/kg BW i.p.), Midazolam (5 mg/kg BW i.p.), Meditomidin (0.5 mg/kg BW i.p.) and heads were shaved and sterilized. Mice were positioned in a stereotactic apparatus and the skull was opened sufficiently to reveal the lambda and bregma points. The injection needle was positioned to target the desired coordinates. Fascia and pericranium were removed with forceps. A burr hole (0.5 – 1.0 mm) was drilled through the skull using a sterile bone drill. The injection needle containing cell suspension was lowered slowly (~1 mm/5 sec) down to the target depth, and the cell suspension was injected slowly (~1 μl/min). Following injection, the needle was slowly withdrawn and bone wax was applied to seal the hole in the skull. Skin was closed with wound clips and mice were transferred to a warming pad for standard post-operative care. Mice were given Naloxon (0,4 mg/kg BW s.c.), Flumazenil (0.5 mg/kg BW s.c.) and Atipamezol (5 mg/kg BW s.c.) to stop anesthesia and Carprofen (50 mg/kg BW s.c.) against pain. Following operation, mice were routinely checked for health and behavior.

3.15.2 Generation of epileptic animals by injection of pilocarpine

For evaluation of this epilepsy model C57/Bl6 mice were chosen. To limit peripheral parasympathetic effects like the excessive dehydration, methylscopalamine (Sigma) was applied (1mg/kg body weight). Mice of 60 days age and body weight over 20 g received a pilocarpine (Sigma) dosage of 340 mg/kg body weight s.c. Pilocarpine was administered stepwise until status epilepticus was reached. Mice were observed for signs of seizures according to the following acute stages of Racine's classification (Racine, 1972): Stage 1: Immobility, eye closure, twitching of vibrissae, facial clonus. Stage 2: Head nodding, chewing, severe facial clonus, wet dog shakes, repetitive movements. Stage 3: Clonus of one forelimb. Stage 4: Rearing, bilateral forelimb clonus. Stage 5: Rearing, bilateral forelimb clonus, loss of balance and falling, status epilepticus (SE). If mice did not show signs of SE within 45 min of pilocarpine injection, a second dosage of 170 mg/kg body weight was applied. After 40 min in SE, diazepam (Roche) 4mg/kg body weight was injected s.c. to stop

the convulsion. Diazepam injection was eventually repeated after 30 min until the convulsions stopped. Each animal was placed on a warming pad and given liquids according to weight loss during the treatment. For the following two days, animals received oral glucose and soaked food.

3.15.3 The kainate model of epilepsy

Kainate injection into the mouse brain was performed by standard procedures of the Institute of Neurology in cooperation with Peter Bedner. For intracortical kainate injections, mice were anesthetized with a mixture of Medetomidine (Novartis) and Ketamine (Pfizer) and placed in a stereotactic frame equipped with a manual microinjection unit. The skull was prepared as detailed in the transplantation section. A 0.7 mm hole was drilled into the skull at coordinates 1.9 mm anterior, 1.5 mm medial und 1.8 mm depth. 70 nl of a 20 mM solution of kainic acid (Sigma) in 0.9% sterile NaCl were stereotactically injected into the cortex just above the right dorsal hippocampus using a microsyringe equipped with a micrometer screw. Each injection was performed over a period of two minutes. After injection, the canula is left for two additional minutes in situ to limit reflux along the canula track. Skull surface electrodes for EEG measurements were implanted directly after kainate injection. Telemetric implants were placed subcutaneously on the right abdominal region with two monopolar leads connected to stainless steel screws of 2 mm length positioned bilaterally 1.5 mm from sagittal suture and 1.9 mm posterior. The leads were covered with dental cement, the sculp incision sutured and anesthesia stopped with Atipamezol (Pfizer). Mice were kept warm under a heating lamp until complete recovery from anesthesia and injected with 4 mg/kg body weight Carprofen i.p. (Pfizer) for 3 days. The telemetry system used consisted of a transmitter implant (TA10EA-F20; DSI), which telemeters EEG data from the mice to the receiver (RPC-1; DSI), further processed to a data exchange matrix. Data was analyzed using Dataquest ART software (DSI).

3.15.4 The kindling model in mice

All kindling experiments were performed by Robrecht Raedt and Lisa Thyrion from the group of Paul Boon at the University Hospital of Ghent, Belgium, with animals previously transplanted in Bonn. Mice were placed in a stereotactic frame. After exposure of the skull, eight small burr holes were drilled for the placement of anchor screws and electrodes. Two epidural electrodes were used for the recording of surface EEG. One was placed on the left side of the skull at the height of the frontal cortex and one on the left side at the height of the

parietal cortex. One epidural electrode was placed at the height of the sutura lambdoidea and was used as reference/ground electrode. A quadripolar registration/stimulation electrode was inserted in the right hippocampus, 2.9 mm posterior to bregma, 3 mm to midline and 3 mm depth from dura. In the remaining four burr holes, anchor screws were placed to fix the electrodes on the skull by dental cement. All electrodes were lead to a connector that could be attached to the EEG cables.

Following surgery, mice were allowed to recover for at least 1 week. The after-discharge threshold (ADT) was determined by application of 1 sec train of 1 msec biphasic rectangular pulses at 60 Hz beginning at 60 µA; additional stimulations increasing by 20 µA were administered at 1 min intervals until an electrographic seizure lasting at least 5 sec was detected on the EEG. Subsequently, experimental animals were stimulated twice each day at a stimulus intensity 100 µA above the ADT, with an interstimulus interval of at least 4 hr until three consecutive seizures of class 4 or greater with limb clonus and/or tonus lasting at least 12 sec were evoked. The behavioral manifestations of seizures were classified according to a modification of Racine's classification (Racine, 1972): 1, facial clonus; 2, head nodding; 3, unilateral forelimb clonus; 4, rearing and bilateral forelimb clonus; 5, rearing and falling (loss of postural control); 6, running and bouncing; and 7, tonic hindlimb extension. Control animals included buffer-injected as well as wildtype cell-transplanted mice.

The duration of all ADs was also measured on the EEG. To check for a retained kindling response, animals were retested one and 2 weeks after the end of the acquisition phase. On these retest days ADT, seizure stage and afterdischarge duration (ADD) were evaluated.

3.15.5 Transcardial perfusion and immunohistochemical analysis

Anesthetized mice were opened along abdomen and thorax. A canula was put into the left ventricle of the heart and the right atrium was opened with a small cut. After rinsing of the blood system with 20 ml of PBS, the animal was perfused with 4% PFA until limbs were fixed. The brain was removed and postfixed at 4°C in 4% PFA overnight and cryoprotected in 30% sucrose solution for 48 h. The tissue was embedded into TissueTek (Weckert Lab.), frozen and cut into coronal sections 30 µm thick using a cryostat (Leica) at –20°C, mounted on slides, air dried, frozen, and stored at –80°C until use.

3.16 Hematoxylin and eosin stain

For histological analysis of brain tissue sections, hematoxylin and eosin (H&E) stain was applied. Sections were first dried after thawing and incubated for 2 min in PBS. After 5 min in

hematoxylin solution (Sigma), sections were washed for 5 min under streaming tap water. Eosin solution (Sigma) was applied for 30 sec, followed by 6 washing steps in 100% ethanol, 3 washing steps in isopropanol and 3 washing steps in xylol. After removal of xylol by careful draining of the glass slide, sections were embedded with Cytoseal (Microm).

3.17 Gene expression analysis

For gene-expression microarrays, mRNA samples of It-NES cells and its derived neurons enriched via DCX-labeling (Ladewig et al., 2008) were isolated using an mRNA extraction kit (Qiagen) according to the manufacturers' instructions. Samples were analyzed in duplicates on the HumanHT-12 v4 Expression BeadChip (Illumina). RNA samples were handled following Illumina's laboratory guidelines. Data processing was performed using GenomeStudio V2010.3 Gene Expression Module (V1.8). Data normalization was performed following previously published protocols (Müller et al., 2008; Müller et al., 2011). Briefly, raw-probe and gene-level data were extracted without background subtraction, selecting those probes with a detection *P* value of <0.01 as computed by GenomeStudio and quantile-normalized the resulting probe-intensity values across the data set (Barnes et al., 2005).

3.18 Statistical analysis

Quantitative data was generated in biological replicates. Means and standard deviations (SD) were computed using Microsoft Excel and GraphPad Prism software. All results presented as bar graphs show mean ± SD. Student's t test was performed to determine whether a significant difference exists between groups (*p <0.05; **p<0.01; ***p <0.001).

4 Results

4.1 Genetic manipulations in human neuroepithelial-like stem cells for the generation of modified neuronal cultures

Long-term self-renewing neuroepithelial-like stem (lt-NES) cells represent a stable intermediate stem cell population between pluripotent stem cells and differentiated neuronal cultures that can be generated from any hES- and iPS cell line, self-renew in a virtually unlimited fashion and stably give rise to mature cultures of postmitotic human neurons (Falk et al., 2012). Human long-term self-renewing neuroepithelial-like neural stem (lt-NES) cells were established from hESC or iPSC lines as previously described (Koch et al., 2009). Homogenous lt-NES cell lines were cultured in the presence of FGF2, EGF and B27. Upon growth factor withdrawal, lt-NES gave rise to a dominant fraction of neurons expressing beta III tubulin, while the prolonged differentiation additionally promoted differentiation into astrocytes characterized by GFAP expression as well as oligodendrocytes expressing O4. Growth capacity as well as the differentiation potential in these cells is stable for more than 100 passages, thus allowing genetic manipulation and propagation at the neural stem cell state.

Due to their ability for clonal growth in culture, lt-NES cells are amenable to convenient and quick genetic manipulation enabling the derivation of poly- as well as monoclonal cell lines. In this thesis, two different approaches of genetic manipulations to generate monoclonal cell lines were used; first the correction of an expanded allele to its wildtype variant by the application of engineered adeno associated virus (AAV), and second, the biallelic destruction of a gene with zinc finger nucleases (ZFN).

4.2 Generation of gene-corrected neural stem cells from MJD patient-derived iPS cells

Our lab recently generated iPSC-derived lt-NES cells from patients suffering from Machado-Joseph-Disease (MJD) and healthy controls (Koch et al., 2011). In MJD, an expansion of CAG repeats in the *ATXN3* gene is translated into an expanded poly-glutamine (PolyQ) tract in its gene product ataxin-3. MJD-lt-NES cells and healthy controls (Ctrl-lt-NES cells) can be kept in culture as a homogenous population and upon growth factor withdrawal give rise to mature neuronal cultures. Importantly, it was found that MJD-neurons form SDS-insoluble microaggregates of ataxin-3 upon excitation with the neurotransmitter L-glutamate. Such microaggregates are discussed to represent an early manifestation of pathological protein

processing that culminates in the formation of nuclear ataxin-3-containing inclusions and neuronal degeneration (Chai et al., 2001; Williams et al., 2009) The following part shows the correction of the expanded disease-associated allele of the ataxin-3-coding gene *ATXN3* in MJD-lt-NES cells using a site-directed AAV system. Following transduction and selection of gene-corrected lt-NES cells, healthy neurons could be generated that represent an isogenic control population for direct comparison.

4.2.1 Successful generation of AAV-vectors for gene correction of elongated ATXN3 gene variants

The *ATXN3* gene consists of 12 exons, of which exon 10 contains a polyglutamine encoding CAG repeat motif commonly 13-36 repeats in length. Elongation of this polyQ stretch in its gene product ataxin-3 is believed to cause Machado-Joseph Disease (MJD).

PCR analysis of exon 10 showed two alleles of about the same size in the control cells whereas the patient-derived cells contained one long allele harboring the mutation (Fig. 4.1a). Sequencing of the PCR products of the patient-derived cells revealed one allele containing 22 CAG repeats while the second allele contains 74 CAG repeats (Fig. 4.1b).

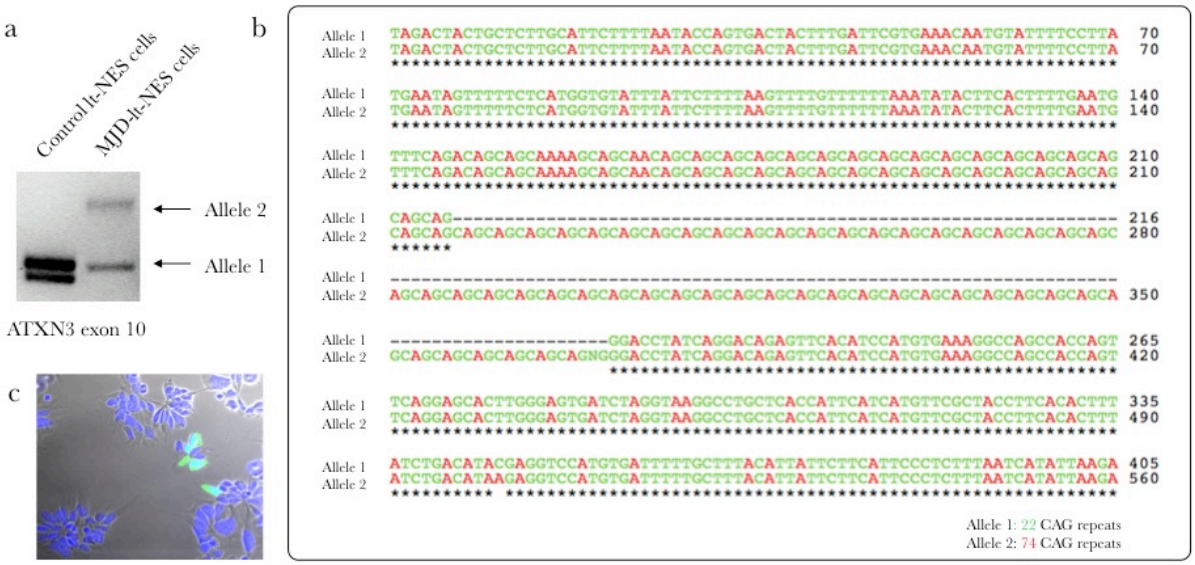

Figure 4.1: MJD-patient-derived lt-NES cells and their suitability for AAV-transduction
a: *PCR amplification of exon 10 of the* ATXN3 *gene shows two different alleles in control and MJD-derived lt-NES cells respectively, representing different CAG repeat numbers. The control cells repeat lengths are both in physiological range while MJD cells show one expanded allele.* ***b:*** *Sequencing of the PCR products reveals 22 CAG repeats for allele 1 and 74 CAG repeats for allele 2 of MJD cells.* ***c:*** *lt-NES cells can be transduced by AAV particles with stable integration into the cells genome as shown by a GFP-expressing control vector.*

Recombinant AAV vectors can be engineered for site-directed integration, using gene-specific homology arms. From previous experiments it was known that AAV particles of subtype 2 are able to transduce lt-NES cells and can integrate permanently into the cell genome (Fig. 4.1c). Furthermore, RT-PCR confirmed that *ATXN3* is actively transcribed already in lt-NES cells, which allows selection with the chosen targeting strategy.

AAVs were generated to specifically target the *ATXN3* locus in order to replace the elongated allele with the unaffected allele from the same patient. The downstream homology arm carried exon 10 in its wildtype variant (Fig. 4.2, green) and adjacent intronic sequences (gray), while the upstream homology arm consisted only of intronic sequences. Both homology arms flank a floxed SEPT-selection cassette. The SEPT cassette consists of a splice acceptor (SA), an internal ribosome entry site (IRES), a neomycin resistance (Neo) gene and a polyA-signal (pA) allowing selection with G148 when the cassette is integrated in an actively transcribed locus. In turn the full-length gene is not expressed anymore from this allele. Consequently, to regain expression of the corrected allele the cassette had to be excised by Cre recombinase.

To facilitate recognition of corrected and original wildtype alleles, the targeting vector was further modified by incorporating an exchange of one adenosine to guanosine within exon 10, downstream of the CAG repeats, using the Quikchange® mutagenesis kit (Stratagene). This modification was a silent mutation that did not change the translated amino acid but enabled discrimination of both alleles on genomic DNA and mRNA level. Sequencing of the modified targeting vector confirmed successful mutagenesis.

4.2.2 AAV vectors targeted the elongated polyQ-allele site-specifically

AAVs were produced in AAV-293 cells and cotransfection with GFPmax allowed optical confirmation of successful calcium phosphate transfection. After transduction of around 750.000 MJD-lt-NES cells with AAV particles and two rounds of selection with G418, 220 ± 40 clones could be gained. Due to the high specificity for its target locus and the use of the promoter-less SEPT cassette, which only allows G418 expression when integrated into an active locus, a large number of positive clones was expected. Screening for targeting events was performed with PCR for exon 10 of *ATXN3* gene, using an amplicon not overlapping with the viral vector to avoid false-positive results. Of the 60 clones analyzed by PCR, 58 showed the loss of the longer, pathogenic allele (Fig. 4.3a shows 3 representative examples). To confirm that this resulted also in a change in protein expression, western blotting was performed.

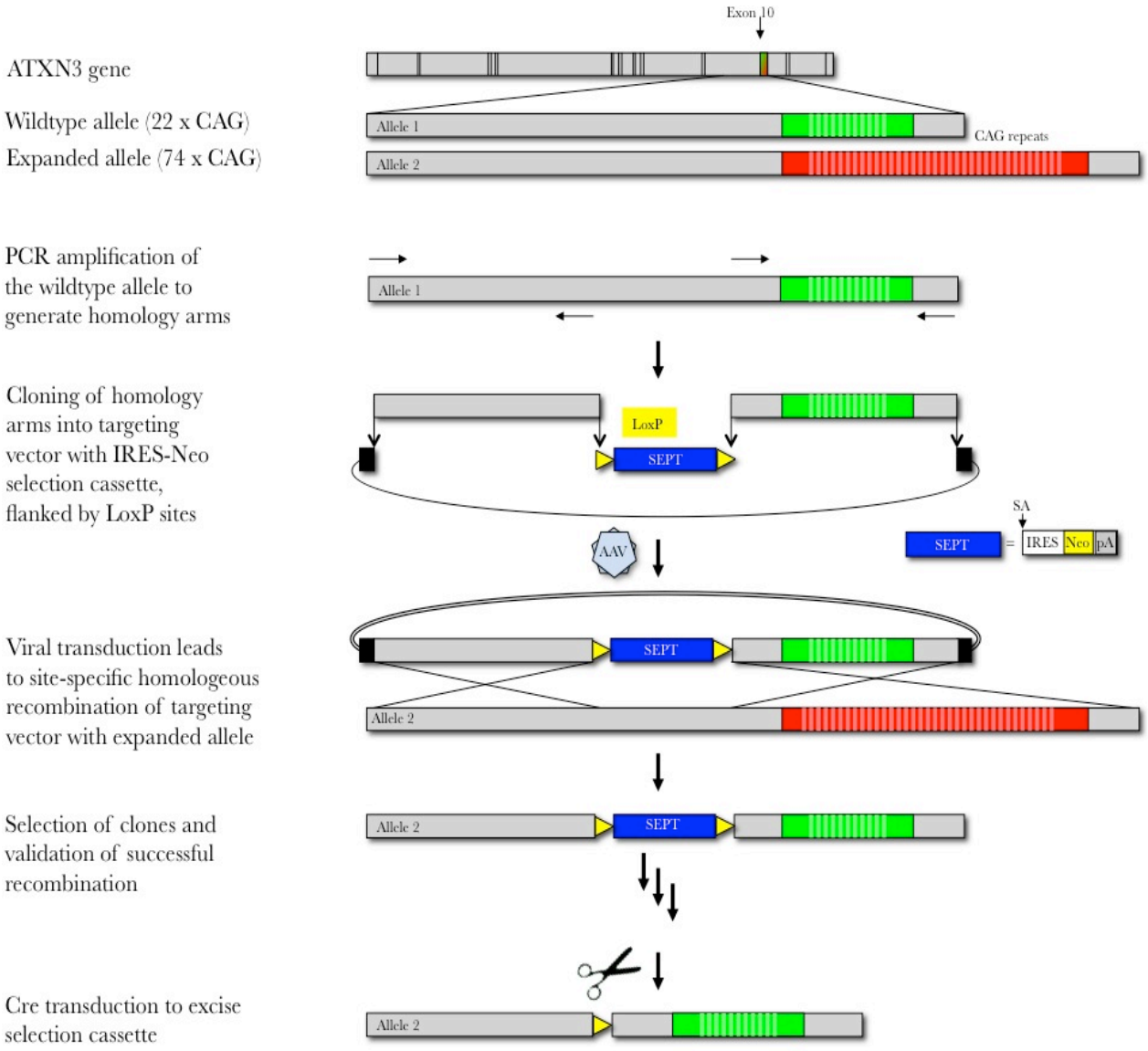

Figure 4.2: Gene correction strategy for the* ATXN3 *gene with adeno-associated viral vectors.

Indeed, analysis for ataxin-3 also showed a loss of the polyQ-elongated protein variant for all 22 clones analyzed (Fig. 4.3b shows 3 representative examples). Southern blotting with probes for the G418 resistance gene showed that in every second clone, only one viral integration occurred (Fig. 4.3c). Additionally, at the position of base modification in the targeting vector, sequencing reveals a mosaic signal for adenosine and guanosine at equimolar ratio (Fig. 4.3d), indicating the same amount of both variants within the genome and thus only one integration of viral sequence into the cells. Taken together, these results confirmed the integration of the targeting vector in the genome at the desired location while unwanted off-target integrations seemed rare. Based on these findings, it was concluded that the generated AAV integrates with high specificity into the desired locus, disrupting the pathogenic allele of the *ATXN3* gene.

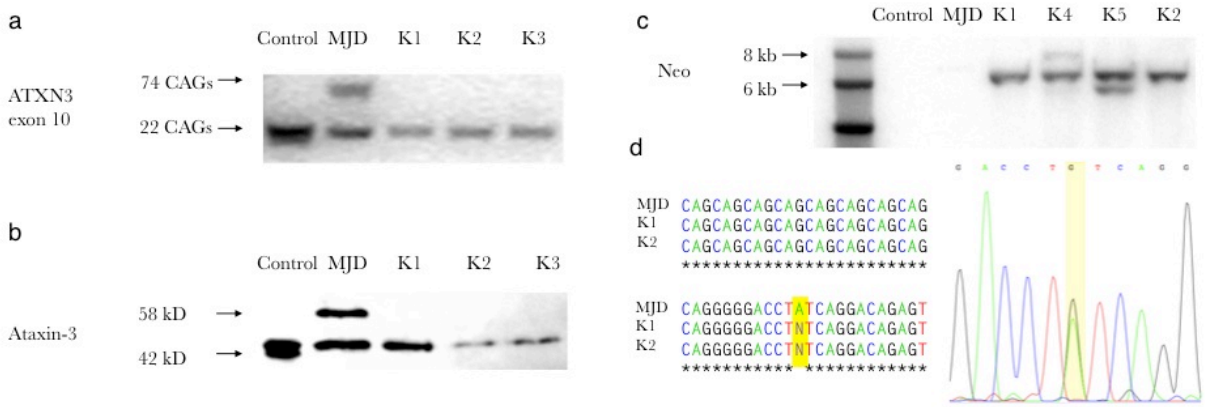

***Figure 4.3: Site-specific targeting of AAV vectors into the expanded allele of* ATXN3**
a: *PCR amplification of exon 10 of the* ATXN3 *gene reveals the diminishment of the expanded allele in 96,7% of PCR-screened clones.* ***b:*** *Western blotting confirms the absence of the pathogenic 58 kD protein variant of ataxin-3 after AAV application in all analyzed clones.* ***c:*** *Southern blotting was used to check for multiple viral integrations. Probes for the G418 resistance of the viral vector were used, resulting in no signal in control- and MJD cells. Half of the clones showed only one integration. These were used for genomic sequencing.* ***d.*** *Sequencing of the part of exon 10 that was mutated in the targeting vector showed equimolar amounts of adenosine and guanosine at the modified base. Adenosine originated from the physiological, unaltered shorter allele while guanosine originated from the viral variant which substitutes for the pathogenic, longer allele. This again confirmed that only one viral integration occurred while PCR and western screens indicated the correct site of integration.*

4.2.3 Efficient removal of selection cassette by Cre transduction

As long as the selection cassette is integrated in front of the corrected exon 10, no functional protein can be generated form this allele as the splice acceptor diverts transcription to the G418 resistance gene. The cassette is flanked with loxP sequences, allowing its excision with Cre activity. To remove the integrated selection cassette for re-expression of *ATXN3* from the recombined allele, a Cre-coding modified mRNA was transfected twice. Western blotting 12 hours after Cre-mRNA-transfection of clones showed an increase of the total protein levels of wildtype ataxin-3 at ~ 42 kD (Fig. 4.4a). Quantification of wildtype ataxin-3 increase ranged from 20% to 80% (presumably dependent on transfection efficiencies, Fig. 4.4b). A fragment of ~ 30 kD which matches the expected protein size of truncated ataxin-3 due to the integration of the SEPT cassette is diminished after Cre treatment (Fig. 4.4a). This observation supports the idea of physiological function of both alleles; prior to Cre application, the targeted allele is not functional leading to a stronger translation of both alleles to generate sufficient amount of protein. As soon as the targeted allele gives rise to functional protein, the higher translation leads to an increase in ataxin-3 protein. Efficient excision of the SEPT cassette was further validated by genomic PCR. In cells not transfected with Cre-mRNA a PCR product of ~ 2000 bp is amplified from the wildtype allele and the allele containing the SEPT cassette leading to two PCR products of approximately the same size,

which could not be separated by gel electrophoresis. Following Cre-transfection the SEPT cassette is excised leading to a smaller PCR product of ~ 400 bp (Fig. 4.4c). To validate functional expression of both alleles, mRNA of corrected MLD-It-NES cells was extracted and subsequently transcripted into cDNA. Sequencing of the previously modified base position of the *ATXN3*-mRNA transcript revealed a mosaic signal of adenosine from the wildtype allele and of guanosine from the virus-derived corrected allele (Fig. 4.4d). The equimolar amount of both signals indicates a physiological and balanced transcription of mRNA from both alleles. Based on these findings, it was concluded that the chosen approach resulted not only in the diminishment of the pathogenic allele but also in a functional gene correction with expression of physiological protein from both alleles.

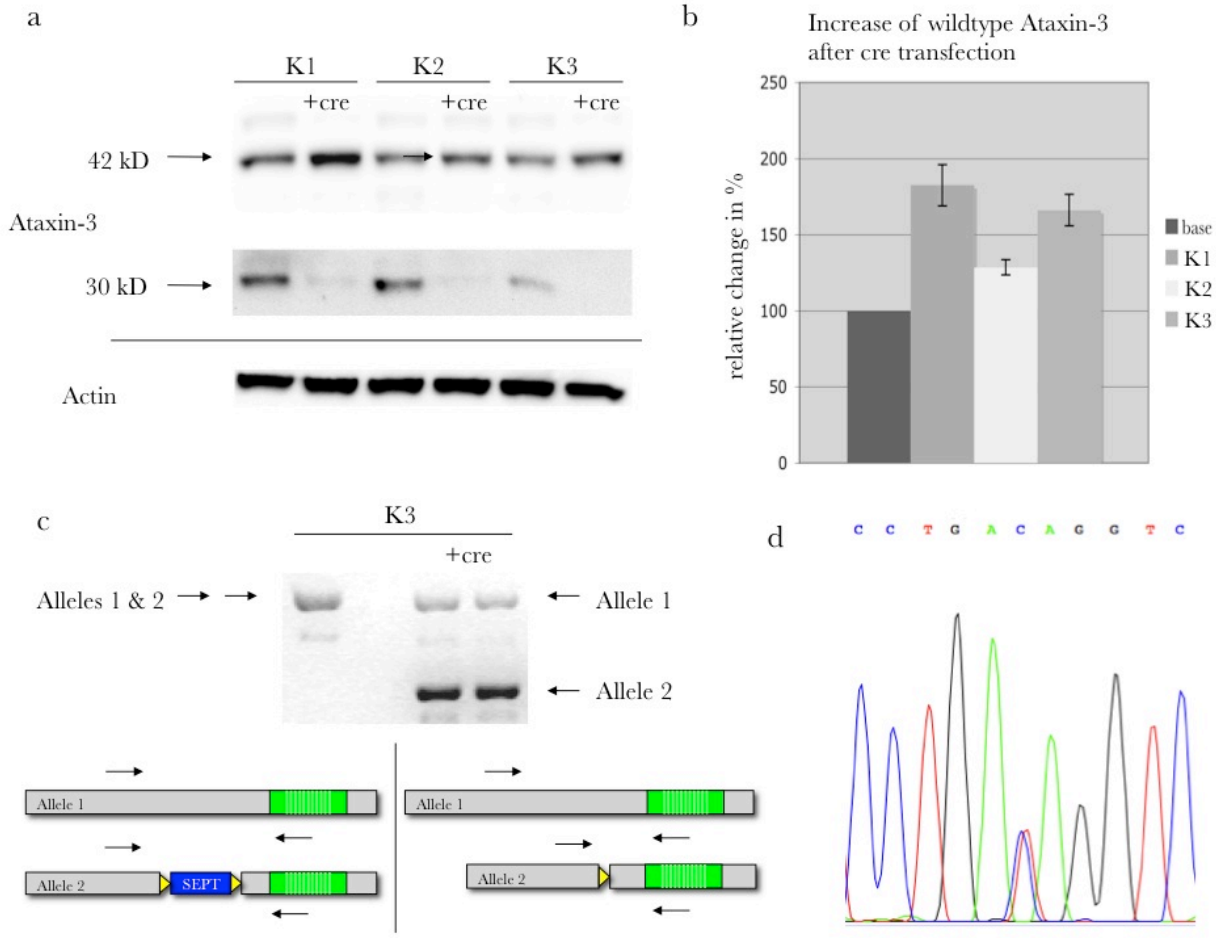

Figure 4.4: Excision of the selection cassette with Cre activity to regain a functional allele
a. *Western blotting of clones 12 h after Cre-mRNA-transfection shows an increase of the total protein levels of wildtype ataxin-3 at ~ 42 kD.* ***b.*** *Quantification of wildtype ataxin-3 increase ranges from 20% to 80% (presumably dependent on transfection efficiencies). A fragment of ~ 30 kD which matches the expected protein size of truncated ataxin-3 due to the integration of the SEPT cassette is diminished after Cre treatment.* ***c.*** *Efficient excision of the SEPT cassette was further validated by genomic PCR. In cells not transfected with Cre-mRNA a PCR product of ~ 2000 bp is amplified from the wildtype allele and the allele containing the SEPT cassette leading to two PCR products of approximately the same size, which could not be separated by gel electrophoresis. Following Cre-transfection the SEPT cassette is excised leading to a smaller PCR product of ~ 400 bp.* ***d.*** *Sequencing of cDNA of corrected and Cre-transfected cells showed mosaic signal at the position of base modification of the targeting vector indicating generation of mRNA from both alleles to the same amount.*

4.2.4 Characterization of morphology and marker expression reveal no significant alterations despite genetic manipulation

It was further validated whether genetic manipulations, the selection and clonal propagation resulted in changes in the differentiation potential and marker expression of isolated clones. Therefore, the morphology and marker expression of gene corrected lt-NES cells and their differentiated progeny were analyzed in parallel (Fig. 4.5a). The uncorrected MJD-lt-NES cells showed a polar, rosette-like structure and expressed the neural stem cell markers Nestin and Sox2 as well as rosette markers DACH1 and PLZF. The tight junction protein ZO-1 is expressed at the luminar side of the rosettes (Fig. 4.5a). After growth factor withdrawal, these cells differentiate into a major fraction of beta III-tubulin(+) and MAP2ab(+) neurons and a minor fraction of GFAP(+) astrocytes (Fig. 4.5b). The gene corrected MJD(corr)-lt-NES cells (depicted are representative stainings of K2) show comparable morphological characteristics, expression of stem cell and rosette markers.

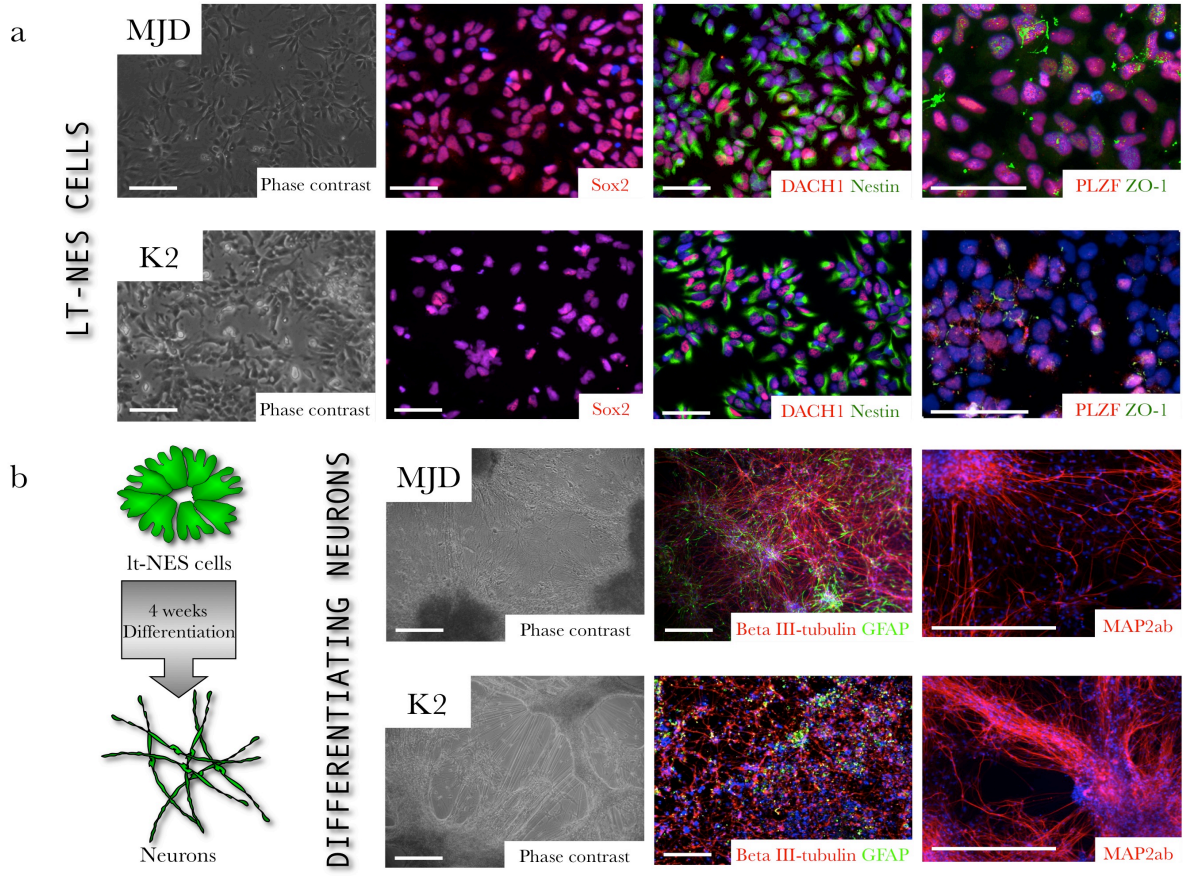

Figure 4.5: Gene targeting does not influence the ability of MJD(corr) cells to differentiate. ***a.*** *The uncorrected MJD-lt-NES cells show a polar, rosette-like structure and express the neural stem cell markers Nestin and Sox2 as well as rosette markers DACH1 and PLZF. The tight junction protein ZO-1 is expressed at the luminar side of the rosettes The gene corrected, MJD(corr)-lt-NES cells (depicted are representative stainings of K2) show comparable morphological characteristics, expression of stem cell and rosette markers* ***b.*** *Four weeks after growth factor withdrawal, cells of both populations differentiate into a comparable number of beta III-tubulin(+) and MAP2ab(+) neurons and a minor fraction of GFAP(+) astrocytes. Scale bars: lt-NES cells: 50 µm, diff. neurons: 200 µm.*

Four weeks after growth factor withdrawal a comparable number of the cells expressed neuronal and glial antigens. Thus, the viral targeting strategy, selection of clones and Cre treatment did not significantly alter the characteristics of MJD(corr)-lt-NES cells.

4.2.5 Gene corrected MJD-lt-NES cells no longer form microaggregates

After glutamate induced activation of MJD-neurons, an insoluble fraction of ataxin-3-positve smear could be detected in western blot (Fig. 4.6). These microaggregates are very likely to be the first detectable signs of defects in protein degradation and accumulation of misfolded proteins, which finally leads to the loss of frequently used neuron populations in MJD patients. As a consequence, the microaggregate formation can be seen as one of the hallmarks of MJD pathology. Neurons made from control lt-NES cells, MJD-lt-NES cells and two corrected MJD-lt-NES cells were subjected to two 30 min-stimuli of glutamate-induced activation. Protein lysates were gained 24 h later and separated into Triton X-100-soluble, SDS-soluble and SDS-insoluble fractions as described (Koch et al., 2011). MJD-neurons showed several prominent fragments of about 25-45 kD and a high molecular smear indicating the presence of fragmented and aggregated ataxin-3 in these cultures (Fig. 4.6). Control cells and corrected clones (K1+K2) shown have no ataxin-3-positive fragments in the formic acid fraction. As microaggregate formation is an important biochemical phenotype of MJD-lt-NES cell-derived neurons, the normalization to physiological value is a good indicator for a full functional rescue of patient-derived cells.

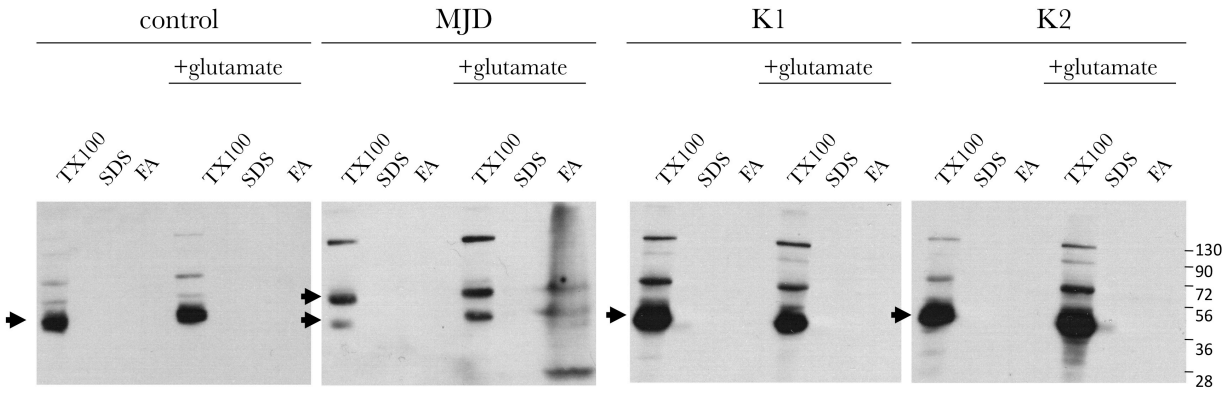

Figure 4.6: Gene corrected MJD-Neurons no longer form microaggregates.
The most important biochemical difference between neurons generated from control cells and those from MJD cells is the formation of SDS-insoluble, Ataxin3-positive high molecular smear. This smear is considered to consist of microaggregates, the first step in the formation of aggregated protein plaques within the cells. These microaggregates can only be detected in neurons, not in neural stem cells or their glial progeny. Furthermore, activation of neurons by glutamate-treatment is essential as seen above. Arrows indicate ataxin-3 variants present in the cells. Control cells have both alleles of similar size, forming one large signal, while in MJD cells, the variant with expanded polyQ tract is seen in a signal of higher protein weight. The SDS-insoluble fraction (FA for formic acid) contains ataxin-3-containing smear after glutamate-treatment in MJD cells. After gene-correction, only one ataxin-3 protein variant is seen in the TX100 lane. Shown are results for two different clones. Following glutamate treatment, no microaggregate formation could be observed.

4.3 Therapeutic intervention in epilepsy: *In vitro* generation and validation of an adenosine releasing neuronal cell population

4.3.1 Zinc-finger nuclease-mediated knock out oft he adenosine kinase gene results in adenosine-releasing neural stem cells

Adenosine is a potent suppressor of excitatory neural transmission and has been shown to inhibit seizure activity upon direct delivery into the central nervous system *(Li et al., 2007b)*. The second targeting project aims at exploiting human stem cell-derived neurons for activity-dependent release of adenosine to the epileptic hippocampus. To that end, both alleles of the adenosine kinase gene in human It-NES cells have been targeted by zinc finger nuclease technology.

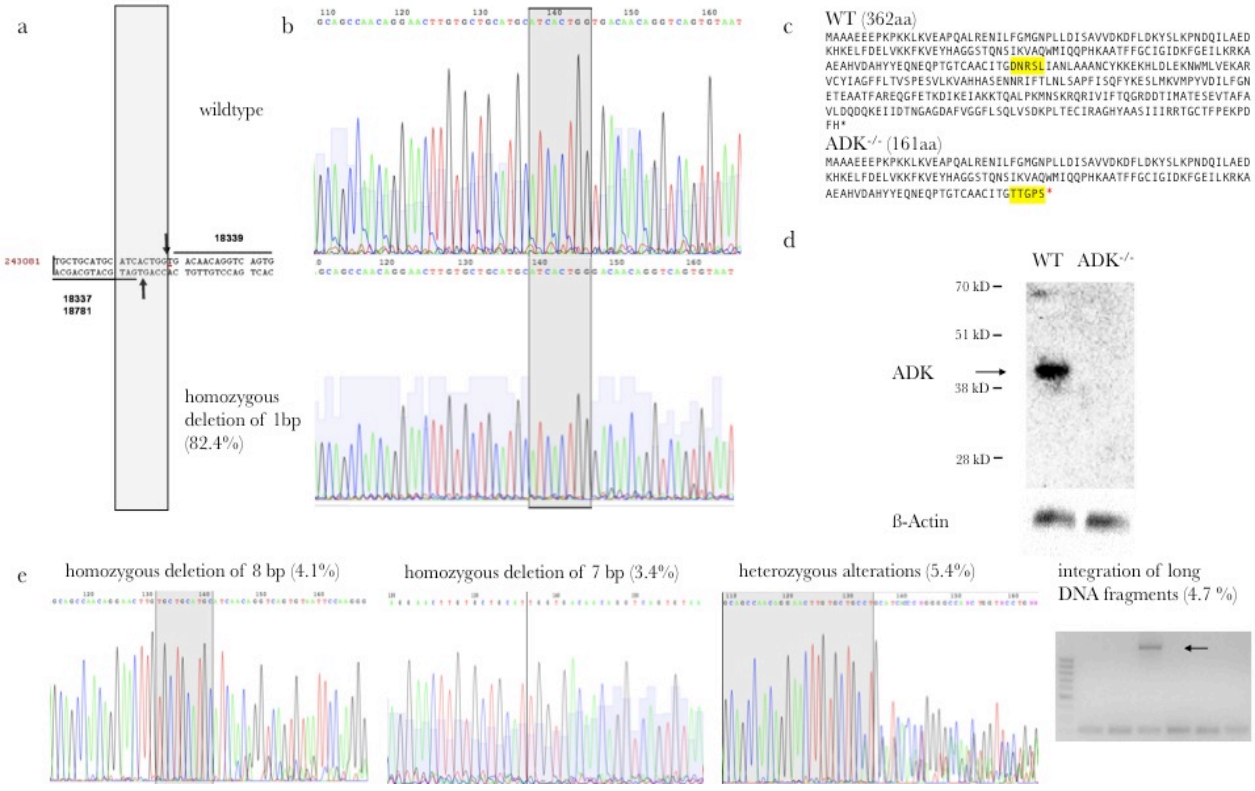

Figure 4.7: Disruption of the ADK gene by zinc finger nucleases.
a. *Position of zinc finger nuclease binding sites within exon 5 of the ADK gene, cleavage site is indicated by arrows. ZFN 18337 and 18781 bound upstream of the cleavage site, ZFN 18339 downstream of it.* ***b.*** *Sequencing of the target locus revealed a homozygous deletion of 1 bp in 82.4% of the 148 analyzed clones.* ***c.*** *This deletion led to a frame shift resulting in premature disruption of translation (marked by asterisk). The accruing protein lacks all catalytic domains, resulting in a complete loss of ADK activity. Translated sequence differing due to frame shift is marked in yellow.* ***d.*** *Western blot analysis confirmed the absence of adenosine kinase. No shorter variants could be detected.* ***e.*** *The remaining 17.6% of clones gained showed the following alterations: 4.1% with an 8 bp deletion, 3.4% with a 7 bp deletion, 5.4% with differing heterozygous alterations and 4.7% with the integration of differing long DNA fragments as shown here by a large product in the screening PCR.*

Depletion of ADK was expected to result in elevated intracellular adenosine levels and thus increased basal release of adenosine via equilibrative nucleoside transporter (ENT). In neurons, additional activity-dependend release was described. For the functional disruption of ADK, three different zinc finger nucleases (ZFN) of Sangamo (Richmond, USA) were used, directed against exon 5 of the ADK gene. The three ZFNs formed two different pairs, binding the same target locus with its DNA-binding zinc finger domain. Dimerization of its double strand break-inducing nuclease domain is necessary for target cleavage. The cellular machinery for non-homologous end joining (NHEJ) is involved in repairing the double strand break, but this mechanism is error-prone and can thus result in disruption of the target gene. Plasmids coding for zinc finger nucleases were electroporated into lt-NES cells derived from the I3 line. ZFNs 18337 and 18781 bound upstream of the cleavage site inside exon 5 of the ADK gene, while ZFN 18339 bound downstream of it (Fig. 4.7a). After binding their target sequences, the close proximity between two ZFNs leads to induction of nuclease activity at positions indicated by arrows (Fig. 4.7a). Without the addition of a selectable marker, to enrich positively targeted cells it was yet possible to exploit the enzymes ability to metabolize adenosine analogues like 8-Chloro-Adenosine and 8-Chloro-cAMP. These two analogues are transformed to cytotoxic variants by metabolization through ADK. Only cells without a functional ADK would survive the selection process and single clones could be derived. Application of chemoselection for 3 weeks was sufficient to eliminate all untargeted cells. DNA from single clones was isolated and examined for alterations in the target locus of the ZFNs. Sequencing revealed a homozygous deletion of 1 bp in more than 82% of the 148 analyzed clones. (Fig. 4.7b) This deletion leads to a frame shift resulting in premature disruption of translation (indicated by asterisk, Fig. 4.7c). The accruing protein lacks all catalytic domains, resulting in a complete loss of ADK activity. Western blot analysis confirmed the absence of adenosine kinase of normal size, while truncated variants could not be detected on the western blot (Fig. 4.7d). Despite the above-mentioned 1 bp deletion, most abundant variations were found to be deletions of 8 and 7 bp. The remaining 10% of clones showed either heterozygous alterations as seen by the mixed, double signals in the sequence occurring after the site of double strand break induction (Fig. 4.7e) or the integration of large fractions of random DNA pieces.

As previously reported (Gupta et al., 2011), the application of zinc finger nucleases carries the risk of off-target cleavage. High-resolution SNP-analysis was carried out to check for chromosomal abnormalities. Many of the derived clones showed duplications or deletions of chromosomes and few had a massive accumulation of such modifications (Fig. 4.8a).

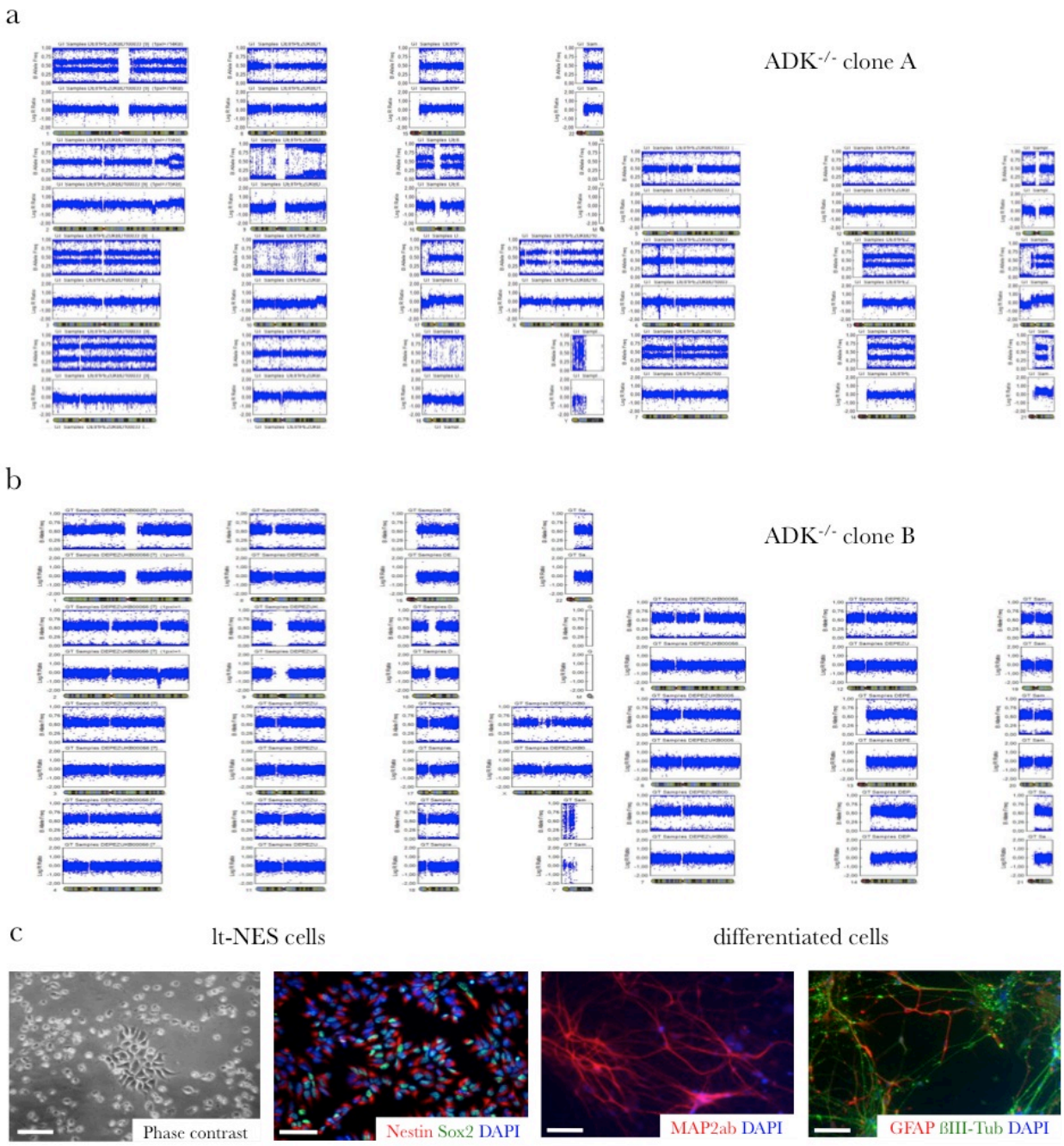

Figure 4.8: Selection of clones without off-target damages.
a. *Full genome-SNP analysis of an ADK-knock out clone showing massive chromosomal changes like duplications (chromosomes 1, 2, 3, 4, 7 13, 14, 16, 19, 20, 21 and X) and deletions (chromosomes 9,10, 17, 18, 20 and 21).* ***b.*** *Full genome SNP analysis of an ADK-knock out clone without detectable alterations that resulted from the ZFN targeting. The deletion in chromosome 2 was already present in the founding cell line derived from I3 ES cells.* ***c.*** *Morphology and marker expression of ADK$^{-/-}$ clone B did not differ from wildtype cells in the neural stem cell state with rosette-like appearance and the expression of Nestin and Sox2. After 4 weeks of differentiation, MAP2ab- and ßIII-tubulin neurons as well as GFAP-positive astrocytes could be detected which indicated a differentiation potential normal for lt-NES cells. Scale bars: 50 µm.*

Chromosomal abnormalities are a major risk factor for possible tumor formation. For grafting into animals it is important to have a cell population that is not prone to malignancy, for which reason clones without detectable genetic alterations (Fig. 4.8b) were selected before moving on. The deletion on chromosome 2 seen in all SNP analysis was already present in the founder cell line I3. It is not related to the application of ZFNs on the cells and clone B was used for the following experiments.

The chosen clone of $ADK^{-/-}$ lt-NES cells could be maintained as a homogenous population of Sox2- and Nestin-positive neural stem cells, morphological identical to the founder cell line and expressing the same markers. Following growth factor withdrawal, these cells efficiently generated ßIII-tubulin- and MAP2ab-positive neurons and GFAP-positive astrocytes (Fig. 4.8b).

4.3.2 ADK stays expressed after differentiation into neurons

The efficiency of secreted adenosine not only depends on its removal by metabolization through the enzymes adenosine kinase and adenosine deaminase but also on the expression of the respective adenosine receptors. To check if the receptors needed for adenosine-mediated inhibition and the key metabolizing enzymes are still present after differentiation of lt-NES cells into neurons, expression profile analysis was performed comparing lt-NES cells with their neuronal progeny generated by a neuron-enrichment method established earlier at our institute (Ladewig et al., 2008). Transcripts of adenosine kinase (ADK), adenosine deaminase (ADA), and adenosine receptors A_1 (ADORA1), A_{2A} (ADORA2A), A_{2B} (ADORA2B) and A_3 (ADORA3) were evaluated as seen in Fig. 4.9. In lt-NES cells, ADK and ADA genes were highly expressed, but diminished after neuronal differentiation. Contrary, expression of A_1 and A_3 receptors was increased in neuronal progeny, while transcripts for the A_2 receptor subtypes A and B are hardly detectable in both populations. Taken together, action of adenosine is expected to be intensified in differentiated neuronal cultures, as the amount of metabolizing enzymes decreases while receptors for adenosine signaling are increased.

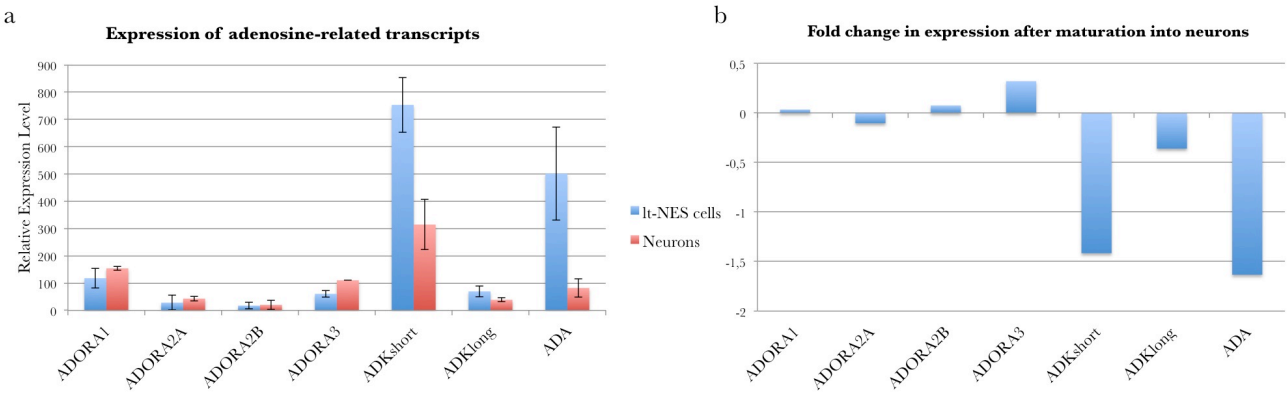

Figure 4.9: Expression of adenosine-related transcripts in lt-NES cells and neurons.
a. *Comparison of relative transcript expression of adenosine receptors A_1, A_{2A}, A_{2B} and A_3 (ADORAx), adenosine kinase (ADK) and adenosine deaminase (ADA) in lt-NES cells (blue) and neurons (red). ADK and ADA are highly expressed in neural stem cells but down regulated after differentiation. ADORA1 and ADORA3 transcripts showed an increase after induction of neuronal commitment while both ADORA2 transcripts are not present.* ***b.*** *Fold change in expression after maturation of lt-NES cells into neurons. Transcript detection performed with n=2 probes per transcript.*

4.3.3 Adenosine kinase deficient cells release adenosine in vitro

After confirming the ADK deficiency on the genomic and proteomic level, adenosine distribution by the $ADK^{-/-}$ lt-NES cells was assessed by collecting cell culture supernatants 2, 8 and 24 hours after media change to analyze for adenosine content. As the second metabolizer of adenosine, the adenosine deaminase is still present in the cells, its inhibitor EHNA (50μM) was added to facilitate measurement. This limitation of the in vitro measurement was found to be neglectable in transplantation approaches as surrounding cells should immediately take up adenosine. Liquid chromatography-tandem mass spectrometry (LC-MS/MS) revealed an up to 200-fold increase in adenosine release compared to wildtype cells, and an accumulation over time (Fig. 4.10a) Different clones of undifferentiated $ADK^{-/-}$ lt-NES cells released comparable amounts of adenosine while differentiated cultures showed variability between different clones (Fig. 4.10b).

It was suspected that the different ratio of neurons and astrocytes within differentiated progeny could be a reason for the differences in adenosine output. Therefore, neuron- or astrocyte-enriched differentiated cultures were generated and again adenosine levels evaluated (Fig. 4.10c). Astrocytes showed a lower basal adenosine release compared to neurons, disagreeing with results from previous work with primary rat cultures (Parkinson et al., 2002). Glutamate lead to an increase of adenosine release in both populations, whilethe effect in neurons was much more prominent (Fig. 4.10d). These observations stand in line with previous reports about activation-dependent release of adenosine (Lovatt et al., 2012).

Based on previous data, a total of 50.000 cells was calculated to be sufficient to yield an anti-epileptic effect after transplantation in affected mouse brains (Huber et al., 2001).

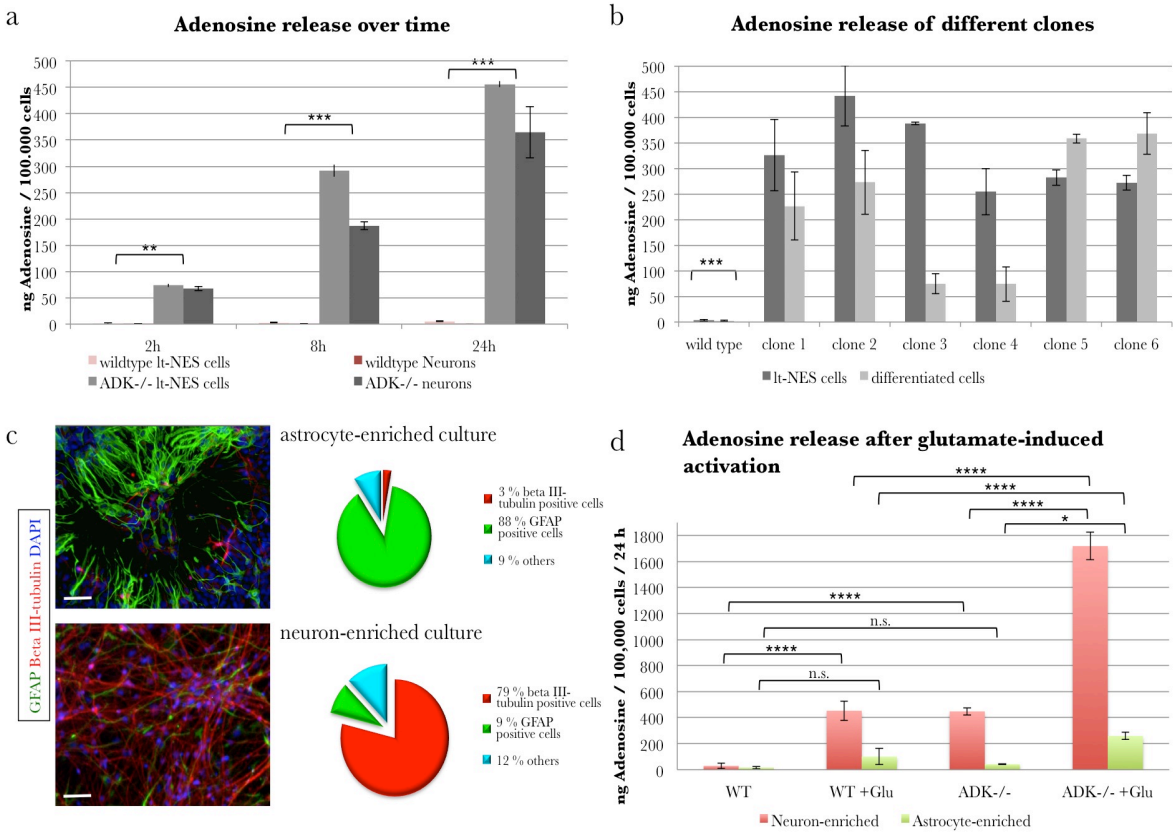

Figure 4.10: Adenosine release of ADK$^{-/-}$ cell cultures.
a. *Comparison of adenosine release into the culture media of wildtype lt-NES cells, ADK$^{-/-}$ lt-NES cells and their differentiated progeny at 2, 8 and 24 h. While adenosine release by wildtype cells is at the detection limit, ADK$^{-/-}$ cells deliver adenosine into the media, where it accumulates over time (n=3 each).* ***b.*** *Various clones of ADK$^{-/-}$ cells showed comparable amounts of released adenosine while after 4 weeks of differentiation the amounts differed largely (n=3 each).* ***c.*** *Astrocyte- or neuron-enriched cultures of ADK$^{-/-}$ lt-NES progeny. Both cultures were stained for beta III-tubulin as neural marker and GFAP as astrocytic marker showing high enrichment for either cell population. Pie chart on the right states the composition of each culture after counting of 3 fields of vision (Astrocyte-enriched: 2.7% neurons, 88% astrocytes, 9.3% other cells. Neuron-enriched: 78.9% neurons, 8.8% astrocytes, 12.3% other cells.) Scale bar = 50 µm.* ***d.*** *Adenosine distribution into supernatants of neuronal and astrocytic cultures of WT and ADK$^{-/-}$ cells were evaluated under standard conditions and following stimulation with glutamate. Glutamate generally induced an increase in adenosine efflux, which is especially prominent in ADK$^{-/-}$ neuronal cultures. Statistical analysis: *, $p < 0.05$; **, $p < 0.01$; ***, $p < 0.001$; ****, $p < 0.0001$*

4.4 *In vivo* application of adenosine-releasing cell populations

4.4.1 lt-NES cells transplanted in the mouse hippocampus show migration and long-term survival

Initial transplantations of lt-NES cells (wildtype and ADK$^{-/-}$) were delivered to the hippocampus of Rag2$^{-/-}$ C57/Bl6 mice to check for migration and survival of grafts. Another important question was how durable these immunodeficient animals would be, as Rag2$^{-/-}$ mice have no functional adaptive immune response, which could be problematic especially for animals with open head wounds after surgery.

A total of 50.000 lt-NES cells were stereotactically delivered to the right hippocampus. Mice recovered well from surgery and around 12 weeks later were sacrificed for histological analysis. Stainings for human axonal microfilaments and human nuclei showed the distribution and maturation state of grafted neural stem cells. Lt-NES cells tended to form transplantation cores of fairly undifferentiated cells at the center of the graft, while cells in the periphery differentiated faster and migrated into the host tissue. Cells showed robust survival with axonal projections across long distances within the ipsilateral hemisphere, approaching the CA3 region, corpus callosum, motor cortex and thalamus. Projections of human neurons could also be found in the fimbria and the contralateral hippocampal pyramidal cell layer (Fig. 4.11a), following a projection pattern typical for commisural hippocampal axons.

Stainings for human synaptophysin showed dotty signals that were arranged like chains (Fig. 4.11b) indicating the functional connectivity with neural dendrites of the host tissue. Based on these findings, it was concluded that lt-NES cells after grafting differentiate into mature neurons, with axons migrating along intrinsic pathways. Long-term experiments showed that animals survived after transplantations up to one year without losing the graft.

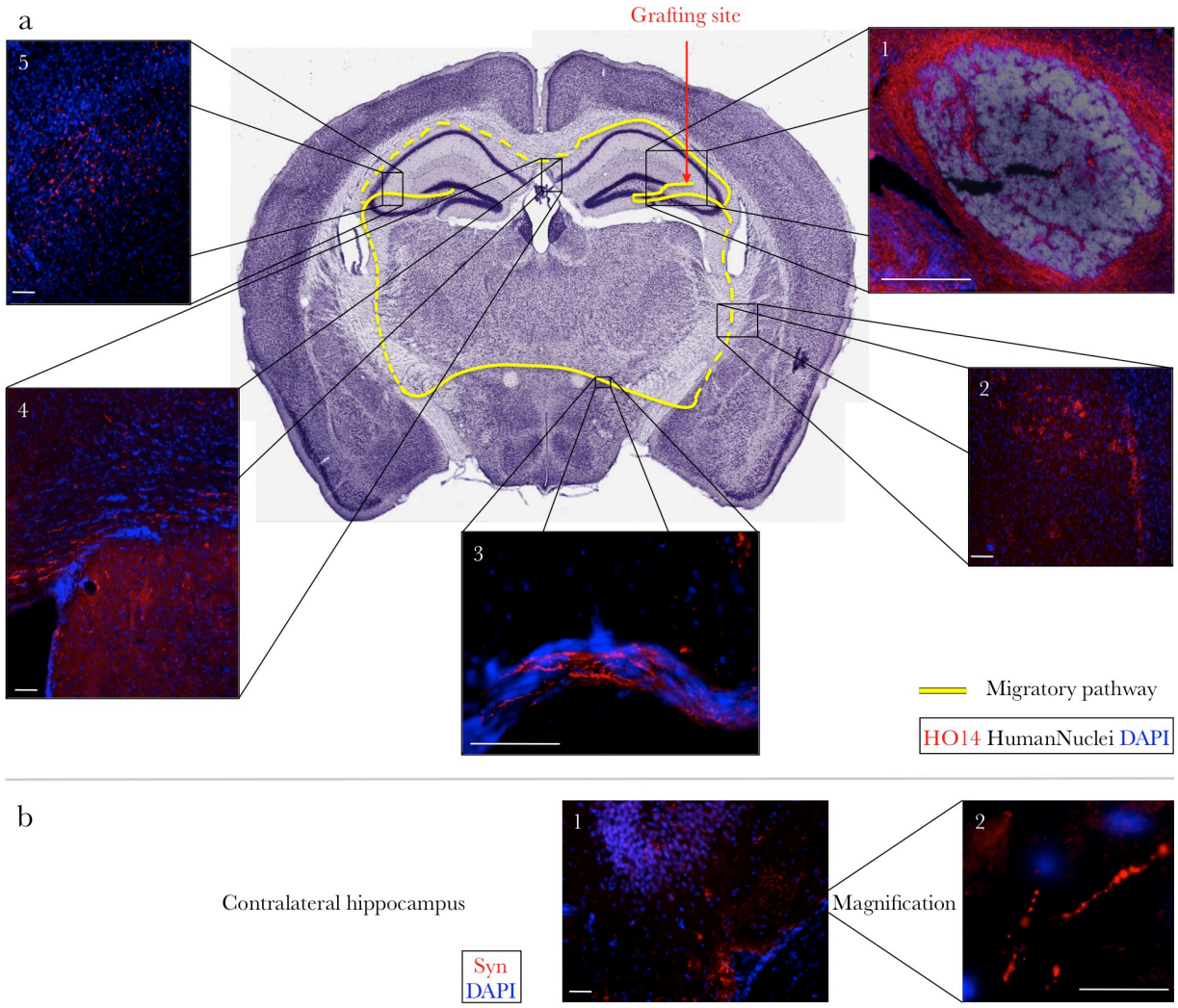

Figure 4.11: Grafting of lt-NES cells into the mouse hippocampus.
A total of 50.000 lt-NES cells were grafted into the right hippocampus as indicated by the red arrow. 12 weeks after surgery, animals were sacrificed for immunohistochemical analysis. ***a.*** *Coronal sections of brain slices stained for human nuclei in white and human axonal neurofilament HO14 in red, counterstained with DAPI in blue, clockwise: A large cluster of undifferentiated lt-NES cells could be detected at the grafting site (1), while at the periphery most of the cells differentiated into mature neurons, that migrated along intrinsic axon guidance pathways throughout the host' tissue as shown by yellow lines in the overview. Human neurons could be detected at the transplantation site (1), beneath the dentate granule cell layer of the ipsilateral hippocampus (2), the corpus callosum (3), the entorhinal cortex (4) and also in CA3 regions of the contralateral hippocampus (5). Scale bars: (1) = 500 µm, (2)-(5) = 50 µm.* ***b.*** *Coronal section of the contralateral hippocampus stained for human synaptophysin showing dotted signals, indicating the establishment of functional synapses with host neurons. Scale bars: (1) = 50 µm, (2) = 20 µm.*

4.4.2 Application of adenosine-releasing It-NES cells in mouse models of epilepsy

For the therapeutic application of adenosine releasing cells, a mouse epilepsy model is a prerequisite for the evaluation of the system. First attempts focused on the pilocarpine model, which was later changed to the kainate model. Both are models for the generation of chronically epileptic mice, which show specific histological alterations in the epileptic hemisphere after application of the compound. In addition, an electric kindling model was used, which is used as a system for the evaluation of the process of epileptogenesis. The grafting of human cells made it necessary to use genetically immunodeficient mice, as the alternative of daily immunosuppressive injections was not an option as based on experiences made in our lab.

4.4.2.1 Pilocarpine or kainate application to generate epileptic mice

For the therapeutic application of adenosine releasing cells, a mouse epilepsy model is a prerequisite for the evaluation of the system. First attempts focused on the pilocarpine model. Pilocarpine is a strong agonist of glutamate receptors leading to a general activation of neuronal activity. It is applied systemically by subcutaneous injection into the animal abdomen. The survival rate using the protocol described in the method section was around 80%, with most animal losses resulting from fulminant seizures that lead to acute death before status could be reached. Within the next 2 weeks, about 15% of the remaining animals died to unknown reasons resulting in an overall survival rate of around 60%. These animals showed spontaneous generalized seizures at least once a day. After the successful establishment of the pilocarpine protocol in normal C57/Bl/6 mice, it was used on immunodeficient $Rag2^{-/-}$ mice of the same C57/Bl/6 background, as these would be needed to tolerate the grafting of human cells. On the day of pilocarpine application, behavior and survival rates of the immunodeficient mice compared to standard mice were very similar. However, in the following 3 weeks, all remaining animals died for unknown reasons. In 3 independent experiments, it was not possible to generate surviving immunodeficient mice with chronic seizures with survival longer then 4 weeks (Fig. 4.12). As these results indicated incompatibility of the pilocarpine mode and the used mouse strain, SCID/beige mice were subjected to the pilocarpine model. Surprisingly, this strain tolerated even very high doses of pilocarpine without showing signs of an epileptic status. The experiments were finally aborted because of severe peripheral effects of pilocarpine, which could no longer be inhibited by the amount of scopolamine given. Despite the successful generation of C57/Bl/6 epileptic animals, failure to transfer the procedure to immunodeficient mice led to the consideration to use kainic acid to induce chronic epilepsy

a

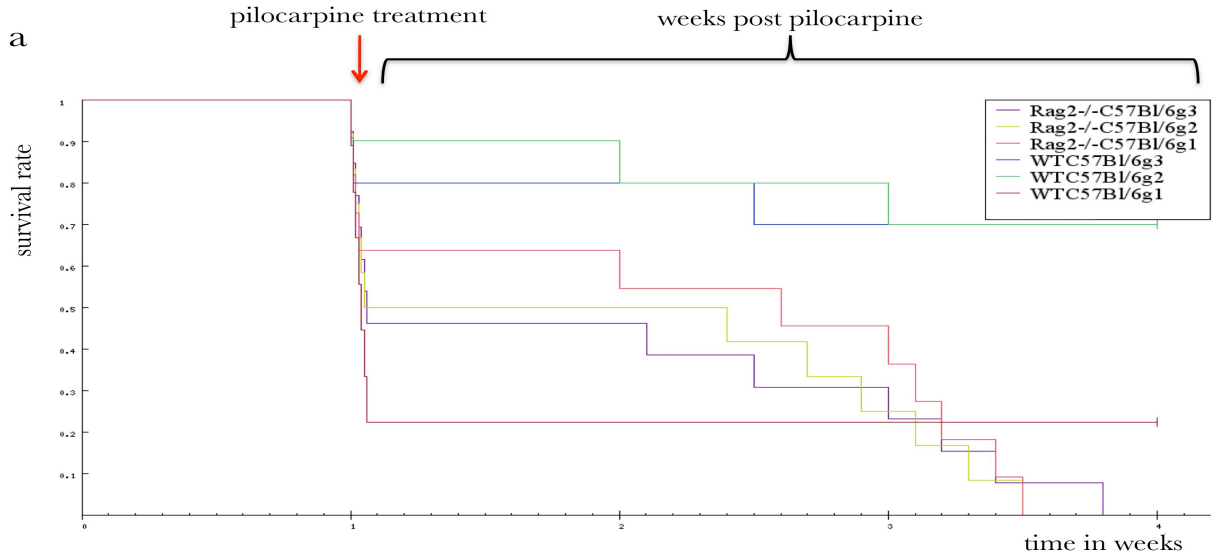

b

Animal numbers / Group	Before pilocarpine treatment	Directly after pilocarpine treatment	3 weeks after pilocarpine treatment
WT-C57Bl/6 g1	9	2	2
WT-C57Bl/6 g2	10	9	7
WT-C57Bl/6 g3	10	8	7
Rag2$^{-/-}$-C57Bl/6 g1	11	7	0
Rag2$^{-/-}$-C57Bl/6 g2	12	6	0
Rag2$^{-/-}$-C57Bl/6 g3	13	6	0
Animals in total	65	38	16

Figure 4.12: Survival of mice after pilocarpine treatment.
a. *Kaplan-Meier survival blot of animals used in the pilocarpine model. Following three experiments with wildtype C57/Bl/6 mice with a success rate of up to 70% in regard to generation of epileptic animals the same protocol was applied to Rag2$^{-/-}$ animals of C57/Bl/6 background. Immediate survival after pilocarpine treatment was 50-63%, while the next 3 weeks following treatment resulted in loss of all immunodeficient animals.* ***b.*** *Tabular summary of the 6 pilocarpine experiments.*

.

Kainic acid is a strong activator of glutamate receptors leading to immediate epileptic seizures and eventually to the manifestation of a status epilepticus (SE). Rag2$^{-/-}$ immunodeficient mice were subjected to kainic acid on the right hippocampus only and EEG electrodes were transplanted immediately afterwards in the same surgical operation. EEG monitoring was used to confirm when SE was reached. Two weeks after the procedure, exemplary histological analysis revealed prominent granule cell dispersion, a main histological feature of chronic epilepsy in the kainate model and also in human patients with chronic temporal lobe epilepsy (Fig. 4.13a, (Houser, 1990)). Within 18 days after surgery, mice showed repeated seizures up to the highest seizure stage Racine 5, so animals could be termed being chronic epileptic. Animals showed robust survival with no obvious variations to standard C57/Bl/6 strains. Therefore, the kainate model system was used for first transplantations of adenosine releasing human neural stem cells and their in vivo arising neurons.

4.4.2.2 lt-NES cells grafted into the epileptic hippocampus show enhanced dispersion and a trend towards reduced spontaneous seizures

Intracerebral injection of kainate into the right hippocampus of immunodeficient Bl/6-Rag2$^{-/-}$ mice was used to induce chronic epilepsy. Two weeks after kainate treatment, a total of 50.000 ADK$^{-/-}$ or wildtype lt-NES cells were transplanted into the ipsilateral hippocampus, along with electrodes for EEG measurements. EEG recordings were obtained for 2 weeks until mice were sacrificed for histological analysis. Transplanted lt-NES cells integrated well into the kainate-treated hippocampus and migrated along the CA1 and CA3 layers as depicted by staining for the human nuclear antigen (Fig. 4.13a). Remarkably, and in contrast to grafts into the healthy hippocampus, the cells showed pronounced dispersion without formation of a transplantation core. EEG recordings, supported by video analysis, were used to assess the total number of grade 5 seizures across 14 consecutive days. Recipients of wildtype cells showed an average of 27.8 seizures while recipients of ADK$^{-/-}$ cells had an average of 11.8 seizures (Fig. 4.13b). Due to a large dispersion of effects and insufficient amounts of number of animals used, this trend was not statistically significant.

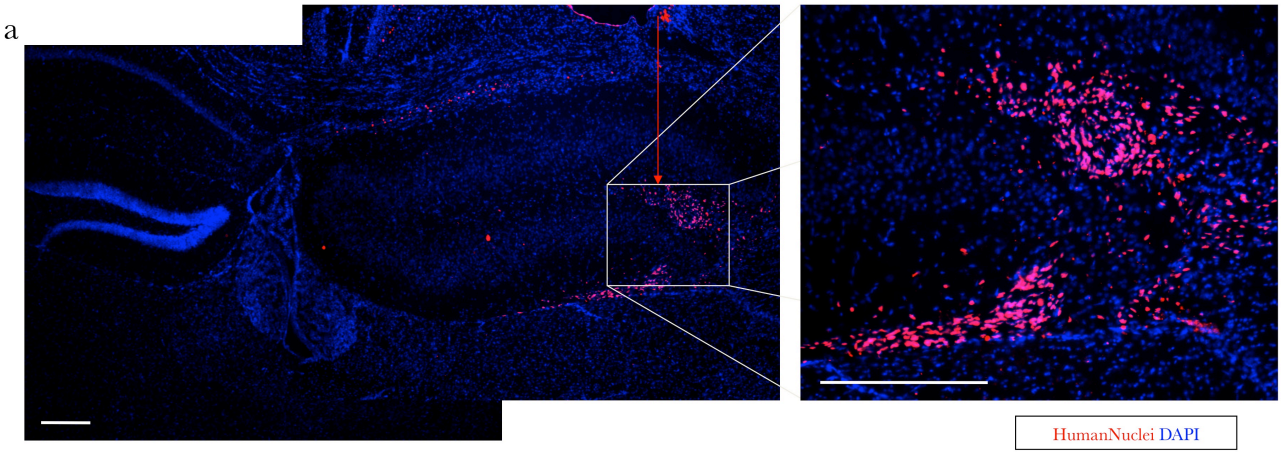

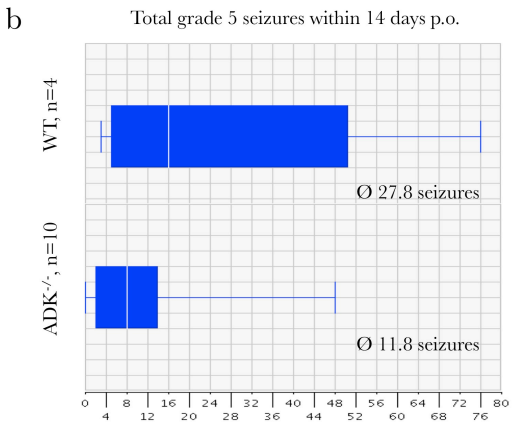

Figure 4.13: Grafting of adenosine-releasing lt-NES cells into the kainate-treated hippocampus.
a. *Coronal section of a kainite-treated hippocampus with prominent granule cell dispersion. Two weeks after kainate treatment, a total of 50.000 ADK$^{-/-}$ or wildtype lt-NES cells were transplanted into the ipsilateral hippocampus at the position marked by red arrow. Sections were stained for human nuclear antigen, illustrating the pronounced dispersion without formation of a transplantation core. Scale bars: 200 µm.* ***b.*** *Box blot diagram showing the number of grade 5 seizures across 14 consecutive days. Recipients of wildtype cells showed an average of 27.8 seizures while recipients of ADK$^{-/-}$ cells had an average of 11.8 seizures.*

4.4.3 Diagonal grafting of lt-NES cells results in distribution throughout the hippocampus in a kindling model of epilepsy

As adenosine does not only have an effect as suppressor of seizures but has also been described to modulate epileptogenesis, we were interested whether transplanted ADK$^{-/-}$ cells would suppress epileptogenesis in a kindling model of epilepsy. To that end we kindled immunodeficient C57/Bl6 and Rag2$^{-/-}$ mice and analyzed epileptogenesis. These results were compared to wildtype animals. The stimulation electrode was placed into the amygdala, while a set of measuring electrodes was placed epidurally to enable EEG recordings. After determination of electrographic seizure threshold (EST), animals were kindled twice daily at EST until three consecutive seizures of class 4 or greater lasting at least 12 sec were observed to term animals fully kindled. Parameters evaluated during kindling contained seizure grade based on the extended scale of Racine, seizure duration and afterdischarge threshold (ADT). Beside a delay in the development of seizures in regard to severity and duration in the immunodeficient mice within days 3 to 8, there was no difference in the reaction to the kindling paradigm. The delay was caught up and after 3 weeks, animals of both groups were fully kindled with daily seizures of grade 5 First experiment with cells grafted into the anterior hippocampus, the same grafting site as used with the kainate model, were performed. Either wildtype (WT) or ADK knockout (KO) cells were grafted into the right hippocampus, 50.000 cells each, while control animals only received saline buffer. After two weeks of recovery, mice were transferred to the kindling facility and after 2 additional weeks of adaption, kindling was started. Using the same kindling protocol resulted in a total of 3 Sham animals, 6 WT cell-grafted animals and 5 KO cell-grafted animals fully kindled. After the first two weeks, the duration and severity of seizures became very uniform, and in the end, no differences could be observed between differently grafted groups Histological analysis revealed a widespread migration of grafted cells with extensive axonal outgrowth into the host tissue, as judged by immunochemical staining for human nuclei and HO14 (data not shown). Cell maturation and survival was not affected by the kindling procedure.

We reasoned, that the size of the graft and the inappropriate innervation of the entire hippocampus were responsible for the negative outcome. Ideally, a graft would distribute along a large portion of the hippocampal structure from anterior to posterior so that commissural projections would also innervate the amygdala. Due to the crescent-like, winded anatomy of the mouse hippocampus, the only way to achieve a grafting tract through the hippocampus without touching the lateral ventricle was to inject diagonally instead of vertically from the skull surface. It would be important not to hit the fissure between hippocampus and thalamus or the lateral ventricle while generating the cannula tract, or cells would evade into these more space-affording rooms, leaving only few of the grafted cells

within the hippocampal formation. From coordinates +0.9 mm posterior and +0.5 lateral to bregma a 45° angle from vertical and 47.5° angle from the midline was used, creating a diagonal injection tract aiming at a coordinate of 3.9 mm posterior to bregma (AP), 3.0 mm lateral to the midline (ML) and 3 mm below the dura (DV). Cells were injected during retraction of the cannula at a rate of 1 μl per mm and min. This enabled us to deposit the cells over a relatively long injection tract within the right hippocampus and adjacent to the stimulation electrode implantation site.

Histological analysis of diagonally grafted animals revealed that this cell injection approach covered most of the dorso-ventral extent of the hippocampus by placement of the grafted cells into the infra-hippocampal cleft and minimized the damage to the ipsilateral hippocampus (Fig. 4.14a-d). From anterior to posterior, the graft followed the hippocampus going to ventral and lateral direction and was found at similar positions within the dentate gyros along its way. The $Rag2^{-/-}$ mice showed larger variations in skull anatomy then the standard C57/Bl/6 mice, which most likely resulted also in differences of brain anatomy. During surgery, these differences in grafting trajectory were tried to be equalized by measuring the distance between bregma and lambda suture and eventually adjusted the point of cannula entry as determined by skull coordinates measured from bregma. Still, in about 25% of all animals transplanted, graft position was suboptimal. This made a histological analysis essential, allowing to exclude animals after all experiments were performed. During application of the diagonal grafting technique, the loss of animals due to trauma or injuries was not found higher as in the classical vertical grafting approach.

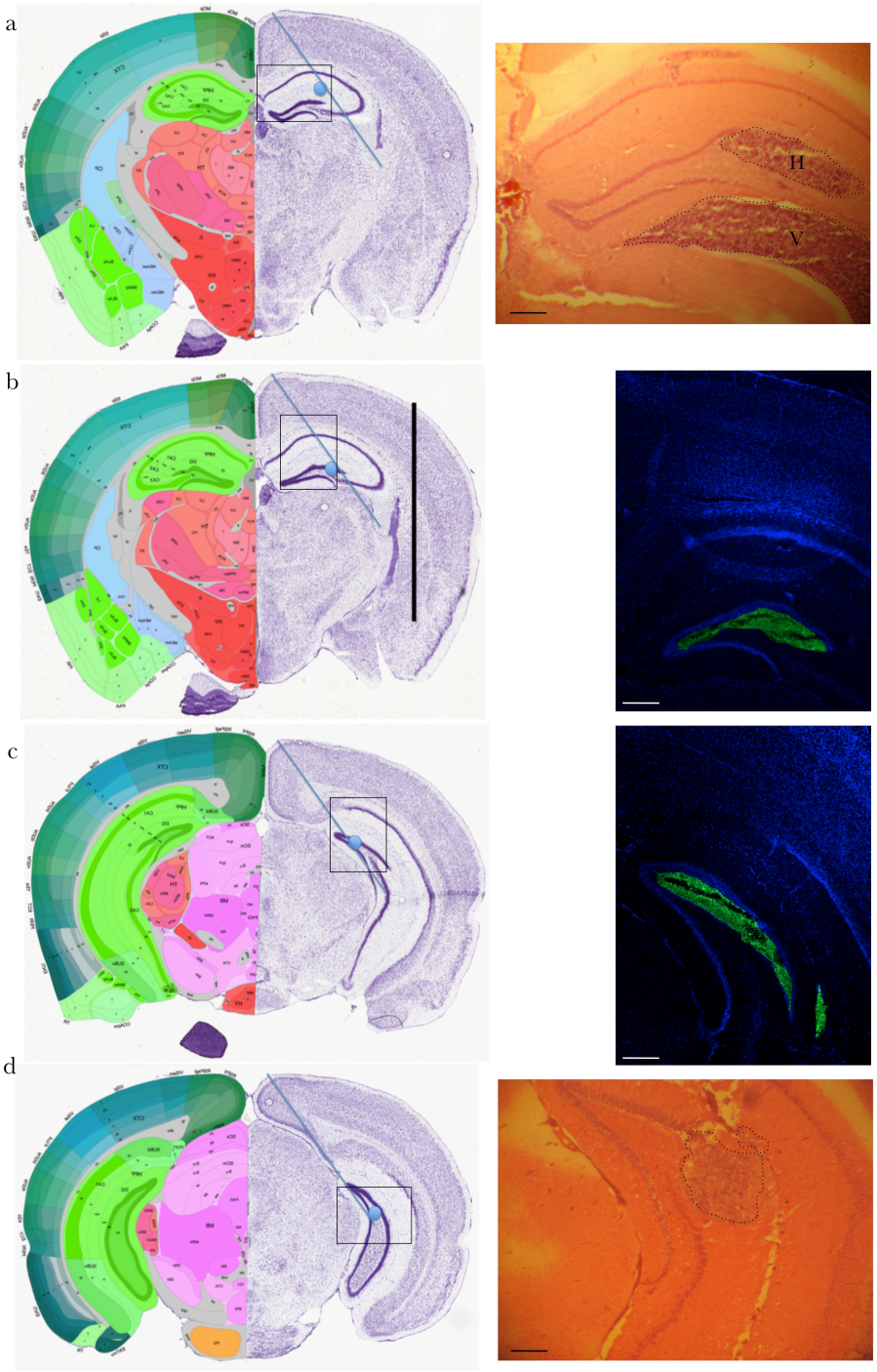

Figure 4.14: Diagonal transplantation of lt-NES cells into the mouse hippocampus.
The blue line indicates the trajectory of diagonal transplantation into the right hippocampus using an angle of 47.5° from the midline and 45° from vertical. The blue circle defines locations where human cells have been found in the respective section, supported by HE and immunohistological stainings as shown on the right. ***a.*** *Coronal section 1.7 mm posterior to bregma. HE staining showed the delivery of cells within the inner granule cell arch of the frontal lateral hippocampal formation (H). If cells were also deposited within the lateral ventricle, they could be found until the upper anterior part of the ventricle (V).* ***b.*** *Coronal section 2.5 mm posterior to bregma. Immunohistological staining for human nuclear filament in green. The black bar indicates the stimulation electrode transplantation site.* ***c.*** *Coronal section 3.3 mm posterior to bregma. Immunohistological staining for human nuclear filament in green revealed grafted cells within the inner granule cell arch and in the lateral ventricle.* ***d.*** *Coronal section 3.8 mm posterior to bregma. This is the most posterior and most ventral point of cell disposal. Scale bars: 200 µm. Pictures on left side derived from the Allen Mouse Atlas (Lein et al., 2007).*

4.4.4 Additional ventricular deposition of adenosine-releasing It-NES cells results in an increased after-discharge threshold in a kindling model of epilepsy

In addition to the diagonal grafting tract, it was also decided to switch the place of kindling from the amygdala to a position more anterior and dorsal within the hippocampus, thereby increasing the proximity of stimulation electrode and graft. New coordinates for transplantation of the stimulation electrode were 2,9 mm AP, 3 mm ML, and 3 mm DV. Kindling was again performed with WT cell-grafted, $ADK^{-/-}$ cell-grafted animals and sham controls, using the same parameters as for the amygdala kindling. Surprisingly, using these conditions resulted in a lack of afterdischarge generation in many of the animals. Of the sham group, 3 out of 7 animals were excluded, of the WT cell grafted group 2 out of 6 animals and of the $ADK^{-/-}$ cell grafted group 2 out of 5 animals because no AD could be generated. As result, animal numbers for each group were only small, leading to a high degree of variation as seen by the large standard error values in the diagrams (Fig. 4.15a). Animals which only received sham buffer showed weak responses to electrical stimulation while animals obtaining $ADK^{-/-}$ cells could be kindled as in previous experiments and developed stage 4 seizures in adequate time. Animals grafted with wildtype cells responded also well to kindling but did not reach values as high as the $ADK^{-/-}$ group. These results were not of the expected outcome, as adenosine-releasing grafts should decrease the severity and duration of seizure events. In the next experiment, a higher number of cells was grafted to facilitate a possible effect. Following suggestions of the Li publication (Li et al., 2007b), an additional graft was deposited in the lateral ventricle. From there, cells would spread over the whole right ventricle and also into the fissure between thalamus and hippocampus, thereby supporting the intra-hippocampal graft with adenosine efflux from outside the hippocampal structure. The kindling of this second diagonal grafting approach was performed with the same parameters as before (Fig. 4.15b). In this experiment, the sham group could be kindled much better and reached seizure stage 4 in the fourth week, while the $ADK^{-/-}$ cell grafted group still showed stronger seizures in respect to duration or class, not supporting the thesis. However, animals with $ADK^{-/-}$ cells needed a much higher electrical stimulation to generate seizures, as the evaluation of the afterdischarge threshold (ADT) revealed. A higher current had to be applied to provoke a reaction, resulting in a seizure that was stronger and lasted longer than in the sham animals stimulated at lower currents (Fig. 4.15c). The increase in ADT was significant compared to both sham and WT cell grafted groups only in the experiment with diagonal grafting and ventricular deposit, while values with diagonal grafting tract only were much lower and more even.

a

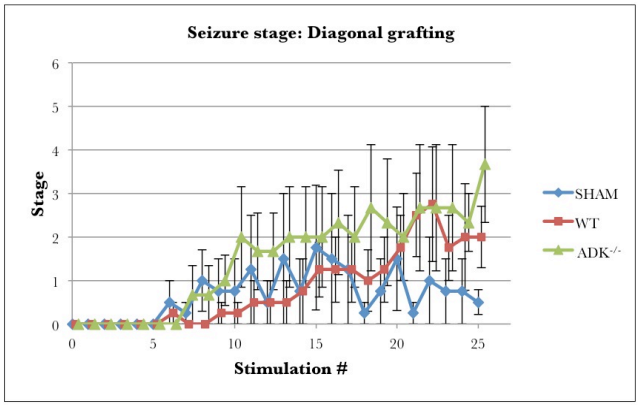

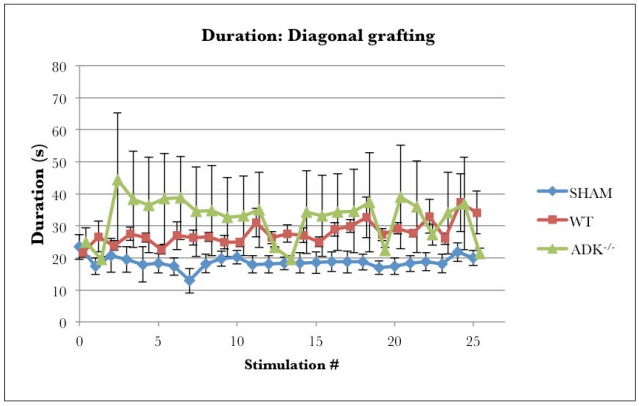

b

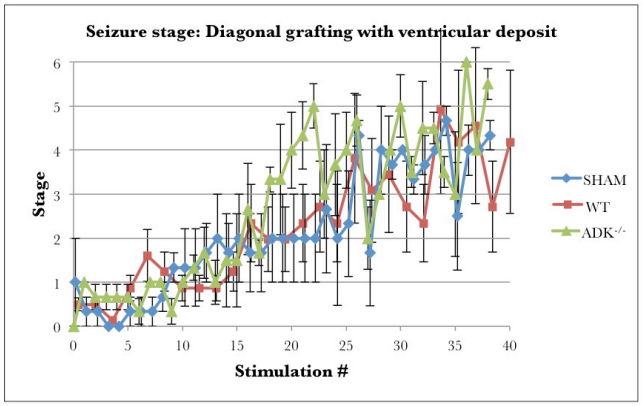

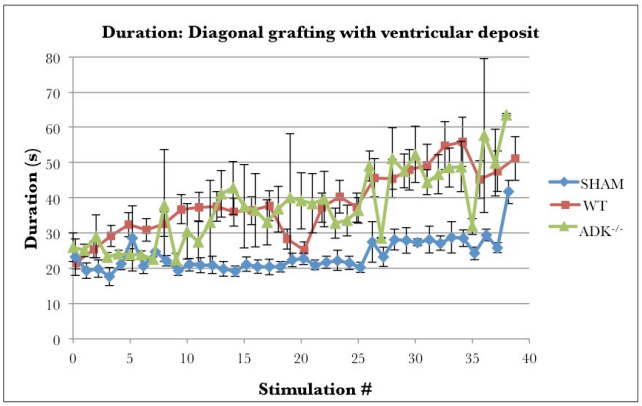

c

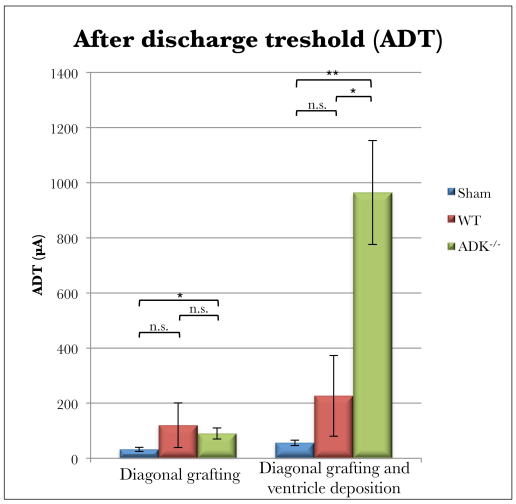

	Diagonal			Diagonal + Ventricle		
Group	Sham	WT	ADK-/-	Sham	WT	ADK-/-
ADT (µA)	32,50	120,00	90,00	56,00	226,67	964,29
SEM of ADT (µA)	7,50	80,83	20,00	9,80	146,67	188,58

Figure 4.15: Kindling of diagonally transplanted animals.
a. *Seizure class and seizure duration during 24 consecutive days of kindling in Rag2-/- mice grafted with wildtype, or ADK$^{-/-}$ lt-NES cells or buffer as sham control using a diagonal injection tract. No visual detectable seizures of the animals on the first 5 days of kindling could be observed. Especially the sham group did not reach seizure classes comparable to previous attempts. Size of groups: n_{SHAM} = 4, n_{WT} = 4, n_{KO} = 3.* ***b.*** *Seizure class and –duration of wildtype or ADK$^{-/-}$ lt-NES cells grafted and buffer sham control treated animals using one diagonal injection tract and an additional ventricular deposit. Again, the sham group did not behave optimal without increase in seizure duration during the experiment. Size of groups: n_{SHAM} = 5, n_{WT} = 4, n_{KO} = 7.* ***c.*** *Afterdischarge threshold after kindling procedure. Left group with diagonal grafting only while right group had also a ventricular deposition of either wildtype- or ADK$^{-/-}$ cells or buffer. ADT significantly increased with the additional ventricular deposit. Due to the small animal numbers of the WT group, SEM is quite high, not allowing any significant statistical differences compared to sham control.*

The results were subsequently correlated to the history of the brains after the experiment was terminated. Mouse brains showed prevalent indentations of the electrodes used, which were originally designed for use in much larger rats (Fig. 4.16a). All animals were analyzed with HE stainings to check for inflammation, scar formation or signs of intracranial hypertension, but no general damage to hippocampal structures could be detected. The grafts were found in the desired location (Fig. 4.16b), and immunohistochemical-staining was performed to address neuronal maturation and integration. A total of 6 animals had blood coagulates either at the stimulation electrode site or the cannula tract, likely resulting from the removal of electrodes prior to sedating the animals for fixation. No augmented presence of astrocytes or immune cells was observed at the cannula tract. In 3 out of 30 animals used in this experiment, a leucocytic invasion deriving from the dural surface electrodes, which proceeded into the brain tissue, was found (Fig. 4.16c). The surface electrodes were fixed with screws in the dura, which could have irritated the surrounding tissue, thereby provoking an inflammation. All these injuries were found in sham animals, only receiving buffer. One general problem, which was found in around 25% of all animals irrespective to the grafted population, was that the location and the size of the stimulation electrode led to a dissection of the whole hippocampal structure (Fig. 4.16d). Such a damage would very likely result in unexpected kindling responses. All animals that showed the mentioned obstacles were excluded from the experiment, but the overall result did not change. Noteworthy is, that besides the large cavities that were caused by the stimulation electrode, they were not colonized by grafted cells, which would also have very likely resulted in a kind of isolating effect on the stimulation currents.

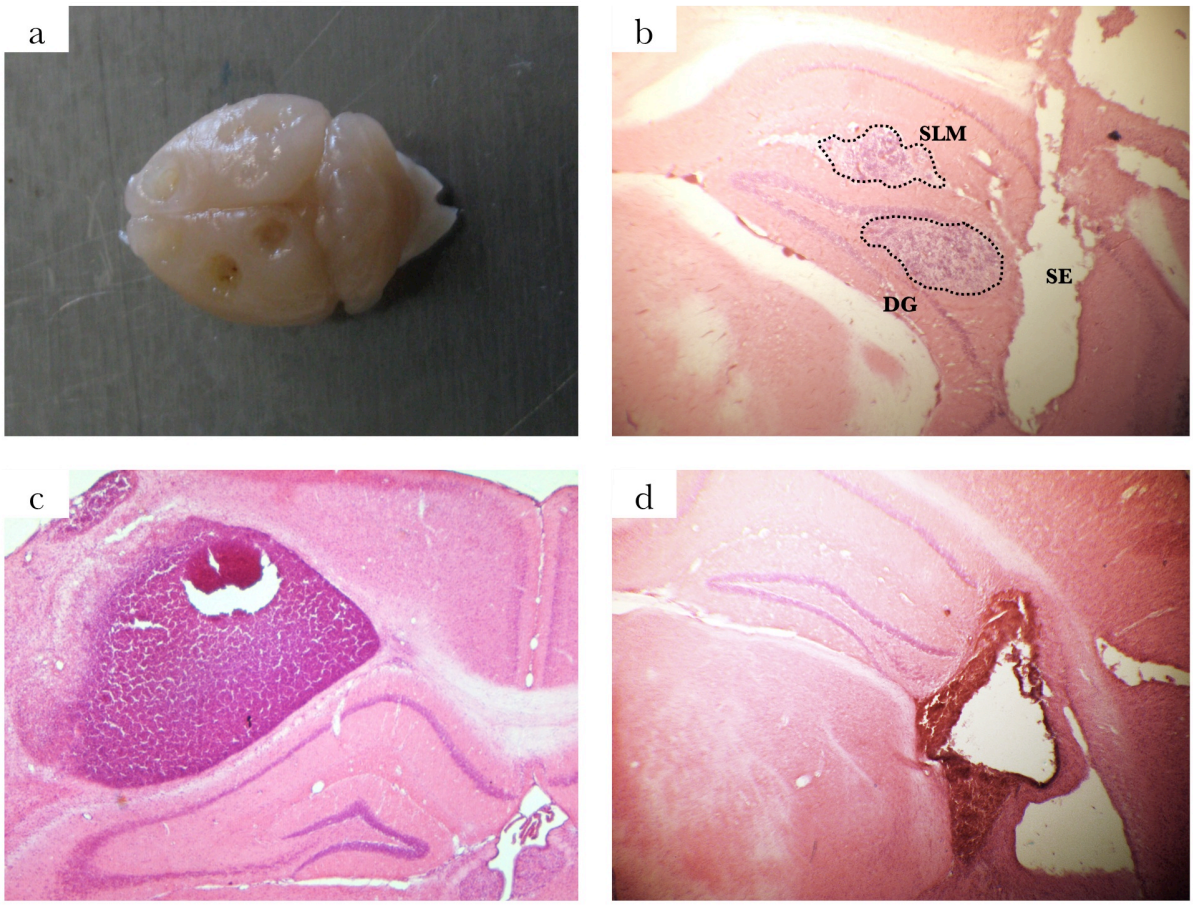

Figure 4.16: Histological analysis of animals after application of full kindling protocol.
a. *Brain of a kindled mouse after removal of the skullcap. The six electrodes used in each animal left clearly visible dents in the brain, extending up to 5 mm into the tissue. This irritation of brain tissue is further shown in the following sections.* ***b.*** *Coronal section 2.6 mm posterior to bregma. HE staining showed the delivery of cells (graft is indicated by dotted line) into the hippocampus within the polymorph layer of the dentate gyros (DG) and the stratum lacunosum-moleculare (SLM). Overall structure of HC is intact beside the former location of the stimulation electrode, as seen by the large rupture lateral to the graft (SE).* ***c.*** *In two animals, leucocytic invasions of the contralateral striatum were found, invading the tissue from the site where subdural measuring electrodes were placed.* ***d.*** *In around a quarter of total animals, placement of the stimulation electrode dissected the whole hippocampus within a coronal section.*

5 Discussion

5.1 AAV-mediated gene targeting in lt-NES cells

We recently showed the generation of patient-specific neurons differentiated from lt-NES of patients with Machado-Joseph disease (Koch et al., 2011). Patient-specific cells show an elongation of CAG repeats in exon 10 of the *ATXN3* gene, resulting in a polyQ-elongated variant of ataxin-3 protein. The first genetic modification of this study used engineered adeno-associated virus to exchange the expanded allele of the *ATXN3* gene with its wildtype variant. The applied method was found to be highly efficient and resulted in clones that no longer possessed the pathogenic variant of *ATXN3*/ataxin-3 on a genomic or protein level. After Cre-mediated excision of the selection cassette, both alleles showed expression of the wildtype protein. The gene-corrected lt-NES cells had the same morphological characteristics as the founder cells and could be efficiently differentiated into human neurons, which is the cell type affected by the disease. These results show that AAV particles are a powerful tool even for complex genetic manipulations (Fig 5.1).

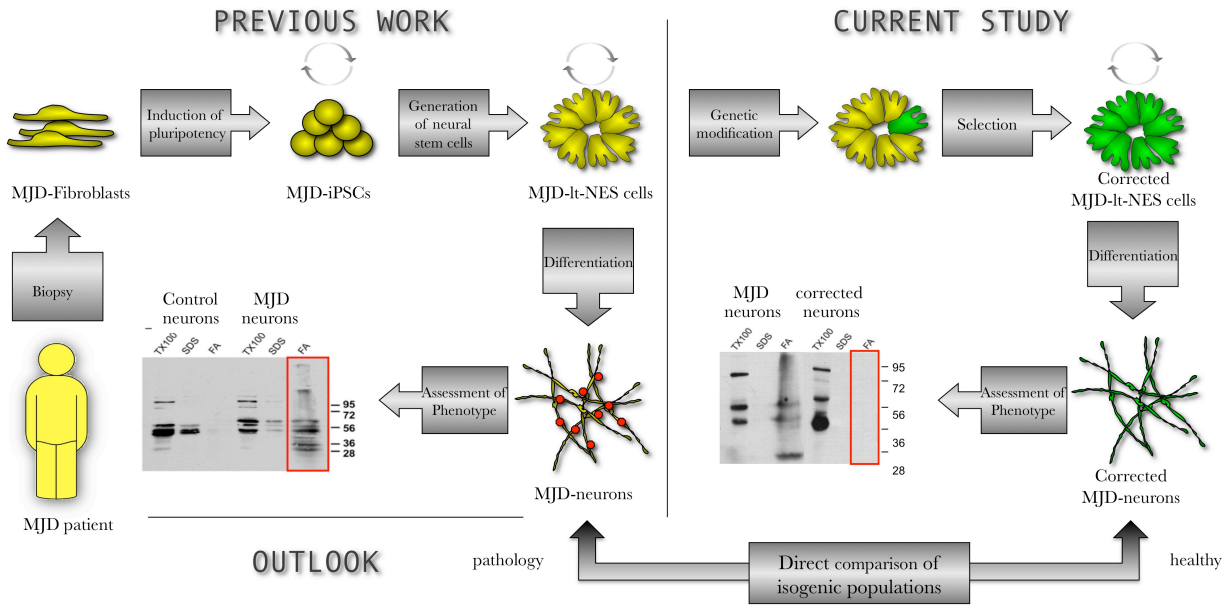

Figure 5.1: Overview of AAV-mediated gene correction in context of previous and perspective work.

It is interesting to note that before using zinc finger nucleases, targeting of the adenosine kinase gene was tried with AAV vectors, similar to the approach used for the *ATXN3* targeting. Yet, several attempts were not successful, very likely because of the genome structure of the ADK gene contains large introns bearing a lot of repetitive sequences, making it difficult to find long homologous sequences needed for AAV targeting (Khan et al., 2011). Zinc finger nucleases on the contrary only need a relatively small DNA sequence to act site-directed, which can be a large advantage in some genes as seen with the ADK locus. This example already shows that despite its many advantages, AAV-mediated targeting is not possible in every locus to the same extent.

The vast majority of analyzed clones generated during this study showed the exchange of the expanded allele against the virally offered wildtype variant, although homology to the allele of physiological length was higher and thus expected to consequentially be targeted more often. It has been reported that long tracts of CAG repeats can lead to a change in chromatin structure and histone packaging (Wang et al., 1994), and in yeast it was shown that CAG repeats increase the spontaneous exchange of unequal sister-chromatids (Nag et al., 2004). Such an exchange is mediated by the machinery for homologous recombination (Sonoda et al., 1999), which is also needed for AAV-mediated targeting (Vasileva et al., 2006). This raises the possibility that similar mechanisms are responsible for the higher crossing-over efficiencies at the pathogenic allele of the *ATXN3* gene.

5.2 Gene corrected human neurons

Very recently, Ellerby and coworkers presented the genetic correction of Huntington's disease (HD) in iPS cells (An et al., 2012). In HD, just as with MJD, the elongation of CAG repeats within the HTT gene is disease-causative. Via BAC-mediated homologous recombination, the expanded allele was exchanged against a wildtype variant, a technique that proved also to be highly efficient. Other successful site-specific modifications were achieved either with ZFNs by the group of Jaenisch and Zou with coworkers (Hockemeyer et al., 2009; Zou et al., 2009) or AAV-mediated corrections by the group of Russell (Khan et al., 2010). Although more and more examples of successful genome modification are found in the literature, all the above publications mentioned use pluripotent human cells. The use of neural stem cells as in this thesis allows a faster and easier generation of several monoclonal cell lines due to their clonal growth and shorter protocols to generate the differentiated cell type of investigation.

The gene-corrected neurons offer an ideal isogenic control population to the pathogenic MJD-neurons in order to elucidate underlying mechanisms of the disease, and how an

elongated ataxin-3 can mediate cell death of the affected neurons. These kinds of isogenic populations only differing in one specific locus offer new possibilities to overcome cell line specific differences of non-isogenic controls that could cloak disease-relevant subtle changes and should lead to a better understanding of neurodegenerative disorders in the human system. Normally, control cells for experiments with patient-specific iPS-cell derived populations are from healthy individuals, without knowing if such an individual would not suffer from a late-onset neurodegenerative disease several decades later. Additionally, even monogenetic diseases like MJD are affected in their time of onset or severity by many other factors, which can easily be seen by comparing numbers of CAG repeats in *ATXN-3* in patients, which can have as little as 45, while healthy individuals with up to 47 are known. In this overlapping region where the number of repeats alone is not sufficient to state if the disease will develop, a multifactorial nature which normally is more present in other diseases is seen. Accounting for this are SNPs or polymorphisms within the genome, of which many are not known or not studied enough to deduce any relations towards the disease studied. This means that any non-isogenic control population is a kind of black box with uncertain interactions with the studied genes, which can lead to false interpretation of data. A population only modified in one specific allele would allow the true study of functions and interactions of the one protein of interest.

Without reasonable tissue sources till recently, especially cell therapies of the central nervous system benefit immensely from stem cell-derived options. The recent advancements in the generation of patient-specific cell populations via reprogramming also offer possibilities for regenerative therapies. The combination of patient-derived iPS cells with genetic correction of the disease-associated genotype creates the potential to generate autologous cell populations for therapy. On the way towards a general application, highly efficient targeting techniques are needed. As demonstrated in this study, AAV-mediated targeting in combination with a promoterless selection cassette enables the generation of high numbers of clones with a very low number of false-positives, which will help to keep screening efforts to a minimum.

Importantly, the corrected MJD-lt-NES cells gave rise to mature neurons *in vitro*. Furthermore the described procedure reverses the phenotype of the diseased cells, which no longer showed the formation of microaggregates. Previous work with iPS- and ES-cell-derived lt-NES cells and the transplantation of $ADK^{-/-}$ lt-NES as part of this thesis showed that grafting into mice brains results in their maturation into functional neurons, which integrate into the host tissue and migrate along common commissural pathways in vivo (Steinbeck et al., 2011). These findings indicate the possibility of future cell therapeutic attempts.

The establishment of iPS technology enabled us to generate pluripotent cells of any person, and the generation of protocols to generate neural stem cell populations allowed us to generate unlimited numbers of human neurons. Combined application to patients suffering from neurological disorders gives us better possibilities to study disease mechanisms then ever before. The techniques presented in this thesis offer new possibilities not only for the elucidation of disease causation, but also perspective for curing it. The removal of disease-associated mutations or the genetic manipulation to generate a beneficial isogenic cell population prevents all immunogenic rejection problems arising in cell therapeutic approaches. Using a patients own cells, curing them and donating them back to eventually "heal" the person is still a long way off, but comes closer with recent developments in stem cell biology (Fig. 5.2).

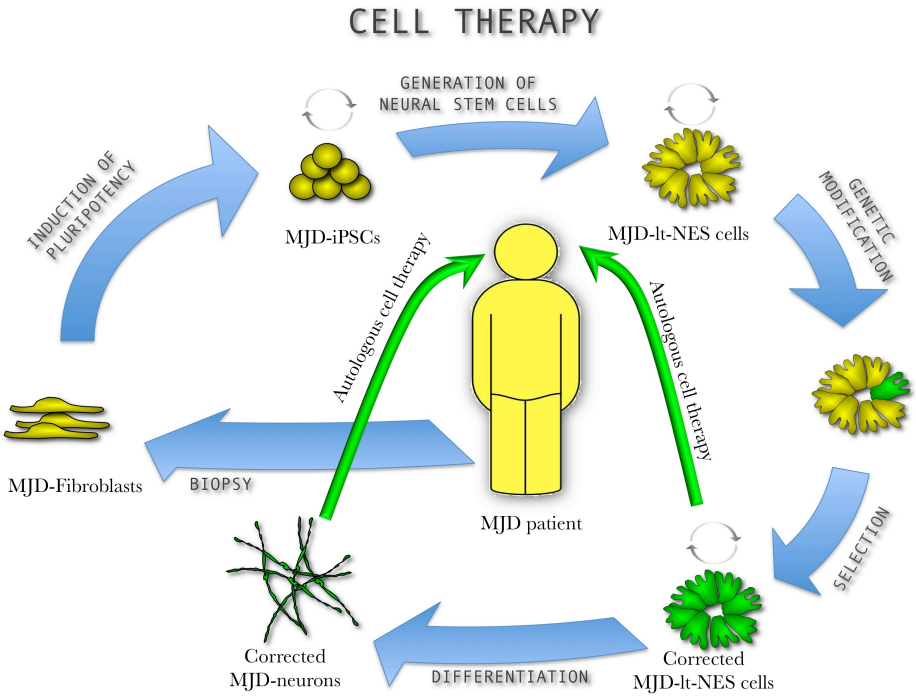

Figure 5.2: Cell therapeutic approach for the central nervous system using iPS-derived, genetically modified neural stem cell-derived neurons.
Fibroblasts are derived form a tissue biopsy from the patient. Under induction of pluripotency, iPS cells are generated, which can be differentiated into neural stem cells (lt-NESCs). They offer a population amenable to genetic manipulation. After enrichment of gene-corrected neural stem cells, they can either be directly delivered to the patients' central nervous system to mature in vivo into neurons to substitute for lost cell populations, or can be prematured in culture and delivered later.

5.3 Zinc finger nucleases for gene targeting in It-NES cells

For the second approach of site-specific genetic manipulation with zinc finger nucleases, the aim was to achieve a biallelic destruction of the adenosine kinase gene, resulting in the secretion of increased levels of adenosine by these cells. ZFNs as synthetic fusion proteins bind with their engineered zinc finger motif domain to a defined DNA sequence. When two of these zinc finger nucleases come into close proximity, a double strand break can be induced. The needed proximity is achieved by designing two ZFN proteins with DNA-binding motifs for sequences at short distance to each other. The induced break can subsequently lead to wrong corrections by the cellular DNA repair machinery. As selection was based on the missing enzymatic activity, only clones with double strand breaks leading to a frame shift and thus an incomplete enzyme translated from both targeted alleles were gained. Multiple monoclonal cell lines were gained, no longer expressing functional ADK enzyme, which as a consequence showed an increased secretion of adenosine into cell culture supernatants.

The destruction of genes in this manner is the easiest way to use the double strand break inducing activity of zinc finger nucleases. Additionally, an open double strand break facilitates the integration of other DNA fragments into the affected position, allowing the addition of genetic information. This has been successfully performed with small oligonucleotides, enabling introduction of single bases, for example for the exchange of amino acids within a gene (Chen et al., 2011a; Radecke et al., 2010). The integration of larger donors with multiple transgenes has also been shown, thereby offering selection capacities similar to viral systems but with the benefit of site-specific integration (DeKelver et al., 2010; Moehle et al., 2007; Zou et al., 2009). In the course of this study, introduction of a larger plasmid into the ADK gene was also attempted by cotransfecting it together with the ZFN coding plasmids to gain a selectable cassette, but integration events were very rare and only monoallelic integrations in the desired locus could be observed (data not shown).

To disrupt the adenosine kinase gene, the use of ZFNs was highly efficient and selection for targeting events by suicide drugs that needed to be metabolized through ADK to become toxic was comparable. If the targeted gene would be not an enzyme offering this possibility, enrichment for positives would become more complicated as short-term selection for transiently co-transfected selection markers or even the stable integration of a selection cassette would be needed.

5.4 Zinc finger nucleases (ZFNs) in comparison to Transcription activator-like effector nucleases (TALENs) and the Crispr/Cas9 system

Recently, another class of custom-made nucleases for gene targeting was described: the transcription activator-like effector nucleases, or TALENs (Cermak et al., 2011; Li et al., 2011). Similar to ZFNs, they consist of the same Fok1 nuclease domain fused to a DNA-binding domain of TAL effectors, and close proximity between two of them leads to nuclease-domain dimerization and thus induction of a double strand break. Like with zinc finger domains, recognition of a specific DNA sequence is achieved by generating a DNA-binding protein by linking together several modular TALE repeats. In contrast to zinc finger domains of 30 amino acids that each recognizes three base pairs, each TALE repeat consists of 34 amino acids and recognizes only a single base pair (Boch et al., 2009; Mak et al., 2012; Moscou and Bogdanove, 2009). This makes the generation of new DNA binding proteins much easier as only 4 different modules are needed to generate TALEs of any specificity compared to 64 different possible modules for zinc finger domains. Several protocols are available that describe the rapid assembly of custom TALE repeat arrays in only a few days using publicly available reagents (Cermak et al., 2011; Reyon et al., 2012; Zhang et al., 2011). In theory, development of ZFNs is also possible in a modular way, but often still needs a combination with 2-hybrid systems (Pruett-Miller et al., 2008) or phage display (Dreier et al., 2005), which is much more work intensive. This is one reason why many ZFNs used in the literature are industrially made, also because the involved biotech companies are rights holders for many proprietary methods for assembling zinc finger proteins.

Meanwhile, TALENs are now commercially available from companies such as Life Technologies. As TALENs are newer to the field, they have been much less studied than zinc finger proteins, and continued work is necessary to fully understand the strengths and weaknesses of the two different techniques. One weakness both technologies share is the danger of off-target cleavage. Again, information about ZFNs is more abundant than about TALENs. Off-target cleavage of zinc finger nucleases resulting in unwanted genetic changes or cytotoxicity has often been reported (Gabriel et al., 2011; Gupta et al., 2011; Pattanayak et al., 2011). Notably, not all of the double-stranded breaks could be predicted by *in silico* methods making its discovery even more complicated. As TALENs become more regularly used, reports about their off-target effects arise (Hockemeyer et al., 2011). In direct comparison of studies using both ZFNs and TALENs for the same target sequence, it is reported that off-target-cleavage related cytotoxicity is much lower in TALEN-treated cultures (Mussolino et al., 2011). Together with their easier assembly, it seems that most of site-directed nuclease approaches of the near future would rely on TALENs rather than on ZFNs.

Shortly after the introduction of TALENs, another system for double strand break induction was established: clustered regularly interspaced short palindromic repeats (Crispr) and their Crispr-related Cas nucleases, forming the Crispr/Cas9 system (Bhaya et al., 2011). This system is originally part of the adaptive immune system of bacteria and archaea, which uses short RNA to direct degradation of alien nucleic acids (Jinek et al., 2012). After modification, it has been shown to work with customized guide RNAs, directing the activity of Cas9 nuclease to a specific sequence in the human genome (Mali et al., 2013). The ease of the system is based on its guide RNAs: engineering of the binding motif of a protein is not required, as it is possible to directly integrate a short sequence into a targeting plasmid, which can easily be done using a quick cloning step. Within a short time, libraries for every gene of the human genome were established, making it very easy for everyone to use this new technology (Shalem et al., 2014; Zhou et al., 2014). One drawback in comparison to TALENS remains: based on its nature, the sequence of the guide RNA is not completely unrestricted, as it has to follow a certain pattern of 23 base pairs of the motif $GN_{20}GG$, thereby reducing the possible sites of application in the genome.

5.5 Genetic aberrations in cultivated stem cells and their progeny

It is not only the use of nucleases that can introduce genomic alterations. The generation of the initial pluripotent cell can incorporate damage into the genome, especially if induced by viral vectors (Nakagawa et al., 2008; Okita et al., 2007). Even the cultivation of pluripotent cells *in vitro* can lead to the accumulation of alterations as often reported (Howden et al., 2011; Maitra et al., 2005; Spits et al., 2008). After the generation of neural stem cells, these are reported to be more susceptible to other kinds of abnormalities in culture, some of which are also found in human tumors of the nervous system (Ben-David et al., 2011; Sartore et al., 2011). Finally, neural stem cells that have been through all of these protocols are subjected to ZFN treatment and clonal selection with toxic components to generate single clones that are used for transplantations into mice, where they are left to mature into neurons for several months. There are therefore many possibilities, and surely enough time, to develop an abnormal genotype. As seen in this study, it is important to carefully monitor the cell population gained by the application of double strand breaks for their chromosomal integrity. Many clones submitted to SNP analysis had prominent duplications or deletions. The selection process used to gain single clones is in part responsible for the enrichment of chromosomal aberrations. Clones of lt-NES cells are picked when they are large enough to be transferred into the next cell culture dish. This means that clones with a growth advantage are automatically the first to be picked, a growth advantage that may result from duplications

of oncogenes or deletions of tumor suppressors. This neoplastic enrichment is seen in the SNP analysis shown in Fig. 4.8: Clone A was derived from the first round of faster growing clones, while clone B was derived from the second round of clone picking, originally slower growing. Differences between the two populations could also be seen in culture, as clone A was growing faster and the media became acidic quicker. Differentiation into neurons was impaired in clone A, and instead the culture kept on proliferating. The same would likely happen within a mouse brain after grafting; a population like clone A could lead to overgrowth or tumor formation, not only diminishing the experiment but also causing avoidable pain to the receiving animal (Wislet-Gendebien et al., 2012). It can be asked if an Illumina chip SNP analysis is sufficient to detect all dangerous alterations, as translocations or single base pair mutations would not be apparent. Nevertheless, in our study it was sufficient, together with observation of the in vitro cultivation, to select for a clone without abnormal growth or differentiation behavior. Generally, phenotypic, functional and genetic assays should be performed on cells that were treated with nucleases before in vivo use to demonstrate whether their biological properties remain suitable for clinical applications. Ultimately, populations that are selected for transplantation might have to be sequenced completely, but with today's advances in sequencing technology, such levels of quality control are more and more broadly accessible.

5.6 ADK$^{-/-}$ It-NES cells as an adenosine releasing cell population

The basic idea of disrupting the adenosine kinase gene was to eliminate the strongest metabolizer of adenosine, thus increasing the total amount of adenosine present in the cells, which would be secreted into the subcellular space. This secretion into cell culture supernatants could be confirmed by using mass spectrometry, but only if the second-most important metabolizer, the enzyme adenosine deaminase (ADA), is inhibited with EHNA. The secretion of adenosine into media supernatants is not an ideal way to mimic an *in vivo* dispersion of adenosine, which is expected to bind to A1 receptors of host cells before being metabolized to inosine by adenosine deaminase. K_m values for interaction with A1 receptors are at least 5 times lower than for adenosine deaminase (Arch and Newsholme, 1978; Yan et al., 2003). In the hippocampus, ADA expression is quite low (Geiger and Nagy, 1986). Additionally, inosine is reported to have anticonvulsant properties acting differently from adenosine (Ganzella et al., 2011). Therefore the observation that adenosine levels after several hours at 37°C are strongly decreased if the adenosine deaminase is not blocked, was not surprising.

The generation of an $ADK^{-/-}/ADA^{-/-}$ double knockout by starting with an ADA-deficient iPS cell line (unpublished data) was also investigated. Despite multiple approaches, no cells could be produced (data not shown). Both adenosine kinase and adenosine deaminase metabolize adenosine as part of metabolic routes enabling the organism to salvage the degradation products of adenosine nucleotides, and recycle them back to nucleotide form. Disrupting both major biochemical pathways for adenosine consumption hinders the synthesis of nucleic acids and leads to an overload with adenosine, two conditions that seem to be toxic to the cells used here. This was also observed while incubating the ADK knock-out cells over more than 24h with EHNA, as this also resulted in complete cell death, while wild type cells were not affected by EHNA application.

5.7 The effect of grafted $ADK^{-/-}$ lt-NES cells in epileptic animals

In a kainic acid model of temporal lobe epilepsies, a trend towards less frequent seizure events compared to a wildtype control cell population was seen. More experiments are needed to conclude whether the ADK knock-out population has a positive effect on seizure development in this paradigm.

In the use of an electric kindling setting, one significantly different parameter between adenosine releasing cells, wildtype cells and sham controls was found as the after-discharge threshold was significantly increased in animals grafted with $ADK^{-/-}$ cells. Normally, during kindling the ADT decreases, making the induction of a seizure easier. At the same time, severity and duration of seizure events increase, which is why the method is called kindling; the increase in response to small stimuli is similar to the way small burning twigs can produce a large fire (Goddard et al., 1969). But what if the stimuli are not small any more but have to become bigger to result in an effect? What does such an increase indicate? Technically, a higher current was needed to provoke an epileptic seizure – but when a seizure was finally initiated it was stronger and lasted longer in these animals. Such insulating effects are observed at scar formation, when astrocytic tissue shields the stimulation electrode, which in turn can no longer act directly on the surrounding neural tissue (Griffith and Humphrey, 2006). Histological analysis of animals of this study after kindling did not show any indication of such a scar formation and thus, other explanations need to be discussed. Another possibility was that the long grafting tract could have damaged the hippocampus and thus led to a state in the buffer-receiving animals which could not longer be kindled, while in the cell-grafted mice the transplanted cells could have filled the damaged area. Also, as cells were grafted in total volumes of 4-5 μl, intracranial

hypertension could have resulted from the procedure and thus might have lead to damage to the brain, but also here, no histological indications for such damage could be found.

The transplantation of wildtype cells increased seizure frequency and duration, which is in contrast to previous reports that showed that grafting of “blank” neural stem cells reduces susceptibility to seizures in a rat kindling model (Shindo et al., 2010).

The most important mediator for the anticonvulsive function of adenosine is the A_1 receptor, whose activation leads to an inhibition of neural activity (Mareš, 2010). It has been reported for temporal lobe epilepsy in humans that A_1 receptors are lost (Glass et al., 1996) and a receptor down-regulation has also been shown to occur during status epilepticus (Hamil et al., 2012). In contrast, the function of the stimulating A_{2A} receptor remains controversial, as it can favor convulsions in certain conditions (Fukuda et al., 2011; Li and Henry, 1998). Reported changes in receptor expressions in kindled animals are also ambiguous, as a recent study depicted an increased expression of A_1 receptor mRNA in several brain areas as well as a decrease in striatal A_{2A} receptor mRNA in rats indicating an adaptive mechanism in the brain (Aden et al., 2004). The opposite results, however, were reported in another study where a decrease in A_1 receptors and increased density of A_{2A} receptor in cortices of rats undergoing amygdala kindling or kainate kindling were monitored (Rebola et al., 2005). Such changes in receptor expression need a certain amount of time. The length of time between grafting and beginning of kindling may be of importance. In the experiments shown, lt-NES cells were given 4 weeks to mature into neurons and innervate the host tissue before kindling started. Most of the studies using adenosine administration for epilepsy treatment, either by sponges, cells or micropumps, were monitored for around just 2 weeks after starting of kindling (Boison et al., 1999; Huber et al., 2001; Li et al., 2007b; Szybala et al., 2009; Van Dycke et al., 2010; Wilz et al., 2008) This time frame coincided with the dry-run of the sponge or the elimination of cells, but also could give a hint that longer time intervals are problematic due to other reasons. With a time frame of 4 weeks it is possible that the critical time window for significant effects has passed, and the permanently higher adenosine level had finally lead to a receptor down regulation, thereby terminating the desired effect before it could be seen on the EEG.

Another explanation could be that the wrong parameters were looked for. The kindling model normally uses the same current which was initially high enough to induce a reaction, throughout the course of the experiment. If antiepileptic effects were present, they emerged by decreased seizure classes and seizure durations over time. In the kindling model used in this study, afterdischarge threshold increased, and the used current was subsequently raised to again provoke a reaction. Increased afterdischarge thresholds were reported for other conditions in the kindling model. After performing kainic acid treatment in rats, kindling of the

epileptic animals resulted in a higher ADT, which was interpreted as a result of natural protective mechanisms, that the epileptic brain develops to suppress seizure activity following the kainate-induced alterations in connectivity and neuronal architecture (Bragin et al., 2002). This would indicate that our cell population mimics such protective mechanisms, maybe by the adenosine increase. Another example is the increase in ADT seen while applying an A_1 receptor agonist as anticonvulsive drug (Potschka et al., 1998). Hereby, duration and severity of seizures were also not improved after applying higher currents to overcome the higher ADT value. Based on mathematical exclusion of all animals with an ADT increase of more than 20 %, they declared their drug to be anticonvulsive. Using the same calculations with our experiment would result in 77,8 % of animals to be named protected from seizures. Another study used adenosine-releasing encapsulated myoblasts that were grafted into the lateral ventricle after animals were fully kindled (Güttinger et al., 2005). Further application of the same electrical current that was used before to kindle the rats showed no effect in animals which received a transplant. It is very likely, that here also the afterdischarge threshold was strongly increased, although it was not mentioned in the study. Using the same paradigm to not increase the currents after kindling started, the experiments performed during this study would declare the used $ADK^{-/-}$ lt-NES cells as acting anticonvulsively.

Taken together, the current literature suggests that an increase in afterdischarge threshold indicates a lower susceptibility towards seizure initiation. Epilepsy can be seen as the state of a neuronal network that shows lower resistance to initial electric stimuli. If larger currents and thus larger stimuli are needed to provoke a seizure, they are harder to generate and thus less likely to occur by coincidence. It is not wrong to call a procedure that increases the energy needed to induce seizures anti-epileptic. As animals in the kindling model show no spontaneous seizures, the use of other epilepsy models would be preferred to validate this conclusion in a better resemblance to the human clinical picture.

5.8 The immune system and epilepsy

Many epileptic events lead to neurodegeneration followed by inflammation (Kan et al., 2012). Concurrently, proinflammatory stimuli exhibit proconvulsant properties (Auvin et al., 2010). This reciprocal amplification is an important promoter of epileptogenesis. To what amount the immune response is accountable for the function of epileptic models is of importance, as the grafting of human cells into mice makes it either necessary to immunosuppress the recipients or to use genetically immunodeficient mouse strains. The first option is not only difficult in regards of handling of the animals, as epileptic animals are much more aggressive than

normal ones, but immunosuppressants such as ciclosporin also have an influence on epileptogenesis and may also cause seizures by themselves in human patients (Navarro et al., 2010; Saner et al., 2010).

Using immunodeficient mice with Rag2 knockout, two important differences were seen in comparison to standard C57/Bl/6 mice. First, kindling was in the beginning not very efficient in regard to seizure development, and second, and more importantly, it was not possible to generate pilocarpine-induced epileptic animals. BALB/c nude mice in a pilocarpine model were reported to be much more vulnerable to status epilepticus (Vignoli et al., 2012) and this may also be the reason for the loss of all $Rag2^{-/-}$ animals in the weeks following pilocarpine treatment in the experiment performed during this study.

Overall, the multiple interactions between the immune system and epilepsy add an additional degree of complexity to the combination of human cell grafting and animal models of epilepsy.

5.9 General conclusion

This study proved that lt-NES cells are very amenable to genetic manipulation, as shown by two different methods. By AAV-mediated targeting, gene correction of the expanded allele of *ATXN3* with its wildtype variant was performed, resulting in a cell population liberated from its pathogenic phenotype. Via ZFN-mediated disruption of the *ADK* gene, an adenosine-releasing cell population with potential anti-convulsive qualities was generated. Both techniques proved to be very efficient to generate a multitude of monoclonal cell lines if combined with a strong selection method. The generated modified lt-NES cells could be differentiated into mature neurons and survived after grafting into animals for several months. Being an isogenic control population, they will offer a valuable addition to current experiments aiming at the deciphering of disease mechanisms and also offer the possibility of future cell therapeutic attempts. Applied to patient-derived iPSCs, such techniques offer new opportunities to generate cell populations that have beneficial effects after autologous transplantation.

5.10 Perspective

The cell populations established during this study form the basis for further investigations. Peculiarly in the neuroscience field, a large fraction of disorders is of late-onset, which - in the limited time of cell culture experiments - presumably results in differences that maybe cannot be distinguished from background-related variations. Isogenic control lines already

set the benchmark for analyses of disease-modeling approaches using iPSC technology, especially where high sensitivity is important.

The indications for antiepileptic activity of adenosine-releasing cells should be addressed in further animal experiments with higher number of animals. It is conceivable that both localization of the grafts or the neural subtype of the grafted cells have an effect on anti-epileptic or anti-epileptogenic abilities. Indications that GABAergic interneurons render a suitable population for antiepileptic cell therapy suggest to further improve differentiation into a more specific interneuron subtype, as most lt-NES cell-derived neurons already are GABAergic following the default differentiation protocol (Cunningham et al., 2014).

The establishment of isogenic control lines of MJD patients allows to conduct a large array of comprehensive experiments: The fixed genetic background with differences in only one specific locus allows for expression profiling methods like DNA microarrays or RNA-seq with much lower background noise and thus higher significance in finding differentially expressed genes. The discrimination between disease-related and background effects is of utmost importance, considering that approximately 5% of all genes are differently expressed due to genetic variation, not even accounting for reprogramming-associated variances (Montgomery et al., 2010; Pickrell et al., 2010).

Gene targeting would also allow generating isogenic populations only expressing the pathogenic allele – for the investigation of MJD this could for example be used to explore differences in protein-protein interactions compared to physiological ataxin-3 or on functionality of the elongated variant by its own. As it is very unlikely that both alleles of *ATXN3* share the same number of CAG repeats, the investigation of ataxin-3 function normally is the result of a combination of two different variants. With the tools developed during this study, it should be possible to extent research on ataxin-3 function to different kinds of polyQ length in an isogenic, one-variant setting.

6 Abbreviations

Abbreviation	Full name
ADA	Adenosine desaminase
ADK	Adenosine kinase
ADT	Afterdischarge threshold
Ado	Adenosine
AMPA	α-Amino-3-hydroxy-5-methyl-4-isoxazolepropionic acid receptor
ATP	Adenosin triphosphate
ATXN3	Ataxin-3
BMP	Bone morphogenic protein
cAMP	Cyclic adenosine monophosphate
CD	Cluster of differentiation
CNS	Central nervous system
DABCO	1,4-Diazabicyclo[2.2.2]octan
Dach1	Dachshund homolog 1
DAPI	4',6-Diamidino-2-phenylindole
DAPT	N-[N-(3,5-Difluorophenacetyl)-L-alanyl]-S-phenylglycine t-butyl ester
DMSO	Dimethyl suphoxide
dNTPs	Nucleoside triphosphate
EB	Embryoid body
EDTA	Ethylenediaminetetraacetic acid
EGF	Epidermal growth factor
EGFP	Enhanced green fluorescent protein
ER	Endoplasmatic reticulum
FCS	Fetal calf serum
FGF	Fibroblast growth factor
GFAP	Glial fibrillary acidic protein
GMP	Guanosine monophosphate
HD	Huntington's disease
HEK	Human embryonic kidney
hES cell	Human embryonic stem cell
hPS cell	Human pluripotent stem cell

Abbreviation	Full name
Ino	Inosine
iPS cell	Induced pluripotent stem cell
IRES	Internal ribosomal entry site
KA	Kainic acid
LIF	Leukemia inhibitory factor
Ln	Laminin
lt-NES cell	long-term self-renewing neuroepithelial stem cell
MAP	Microtubuli-associated protein
MEF	Mouse embryonic fibroblast
miRNA	micro RNA
MJD	Machado Joseph disease
mRNA	messenger RNA
NE	Neuroepithelia
neoR	Neomycin resistance
NMDA	N-Methyl-D-aspartic acid
PAGE	Polyacrylamid gel electrophoresis
PBS	Phosphate buffered saline
PCR	Polymerase chain reaction
PFA	Paraformaldehyde
PO	Poly-ornithine
puroR	Puromycin restance
RNA	Ribonucleic acid
RT-PCR	Reverse-transcriptase PCR
SCA3	Spinocerebellar ataxia type 3
SDS	Sodium dodecyl sulphate
SHH	Sonic Hedgehog
siRNA	small interfering RNA
SMAD	Mothers against decapentaplegic homolog
Sox2	SRY-box 2
SVZ	Subventricular zone
TC	Tissue culture
TE	Trypsin/EDTA
TEMED	Tetramethylethylenediamine

Abbreviation	Full name
TF	Transcription factor
TGFβ	Transforming growth factor β
TI	Trypsin inhibitor
ZFN	Zinc finger nuclease
ZO1	Zona occludens 1

7 Abstract

Modern stem cell technology has made remarkable progress in recent years with the discovery of induced pluripotency, enabling the production of any cell type from any person in unlimited quantities, as well as improved protocols for the generation of stable neural stem cells to generate all cells of the central nervous system. This forms the base to examine neurons derived from patients of neurodegenerative diseases in vitro, allowing elucidation of disease mechanisms, as well as to regenerative production of neurons and other cells of the CNS. This study investigated two different techniques in order to achieve a specific genetic change in human neural stem cells, enabling the generation of modified neurons. A zinc finger nuclease (ZFN) attempt was used for the targeted destruction of the adenosine kinase gene (ADK) to obtain an adenosine releasing cell population comprising anti-epileptic properties. With recombinant adeno-associated virus (AAV), the Machado-Joseph disease (MJD) causing prolonged allele of ataxin-3 was replaced with the other allele of normal length. The destruction of the ADK gene by frame shifting in course of repairing the ZFN-induced double-strand break was confirmed by sequencing and Western blot analysis and led to a strong increase in adenosine efflux in neural stem cells, which was maintained after differentiation into neurons. Use of this cell population in mouse models of epilepsy to test the anticonvulsant properties have so far not led to a clear result. While due to small animal quantities in a kainate-induced model only a statistically non-significant trend toward reduced seizure frequency in animals with $ADK^{-/-}$ cells compared to wild type cells could be observed, in a model of electrical seizure induction (Kindling) animals showed a strongly increased resistance to the amount of current necessary to induce a seizure. After AAV-mediated exchange of the pathogenic *ATXN3*-allele against the physiological length, PCR and Western blot analysis confirmed the loss of extended transcript and protein variants in the cells. Following Cre-mediated removal of the selection cassette, a normal protein variant was transcribed from both alleles. MJD patient-derived neurons showed the formation of insoluble microaggregates following glutamate-induced activation. This aggregation was no longer detectable after gene correction. The method used consequently led to neurons, which no longer showed the disease phenotype. Both techniques used were highly efficient and produced very few false positive clones. These results indicate that neural stem cells are an ideal population for genetic manipulation and that the techniques used provide new perspectives for the study of disease mechanisms in the culture dish as well as open the field towards cell therapeutic applications.

8 Zusammenfassung

Die moderne Stammzell-Technologie hat in den letzten Jahren erstaunliche Fortschritte gemacht, insbesondere durch die Entdeckung der induzierten Pluripotenz, welche ermöglicht, von jedweder Person Zellen beliebiger Gewebe in unbegrenzten Mengen herzustellen. Zusätzlich erleichtern Protokolle, welche die Generierung von stabilen neuralen Stammzellpopulation aus diesen pluripotenten Zellen ermöglichen die Generierung von Zellen des Zentralnervensystems maßgeblich. Damit liegt das Werkzeug bereit, Neurone von Patienten neurodegenerativer Erkrankungen in der Zellkultur zu untersuchen um Krankheitsmechanismen zu erklären als auch regenerativ Neurone und andere Zellen des Gehirns herzustellen, um den Verlust dieser Zellpopulationen während der Erkrankung auszugleichen.

Diese Studie untersucht zwei verschiedene Techniken, um eine gezielte genetische Veränderung in neuralen Stammzellen zu erreichen, welche die Generierung veränderter Neurone ermöglicht. Zum einen wurden Zinkfinger-Nukleasen (ZFN) zur gezielten Zerstörung des Adenosinkinase-Gens (ADK) verwendet, um eine Adenosin-ausschüttende Zellpopulation zu erhalten, die antiepileptische Eigenschaften aufweist. Des weiteren wurde mittels rekombiniertem Adeno-assoziierten Virus (AAV) das Machado-Joseph Krankheit (MJD)-auslösende, verlängerte Allel von Ataxin-3 gegen das andere Allel normaler Länge ausgetauscht.

Die Zerstörung des ADK-Gens durch Verschieben des Leserahmes bei der Reparatur des ZFN-induzierten Doppelstrangbruches konnte mittels Sequenzierung und Western Blot gezeigt werden und bewirkte eine starke Erhöhung des Adenosin-Ausstoßes in neuralen Stammzellen, welcher auch nach Differenzierung zu Neuronen und Astrozyten erhalten blieb. Verwendung der Zellpopulation in Epilepsiemodellen der Maus zur Prüfung der antikonvulsiven Eigenschaften führten bislang zu keinem eindeutigen Ergebnis. Während aufgrund kleiner Tiermengen in einem Kainat-induziertem Modell lediglich ein statistisch nicht signifikanter Trend in Richtung reduzierter Anfallshäufigkeit in Tieren mit $ADK^{-/-}$ Zellen im Vergleich zu wildtypischen Zellen beobachten werden konnte, zeigten Tiere in einem Modell von elektrischer Anfallsinduktion (Kindling) einen stark erhöhten Widerstand gegenüber der notwenigen Stromstärke, die nötig war um einen Anfall zu induzieren.

Nach AAV-vermittelten Austausch des pathogen *ATXN3*-Alleles gegen eine physiologische Länge waren durch PCR und Western Blot keine verlängerten Transkript- und Proteinvarianten in den Zellen mehr auffindbar. Durch Cre-vermittelte Entfernung der Selektionskassette wurde von beiden Allelen die normale Proteinvariante transkribiert. Von

MJD-Patienten abgeleitete Neurone zeigten zuvor die Bildung von unlöslichen Mikroaggregaten nach Glutamat-induzierter Aktivierung. Diese Aggegratbildung war nach der Genkorrektur nicht mehr nachweisbar. Die verwendete Methode führte folglich zu Neuronen, die keinen krankheitstypischen Phänotyp mehr zeigten.

Beide verwendeten Techniken waren hocheffizient und erzeugten nur sehr wenige falsch-positive Klone. Diese Ergebnisse zeigen, dass neurale Stammzellen eine ideale Population zur genetischen Manipulation sind und die verwendeten Techniken neue Perspektiven für die Erforschung von Krankheitsmechanismen in der Kulturschale liefern als auch die Möglichkeit zelltherapeutischer Applikationen eröffnen.

9 References

Abranches, E., Silva, M., Pradier, L., Schulz, H., Hummel, O., Henrique, D., Bekman, E., and Parise, G. (2009). Neural Differentiation of Embryonic Stem Cells In Vitro: A Road Map to Neurogenesis in the Embryo. PLoS ONE *4*, e6286.

Amit, M., Carpenter, M.K., Inokuma, M.S., Chiu, C.P., Harris, C.P., Waknitz, M.A., Itskovitz-Eldor, J., and Thomson, J.A. (2000). Clonally derived human embryonic stem cell lines maintain pluripotency and proliferative potential for prolonged periods of culture. Dev. Biol. *227*, 271-278.

An, M.C., Zhang, N., Scott, G., Montoro, D., Wittkop, T., Mooney, S., Melov, S., and Ellerby, L.M. (2012). Genetic Correction of Huntington's Disease Phenotypes in Induced Pluripotent Stem Cells. Cell Stem Cell *2*, 253-263.

Anokye-Danso, F., Trivedi, C.M., Juhr, D., Gupta, M., Cui, Z., Tian, Y., Zhang, Y., Yang, W., Gruber, P.J., Epstein, J.A., and Morrisey, E.E. (2011). Highly Efficient miRNA-Mediated Reprogramming of Mouse and Human Somatic Cells to Pluripotency. Cell Stem Cell *8*, 376-388.

Arch, J.R., and Newsholme, E.A. (1978). Activities and some properties of 5'-nucleotidase, adenosine kinase and adenosine deaminase in tissues from vertebrates and invertebrates in relation to the control of the concentration and the physiological role of adenosine. Biochem. J. *174*, 965-977.

Arrasate, M., Mitra, S., Schweitzer, E., Segal, M., and Finkbeiner, S. (2004). Inclusion body formation reduces levels of mutant huntingtin and the risk of neuronal death. Nature *431*, 805-810.

Athanasopoulos, T., Graham, I., Foster, H., and Dickson, G. (2004). Recombinant adeno-associated viral (rAAV) vectors as therapeutic tools for Duchenne muscular dystrophy (DMD). Gene. Ther. *11 Suppl 1*, S109-121.

Auvin, S., Mazarati, A., Shin, D., and Sankar, R. (2010). Inflammation enhances epileptogenesis in the developing rat brain. Neurobiol. Dis. *40*, 303-310.

Ban, H., Nishishita, N., Fusaki, N., Tabata, T., Saeki, K., Shikamura, M., Takada, N., Inoue, M., Hasegawa, M., Kawamata, S., and Nishikawa, S. (2011). Efficient generation of transgene-free human induced pluripotent stem cells (iPSCs) by temperature-sensitive Sendai virus vectors. Proc. Natl. Acad. Sci. USA *108*, 14234-14239.

Barnes, M., Freudenberg, J., Thompson, S., Aronow, B., and Pavlidis, P. (2005). Experimental comparison and cross-validation of the Affymetrix and Illumina gene expression analysis platforms. Nucleic Acids Res. *33*, 5914-5923.

Ben-David, U., Mayshar, Y., and Benvenisty, N. (2011). Large-scale analysis reveals acquisition of lineage-specific chromosomal aberrations in human adult stem cells. Cell Stem Cell *9*, 97-102.

Berke, S., Chai, Y., Marrs, G.L., Wen, H., and Paulson, H.L. (2005). Defining the role of ubiquitin-interacting motifs in the polyglutamine disease protein, ataxin-3. J. Biol. Chem. *280*, 32026-32034.

Berman, R.F., Fredholm, B.B., Aden, U., and O'Connor, W.T. (2000). Evidence for increased dorsal hippocampal adenosine release and metabolism during pharmacologically induced seizures in rats. Brain Res. *872*, 44-53.

Beutler, E. (1993). Gaucher disease as a paradigm of current issues regarding single gene mutations of humans. Proc. Natl. Acad. Sci. USA *90*, 5384-5390.

Bevivino, A.E., and Loll, P.J. (2001). An expanded glutamine repeat destabilizes native ataxin-3 structure and mediates formation of parallel beta -fibrils. Proc. Natl. Acad. Sci. USA *98*, 11955-11960.

Bhaya, D., Davison, M., and Barrangou, R. (2011). CRISPR-Cas systems in bacteria and archaea: versatile small RNAs for adaptive defense and regulation. Annu. Rev. Genet. *45*, 273-297.

Bibikova, M., Carroll, D., Segal, D.J., Trautman, J.K., Smith, J., Kim, Y.G., and Chandrasegaran, S. (2001). Stimulation of homologous recombination through targeted cleavage by chimeric nucleases. Mol. Cell Biol. *21*, 289-297.

Boch, J., Scholze, H., Schornack, S., Landgraf, A., Hahn, S., Kay, S., Lahaye, T., Nickstadt, A., and Bonas, U. (2009). Breaking the code of DNA binding specificity of TAL-type III effectors. Science *326*, 1509-1512.

Boeddrich, A., Gaumer, S., Haacke, A., Tzvetkov, N., Albrecht, M., Evert, B.O., Müller, E., Lurz, R., Breuer, P., Schugardt, N., Plassmann, S., Xu, K., Warrick, J.M., Suopanki, J., Wüllner, U., Frank, R., Hartl, U., Bonini, N., and Wanker, E. (2006). An arginine/lysine-rich motif is crucial for VCP/p97-mediated modulation of ataxin-3 fibrillogenesis. EMBO J. *25*, 1547-1558.

Boison, D., Scheurer, L., Tseng, J.L., Aebischer, P., and Mohler, H. (1999). Seizure suppression in kindled rats by intraventricular grafting of an adenosine releasing synthetic polymer. Exp. Neurol. *160*, 164-174.

Bongso, A., Fong, C.Y., Ng, S.C., and Ratnam, S. (1994). Isolation and culture of inner cell mass cells from human blastocysts. Hum. Reprod. *9*, 2110-2117.

Bragin, A., Wilson, C., and Engel, J. (2002). Increased afterdischarge threshold during kindling in epileptic rats. Exp. Brain. Res. *144*, 30-37.

Breunig, J.J., Haydar, T.F., and Rakic, P. (2011). Neural stem cells: historical perspective and future prospects. Neuron *70*, 614-625.

Brinkman, R.R., Mezei, M.M., Theilmann, J., Almqvist, E., and Hayden, M.R. (1997). The likelihood of being affected with Huntington disease by a particular age, for a specific CAG size. Am. J. Hum. Genet. *60*, 1202-1210.

Bunz, F. (2002). Human cell knockouts. Curr. Opin. Oncol. *14*, 73-78.

Burnett, B., Li, F., and Pittman, R.N. (2003). The polyglutamine neurodegenerative protein ataxin-3 binds polyubiquitylated proteins and has ubiquitin protease activity. Hum. Mol. Genet. *12*, 3195-3205.

Burnett, B.G., and Pittman, R.N. (2005). The polyglutamine neurodegenerative protein ataxin 3 regulates aggresome formation. Proc. Natl. Acad. Sci. USA *102*, 4330-4335.

Carpenter, M.K., Inokuma, M.S., Denham, J., Mujtaba, T., Chiu, C.P., and Rao, M.S. (2001). Enrichment of neurons and neural precursors from human embryonic stem cells. Exp. Neurol. *172*, 383-397.

Cartwright, P. (2005). LIF/STAT3 controls ES cell self-renewal and pluripotency by a Myc-dependent mechanism. Development *132*, 885-896.

Cermak, T., Doyle, E.L., Christian, M., Wang, L., Zhang, Y., Schmidt, C., Baller, J.A., Somia, N.V., Bogdanove, A.J., and Voytas, D. (2011). Efficient design and assembly of custom TALEN and other TAL effector-based constructs for DNA targeting. Nucleic Acids Res. *39*, e82.

Chai, Y., Wu, L., Griffin, J.D., and Paulson, H.L. (2001). The role of protein composition in specifying nuclear inclusion formation in polyglutamine disease. J. Biol. Chem. *276*, 44889-44897.

Chambers, I., Colby, D., Robertson, M., Nichols, J., Lee, S., Tweedie, S., and Smith, A. (2003). Functional expression cloning of Nanog, a pluripotency sustaining factor in embryonic stem cells. Cell *113*, 643-655.

Chang, B.S., and Lowenstein, D.H. (2003). Epilepsy. N. Engl. J. Med. *349*, 1257-1266.

Chapman, M.S., and Rossmann, M.G. (1993). Structure, sequence, and function correlations among parvoviruses. Virology *194*, 491-508.

Chen, F., Pruett-Miller, S., Huang, Y., Gjoka, M., Duda, K., Taunton, J., Collingwood, T., Frodin, M., and Davis, G. (2011a). High-frequency genome editing using ssDNA oligonucleotides with zinc-finger nucleases. Nat. Methods *9*, 753-755.

Chen, G., Gulbranson, D.R., Hou, Z., Bolin, J., Ruotti, V., Probasco, M., Smuga-Otto, K., Howden, S.E., Diol, N.R., Propson, N., Wagner, R., Lee, G., Antosiewicz-Bourget, J., Teng, J., and Thomson, J. (2011b). Chemically defined conditions for human iPSC derivation and culture. Nat. Methods *8*, 424-429.

Chow, M.K., Mackay, J.P., Whisstock, J.C., Scanlon, M.J., and Bottomley, S.P. (2004). Structural and functional analysis of the Josephin domain of the polyglutamine protein ataxin-3. Biochem. Biophys. Res. Commun. *322*, 387-394.

Christ, M., Lusky, M., Stoeckel, F., Dreyer, D., Dieterle, A., Michou, A.I., Pavirani, A., and Mehtali, M. (1997). Gene therapy with recombinant adenovirus vectors: evaluation of the host immune response. Immunol. Lett. *57*, 19-25.

Colman, A., and Dreesen, O. (2009). Pluripotent Stem Cells and Disease Modeling. Stem Cell *5*, 244-247.

Colosimo, A., Goncz, K.K., Novelli, G., Dallapiccola, B., and Gruenert, D.C. (2001). Targeted correction of a defective selectable marker gene in human epithelial cells by small DNA fragments. Mol. Ther. *3*, 178-185.

Conti, L., and Cattaneo, E. (2010). Neural stem cell systems: physiological players or in vitro entities? Nat. Rev. Neurosci. *3*, 176-187.

Coutinho, P., and Andrade, C. (1978). Autosomal dominant system degeneration in Portuguese families of the Azores Islands. A new genetic disorder involving cerebellar, pyramidal, extrapyramidal and spinal cord motor functions. Neurology *28*, 703-709.

Cox, W.G., and Hemmati-Brivanlou, A. (1995). Caudalization of neural fate by tissue recombination and bFGF. Development *121*, 4349-4358.

Cunningham, M., Cho, J., Leung, A., Savvidis, G., Ahn, S., Moon, M., Lee, P.K., Han, J.J., Azimi, N., Kim, K., Bolshakov, V.Y., and Chung, S. (2014). hPSC-derived maturing GABAergic interneurons ameliorate seizures and abnormal behavior in epileptic mice. Cell Stem Cell *15*, 559-573.

DeKelver, R.C., Choi, V.M., Moehle, E.A., Paschon, D.E., Hockemeyer, D., Meijsing, S.H., Sancak, Y., Cui, X., Steine, E.J., Miller, J.C., Tam, P., Bartsevich, V.V., Meng, X., Rupniewski, I., Gopalan, S.M., Sun, H.C., Pitz, K.J., Rock, J.M., Zhang, L., Davis, G.D., Rebar, E.J., Cheeseman, I.M., Yamamoto, K.R., Sabatini, D.M., Jaenisch, R., Gregory, P.D., and Urnov, F.D. (2010). Functional genomics, proteomics, and regulatory DNA analysis in isogenic settings using zinc finger nuclease-driven transgenesis into a safe harbor locus in the human genome. Genome Res. *20*, 1133-1142.

DeLorenzo, R.J., Sun, D.A., Blair, R.E., and Sombati, S. (2007). An in vitro model of stroke-induced epilepsy: Elucidation of the roles of glutamate and calcium in the induction and maintenance of stroke-induced epileptogenesis. Int. Rev. Neurobiol. *81*, 59-84.

Delorenzo, R.J., Sun, D.A., and Deshpande, L.S. (2005). Cellular mechanisms underlying acquired epilepsy: the calcium hypothesis of the induction and maintainance of epilepsy. Pharmacol. Ther. *105*, 229-266.

Devinsky, O. (1999). Patients with refractory seizures. N. Engl. J. Med. *340*, 1565-1570.

Diakun, G.P., Fairall, L., and Klug, A. (1986). EXAFS study of the zinc-binding sites in the protein transcription factor IIIA. Nature *324*, 698-699.

do Carmo Costa, M., Bajanca, F., Rodrigues, A., Tomé, R., Corthals, G., Macedo-Ribeiro, S., Paulson, H.L., Logarinho, E., and Maciel, P. (2010). Ataxin-3 plays a role in mouse myogenic differentiation through regulation of integrin subunit levels. PLoS ONE *5*, e11728.

Doetschman, T., Maeda, N., and Smithies, O. (1988). Targeted mutation of the Hprt gene in mouse embryonic stem cells. Proc. Natl. Acad. Sci. USA *85*, 8583-8587.

Donaldson, K.M., Li, W., Ching, K.A., Batalov, S., Tsai, C.C., and Joazeiro, C.A. (2003). Ubiquitin-mediated sequestration of normal cellular proteins into polyglutamine aggregates. Proc. Natl. Acad. Sci. USA *100*, 8892-8897.

Doss-Pepe, E.W., Stenroos, E.S., Johnson, W.G., and Madura, K. (2003). Ataxin-3 interactions with rad23 and valosin-containing protein and its associations with ubiquitin chains and the proteasome are consistent with a role in ubiquitin-mediated proteolysis. Mol. Cell Biol. *23*, 6469-6483.

Dreier, B., Fuller, R.P., Segal, D.J., Lund, C.V., Blancafort, P., Huber, A., Koksch, B., and Barbas, C.F. (2005). Development of zinc finger domains for recognition of the 5'-CNN-3' family DNA sequences and their use in the construction of artificial transcription factors. J. Biol. Chem. *280*, 35588-35597.

Dunwiddie, T.V. (1999). Adenosine and suppression of seizures. Adv. Neurol. *79*, 1001-1010.

Dunwiddie, T.V., and Masino, S.A. (2001). The role and regulation of adenosine in the central nervous system. Annu. Rev. Neurosci. *24*, 31-55.

During, M.J., and Spencer, D.D. (1992). Adenosine: a potential mediator of seizure arrest and postictal refractoriness. Ann. Neurol. *32*, 618-624.

Dürr, A., Stevanin, G., Cancel, G., Duyckaerts, C., Abbas, N., Didierjean, O., Chneiweiss, H., Benomar, A., Lyon-Caen, O., Julien, J., Serdaru, M., Penet, C., Agid, Y., and Brice, A. (1996). Spinocerebellar ataxia 3 and Machado-Joseph disease: clinical, molecular and neuropathological features. Ann. Neurol. *39*, 490-499.

Elkabetz, Y., Panagiotakos, G., Al Shamy, G., Socci, N., Tabar, V., and Studer, L. (2008). Human ES cell-derived neural rosettes reveal a functionally distinct early neural stem cell stage. Genes Dev. *22*, 152-165.

Ellis, J., and Bernstein, A. (1989). Gene targeting with retroviral vectors: recombination by gene conversion into regions of nonhomology. Mol. Cell Biol. *9*, 1621-1627.

Engel, J. (1996). Surgery for seizures. N. Engl. J. Med. *334*, 647-652.

Eriksson, P.S., Perfilieva, E., Björk-Eriksson, T., Alborn, A.M., Nordborg, C., Peterson, D.A., and Gage, F.H. (1998). Neurogenesis in the adult human hippocampus. Nat. Med. *4*, 1313-1317.

Etherington, L.V., Patterson, G.E., Meechan, L., Boison, D., Irving, A.J., Dale, N., and Frenguelli, B.G. (2009). Astrocytic adenosine kinase regulates basal synaptic adenosine levels and seizure activity but not activity-dependent adenosine release in the hippocampus. Neuropharmacology *56*, 429-437.

Evert, B.O., Araujo, J., Vieira-Saecker, A.M., de Vos, R.A., Harendza, S., Klockgether, T., and Wüllner, U. (2006). Ataxin-3 represses transcription via chromatin binding, interaction with histone deacetylase 3, and histone deacetylation. J. Neurosci. *26*, 11474-11486.

Falk, A., Koch, P., Kesavan, J., Takashima, Y., Ladewig, J., Alexander, M., Wiskow, O., Tailor, J., Trotter, M., Pollard, S., Smith, A., and Brüstle, O. (2012). Capture of neuroepithelial-like stem cells from pluripotent stem cells provides a versatile system for in vitro production of human neurons. PLoS ONE *7*, e29597.

Fedele, D.E., Koch, P., Scheurer, L., Simpson, E.M., Möhler, H., Brüstle, O., and Boison, D. (2004). Engineering embryonic stem cell derived glia for adenosine delivery. Neurosci. Lett. *370*, 160-165.

Ferré, S., Borycz, J., Goldberg, S.R., Hope, B.T., Morales, M., Lluis, C., Franco, R., Ciruela, F., and Cunha, R. (2005). Role of adenosine in the control of homosynaptic plasticity in striatal excitatory synapses. J. Integr. Neurosci. *4*, 445-464.

Ferrigno, P., and Silver, P.A. (2000). Polyglutamine expansions: proteolysis, chaperones, and the dangers of promiscuity. Neuron *26*, 9-12.

Flotte, T.R., Solow, R., Owens, R.A., Afione, S., Zeitlin, P.L., and Carter, B.J. (1992). Gene expression from adeno-associated virus vectors in airway epithelial cells. Am. J. Respir. Cell Mol. Biol. *7*, 349-356.

Fox, K.R. (2000). Targeting DNA with triplexes. Curr. Med. Chem. *7*, 17-37.

Fredholm, B.B., Chen, J.F., Cunha, R.A., Svenningsson, P., and Vaugeois, J.M. (2005a). Adenosine and brain function. Int. Rev. Neurobiol. *63*, 191-270.

Fredholm, B.B., Chen, J.F., Masino, S.A., and Vaugeois, J.M. (2005b). Actions of adenosine at its receptors in the CNS: insights from knockouts and drugs. Annu. Rev. Pharmacol. Toxicol. *45*, 385-412.

Fukuda, M., Suzuki, Y., Hino, H., Morimoto, T., and Ishii, E. (2011). Activation of central adenosine A(2A) receptors lowers the seizure threshold of hyperthermia-induced seizure in childhood rats. Seizure *20*, 156-159.

Gabriel, R., Lombardo, A., Arens, A., Miller, J.C., Genovese, P., Kaeppel, C., Nowrouzi, A., Bartholomae, C., Wang, J., Friedman, G., Holmes, M., Gregory, P.D., Glimm, H., Schmidt, M., Naldini, L., and Von Kalle, C. (2011). An unbiased genome-wide analysis of zinc-finger nuclease specificity. Nat. Biotechnol. *29*, 816-823.

Gage, F. (2000). Mammalian Neural Stem Cells. Science *287*, 1433-1438.

Gales, L., Cortes, L., Almeida, C., Melo, C.V., Costa, M., Maciel, P., Clarke, D.T., Damas, A.M., and Macedo-Ribeiro, S. (2005). Towards a structural understanding of the fibrillization pathway in Machado-Joseph's disease: trapping early oligomers of non-expanded ataxin-3. J. Mol. Biol. *353*, 642-654.

Ganzella, M., Faraco, R.B., Almeida, R.F., Fernandes, V.F., and Souza, D.O. (2011). Intracerebroventricular administration of inosine is anticonvulsant against quinolinic acid-induced seizures in mice: an effect independent of benzodiazepine and adenosine receptors. Pharmacol. Biochem. Behav. *100*, 271-274.

Geiger, J.D., and Nagy, J.I. (1986). Distribution of adenosine deaminase activity in rat brain and spinal cord. J. Neurosci. *6*, 2707-2714.

Glaser, T., Perez-Bouza, A., Klein, K., and Brüstle, O. (2005). Generation of purified oligodendrocyte progenitors from embryonic stem cells. FASEB J. *19*, 112-114.

Glass, M., Faull, R.L., Bullock, J.Y., Jansen, K., Mee, E.W., Walker, E.B., Synek, B.J., and Dragunow, M. (1996). Loss of A1 adenosine receptors in human temporal lobe epilepsy. Brain Res. *710*, 56-68.

Goddard, G.V., McIntyre, D.C., and Leech, C.K. (1969). A permanent change in brain function resulting from daily electrical stimulation. Exp. Neurol. *25*, 295-330.

Gore, A., Li, Z., Fung, H., Young, J.E., Agarwal, S., Antosiewicz-Bourget, J., Canto, I., Giorgetti, A., Israel, M.A., Kiskinis, E., Lee, J., Loh, Y.H., Manos, P.D., Montserrat, N., Panopoulos, A.D., Ruiz, S., Wilbert, M.L., Yu, J., Kirkness, E.F., Izpisua Belmonte, J.C., Rossi, D.J., Thomson, J.A., Eggan, K., Daley, G.Q., Goldstein, L.S.B., and Zhang, K. (2011). Somatic coding mutations in human induced pluripotent stem cells. Nature *471*, 63-67.

Gouder, N., Scheurer, L., Fritschy, J.M., and Boison, D. (2004). Overexpression of adenosine kinase in epileptic hippocampus contributes to epileptogenesis. J.Neurosci. *24*, 692-701.

Griffith, R.W., and Humphrey, D.R. (2006). Long-term gliosis around chronically implanted platinum electrodes in the Rhesus macaque motor cortex. Neurosci. Lett. *406*, 81-86.

Gunawardena, S., Her, L.S., Brusch, R.G., Laymon, R.A., Niesman, I.R., Gordesky-Gold, B., Sintasath, L., Bonini, N., and Goldstein, L.S.B. (2003). Disruption of axonal transport by loss of huntingtin or expression of pathogenic polyQ proteins in Drosophila. Neuron *40*, 25-40.

Gupta, A., Meng, X., Zhu, L.J., Lawson, N.D., and Wolfe, S.A. (2011). Zinc finger protein-dependent and -independent contributions to the in vivo off-target activity of zinc finger nucleases. Nucleic Acids Res. *39*, 381-392.

Güttinger, M., Padrun, V., Pralong, W.F., and Boison, D. (2005). Seizure suppression and lack of adenosine A1 receptor desensitization after focal long-term delivery of adenosine by encapsulated myoblasts. Exp. Neurol. *193*, 53-64.

Haacke, A., Hartl, F.U., and Breuer, P. (2007). Calpain inhibition is sufficient to suppress aggregation of polyglutamine-expanded ataxin-3. J. Biol. Chem. *282*, 18851-18856.

Haberhausen, G., Damian, M.S., Leweke, F., and Müller, U. (1995). Spinocerebellar ataxia, type 3 (SCA3) is genetically identical to Machado-Joseph disease (MJD). J. Neurol. Sci. *132*, 71-75.

Hackett, C., Geurts, A., and Hackett, P. (2007). Predicting preferential DNA vector insertion sites: implications for functional genomics and gene therapy. Genome Biol. *8 Suppl 1*, S12.

Hamil, N., Cock, H., and Walker, M.C. (2012). Acute down-regulation of adenosine A(1) receptor activity in status epilepticus. Epilepsia *53*, 177-188.

Han, S.S., Williams, L.A., and Eggan, K.C. (2011). Constructing and deconstructing stem cell models of neurological disease. Neuron *70*, 626-644.

Hanson, K.D., and Sedivy, J.M. (1995). Analysis of biological selections for high-efficiency gene targeting. Mol. Cell Biol. *15*, 45-51.

Hazeki, N., Tukamoto, T., Goto, J., and Kanazawa, I. (2000). Formic Acid Dissolves Aggregates of an N-Terminal Huntingtin Fragment Containing an Expanded Polyglutamine Tract: Applying to Quantification of Protein Components of the Aggregates. Biochem. Biophys. Res. Commun. *277*, 386-393.

Hiyama, H., Yokoi, M., Masutani, C., Sugasawa, K., Maekawa, T., Tanaka, K., Hoeijmakers, J.H., and Hanaoka, F. (1999). Interaction of hHR23 with S5a. The ubiquitin-like domain of hHR23 mediates interaction with S5a subunit of 26 S proteasome. J. Biol. Chem. *274*, 28019-28025.

Hockemeyer, D., Soldner, F., Beard, C., Gao, Q., Mitalipova, M., Dekelver, R.C., Katibah, G.E., Amora, R., Boydston, E.A., Zeitler, B., Meng, X., Miller, J.C., Zhang, L., Rebar, E.J., Gregory, P.D., Urnov, F.D., and Jaenisch, R. (2009). Efficient targeting of expressed and silent genes in human ESCs and iPSCs using zinc-finger nucleases. Nat. Biotechnol. *27*, 851-857.

Hockemeyer, D., Wang, H., Kiani, S., Lai, C., Gao, Q., Cassady, J.P., Cost, G.J., Zhang, L., Santiago, Y., Miller, J.C., Zeitler, B., Cherone, J., Meng, X., Hinkley, S., Rebar, E.J., Gregory, P.D., Urnov, F.D., and Jaenisch, R. (2011). Genetic engineering of human pluripotent cells using TALE nucleases. Nat. Biotechnol. *29*, 731-734.

Houser, C.R. (1990). Granule cell dispersion in the dentate gyrus of humans with temporal lobe epilepsy. Brain Res. *535*, 195-204.

Howard, D.B., Powers, K., Wang, Y., and Harvey, B.K. (2008). Tropism and toxicity of adeno-associated viral vector serotypes 1, 2, 5, 6, 7, 8, and 9 in rat neurons and glia in vitro. Virology *372*, 24-34.

Howden, S.E., Gore, A., Li, Z., Fung, H.L., Nisler, B.S., Nie, J., Chen, G., McIntosh, B.E., Gulbranson, D.R., Diol, N.R., Taapken, S.M., Vereide, D.T., Montgomery, K.D., Zhang, K., Gamm, D.M., and Thomson, J.A. (2011). Genetic correction and analysis of induced pluripotent stem cells from a patient with gyrate atrophy. Proc. Natl. Acad. Sci. USA *108*, 6537-6542.

Huber, A., Padrun, V., Déglon, N., Aebischer, P., Möhler, H., and Boison, D. (2001). Grafts of adenosine-releasing cells suppress seizures in kindling epilepsy. Proc. Natl. Acad. Sci. USA *98*, 7611-7616.

Hussein, S.M., Batada, N.N., Vuoristo, S., Ching, R.W., Autio, R., Närvä, E., Ng, S., Sourour, M., Hämäläinen, R., Olsson, C., Lundin, K., Mikkola, M., Trokovic, R., Peitz, M., Brüstle, O., Bazett-Jones, D.P., Alitalo, K., Lahesmaa, R., Nagy, A., and Otonkoski, T. (2011). Copy number variation and selection during reprogramming to pluripotency. Nature *471*, 58-62.

Ichikawa, Y., Goto, J., Hattori, M., Toyoda, A., Ishii, K., Jeong, S.Y., Hashida, H., Masuda, N., Ogata, K., Kasai, F., Hirai, M., Maciel, P., Rouleau, G.A., Sakaki, Y., and Kanazawa, I. (2001). The genomic structure and expression of MJD, the Machado-Joseph disease gene. J. Hum. Genet. *46*, 413-422.

Ikeda, H., Yamaguchi, M., Sugai, S., Aze, Y., Narumiya, S., and Kakizuka, A. (1996). Expanded polyglutamine in the Machado-Joseph disease protein induces cell death in vitro and in vivo. Nat. Genet. *13*, 196-202.

Inoue, H., Nojima, H., and Okayama, H. (1990). High efficiency transformation of Escherichia coli with plasmids. Gene *96*, 23-28.

Irion, S., Luche, H., Gadue, P., Fehling, H.J., Kennedy, M., and Keller, G. (2007). Identification and targeting of the ROSA26 locus in human embryonic stem cells. Nat. Biotech. *25*, 1477-1482.

Jallon, P. (1997). The problem of intractability: the continuing need for new medical therapies in epilepsy. Epilepsia *38 Suppl 9*, S37-42.

Jantz, D., Amann, B.T., Gatto, G.J., and Berg, J.M. (2004). The design of functional DNA-binding proteins based on zinc finger domains. Chem. Rev. *104*, 789-799.

Jinek, M., Chylinski, K., Fonfara, I., Hauer, M., Doudna, J.A., and Charpentier, E. (2012). A programmable dual-RNA-guided DNA endonuclease in adaptive bacterial immunity. Science *337*, 816-821.

Kan, A., van Erp, S., Derijck, A.A., de Wit, M., Hessel, E.V., O'Duibhir, E., de Jager, W., Van Rijen, P.C., Gosselaar, P., de Graan, P.N., and Pasterkamp, R.J. (2012). Genome-wide microRNA profiling of human temporal lobe epilepsy identifies modulators of the immune response. Cell. Mol. Life Sci. *69*, 3127-3145.

Kaplitt, M.G., Leone, P., Samulski, R.J., Xiao, X., Pfaff, D.W., O'Malley, K.L., and During, M.J. (1994). Long-term gene expression and phenotypic correction using adeno-associated virus vectors in the mammalian brain. Nat. Genet. *8*, 148-154.

Kawaguchi, Y., Okamoto, T., Taniwaki, M., Aizawa, M., Inoue, M., Katayama, S., Kawakami, H., Nakamura, S., Nishimura, M., and Akiguchi, I. (1994). CAG expansions in a novel gene for Machado-Joseph disease at chromosome 14q32.1. Nat. Genet. *8*, 221-228.

Khan, I.F., Hirata, R.K., and Russell, D.W. (2011). AAV-mediated gene targeting methods for human cells. Nat. Protoc. *6*, 482-501.

Khan, I.F., Hirata, R.K., Wang, P., Li, Y., Kho, J., Nelson, A., Huo, Y., Zavaljevski, M., Ware, C., and Russell, D.W. (2010). Engineering of human pluripotent stem cells by AAV-mediated gene targeting. Mol. Ther. *18*, 1192-1199.

Kim, D., Kim, C., Moon, J., Chung, Y., Chang, M., Han, B., Ko, S., Yang, E., Cha, K., Lanza, R., and Kim, K. (2009). Generation of Human Induced Pluripotent Stem Cells by Direct Delivery of Reprogramming Proteins. Cell Stem Cell *4*, 472-476.

Kim, H.S., Oh, S.K., Park, Y.B., Ahn, H.J., Sung, K.C., Kang, M.J., Lee, L.A., Suh, C.S., Kim, S.H., Kim, D.W., and Moon, S.Y. (2005). Methods for derivation of human embryonic stem cells. Stem Cells *23*, 1228-1233.

Kim, Y.G., Cha, J., and Chandrasegaran, S. (1996). Hybrid restriction enzymes: zinc finger fusions to Fok I cleavage domain. Proc. Natl. Acad. Sci. USA *93*, 1156-1160.

Kim, Y.G., and Chandrasegaran, S. (1994). Chimeric restriction endonuclease. Proc. Natl. Acad. Sci. USA *91*, 883-887.

Kim, Y.G., Smith, J., Durgesha, M., and Chandrasegaran, S. (1998). Chimeric restriction enzyme: Gal4 fusion to FokI cleavage domain. Biol. Chem. *379*, 489-495.

Klimanskaya, I., Chung, Y., Meisner, L., Johnson, J., West, M.D., and Lanza, R. (2005). Human embryonic stem cells derived without feeder cells. Lancet *365*, 1636-1641.

Kmiec, E.B. (1999). Targeted gene repair. Gene. Ther. *6*, 1-3.

Koch, P., Breuer, P., Peitz, M., Jungverdorben, J., Kesavan, J., Poppe, D., Doerr, J., Ladewig, J., Mertens, J., Tüting, T., Hoffmann, P., Klockgether, T., Evert, B.O., Wüllner, U., and Brüstle, O. (2011). Excitation-induced ataxin-3 aggregation in neurons from patients with Machado-Joseph disease. Nature *480*, 543-546.

Koch, P., Opitz, T., Steinbeck, J.A., Ladewig, J., and Brüstle, O. (2009). A rosette-type, self-renewing human ES cell-derived neural stem cell with potential for in vitro instruction and synaptic integration. Proc. Natl. Acad. Sci. USA *106*, 3225-3230.

Kohli, M., Rago, C., Lengauer, C., Kinzler, K.W., and Vogelstein, B. (2004). Facile methods for generating human somatic cell gene knockouts using recombinant adeno-associated viruses. Nucleic Acids Res. *32*, e3.

Kotin, R.M., Linden, R.M., and Berns, K.I. (1992). Characterization of a preferred site on human chromosome 19q for integration of adeno-associated virus DNA by non-homologous recombination. EMBO J. *11*, 5071-5078.

Kriegstein, A., and Alvarez-Buylla, A. (2009). The glial nature of embryonic and adult neural stem cells. Annu. Rev. Neurosci. *32*, 149-184.

Ladewig, J., Koch, P., Endl, E., Meiners, B., Opitz, T., Couillard-Despres, S., Aigner, L., and Brüstle, O. (2008). Lineage selection of functional and cryopreservable human embryonic stem cell-derived neurons. Stem Cells *26*, 1705-1712.

Ladewig, J., Mertens, J., Kesavan, J., Doerr, J., Poppe, D., Glaue, F., Herms, S., Wernet, P., Kögler, G., Müller, F.J., Koch, P., and Brüstle, O. (2012). Small molecules enable highly efficient neuronal conversion of human fibroblasts. Nat. Methods *6*, 575-578.

Lee, K.S., Schubert, P., and Heinemann, U. (1984). The anticonvulsive action of adenosine: a postsynaptic, dendritic action by a possible endogenous anticonvulsant. Brain Res. *321*, 160-164.

Lein, E., Hawrylycz, M., Ao, N., Ayres, M., Bensinger, A., Bernard, A., Boe, A., Boguski, M., Brockway, K., Byrnes, E., Chen, L., Chen, L., Chen, T., Chin, M.C., Chong, J., Crook, B., Czaplinska, A., Dang, C., Datta, S., Dee, N., Desaki, A., Desta, T., Diep, E., Dolbeare, T., Donelan, M., Dong, H., Dougherty, J., Duncan, B., Ebbert, A., Eichele, G.*, et al.* (2007). Genome-wide atlas of gene expression in the adult mouse brain. Nature *445*, 168-176.

Li, F., Macfarlan, T., Pittman, R.N., and Chakravarti, D. (2002). Ataxin-3 is a histone-binding protein with two independent transcriptional corepressor activities. J. Biol. Chem. *277*, 45004-45012.

Li, H., and Henry, J.L. (1998). Adenosine A2 receptor mediation of pre- and postsynaptic excitatory effects of adenosine in rat hippocampus in vitro. Eur. J. Pharmacol. *347*, 173-182.

Li, L., Yu, Z., Teng, X., and Bonini, N. (2008). RNA toxicity is a component of ataxin-3 degeneration in Drosophila. Nature *453*, 1107-1111.

Li, T., Huang, S., Zhao, X., Wright, D.A., Carpenter, S., Spalding, M.H., Weeks, D.P., and Yang, B. (2011). Modularly assembled designer TAL effector nucleases for targeted gene knockout and gene replacement in eukaryotes. Nucleic Acids Res. *39*, 6315-6325.

Li, T., Quan Lan, J., Fredholm, B.B., Simon, R., and Boison, D. (2007a). Adenosine dysfunction in astrogliosis: cause for seizure generation? Neuron Glia Biol. *3*, 353-366.

Li, T., Steinbeck, J.A., Lusardi, T., Koch, P., Lan, J., Wilz, A., Segschneider, M., Simon, R., Brüstle, O., and Boison, D. (2007b). Suppression of kindling epileptogenesis by adenosine releasing stem cell-derived brain implants. Brain *130*, 1276-1288.

Li, Y. (2005). Murine embryonic stem cell differentiation is promoted by SOCS-3 and inhibited by the zinc finger transcription factor Klf4. Blood *105*, 635-637.

Linden, R.M., Ward, P., Giraud, C., Winocour, E., and Berns, K.I. (1996). Site-specific integration by adeno-associated virus. Proc. Natl. Acad. Sci. USA *93*, 11288-11294.

Lister, R., Pelizzola, M., Kida, Y.S., Hawkins, R.D., Nery, J.R., Hon, G., Antosiewicz-Bourget, J., O'Malley, R., Castanon, R., Klugman, S., Downes, M., Yu, R., Stewart, R., Ren, B., Thomson, J.A., Evans, R.M., and Ecker, J.R. (2011). Hotspots of aberrant epigenomic reprogramming in human induced pluripotent stem cells. Nature *471*, 68-73.

Lombardo, A., Genovese, P., Beausejour, C.M., Colleoni, S., Lee, Y.L., Kim, K.A., Ando, D., Urnov, F.D., Galli, C., Gregory, P.D., Holmes, M.C., and Naldini, L. (2007). Gene editing in human stem cells using zinc finger nucleases and integrase-defective lentiviral vector delivery. Nat. Biotechnol. *25*, 1298-1306.

Löscher, W., and Schmidt, D. (2006). New Horizons in the development of antiepileptic drugs: Innovative strategies. Epilepsy Res. *69*, 183-272.

Lovatt, D., Xu, Q., Liu, W., Takano, T., Smith, N.A., Schnermann, J., Tieu, K., and Nedergaard, M. (2012). Neuronal adenosine release, and not astrocytic ATP release, mediates feedback inhibition of excitatory activity. Proc. Natl. Acad. Sci. USA *109*, 6265-6270.

Lovell-Badge, R. (2001). The future for stem cell research. Nature *414*, 88-91.

Maciel, P., Gaspar, C., DeStefano, A.L., Silveira, I., Coutinho, P., Radvany, J., Dawson, D.M., Sudarsky, L., Guimarães, J., and Loureiro, J.E. (1995). Correlation between CAG repeat length and clinical features in Machado-Joseph disease. Am. J. Hum. Genet. *57*, 54-61.

Maitra, A., Arking, D., Shivapurkar, N., Ikeda, M., Stastny, V., Kassauei, K., Sui, G., Cutler, D., Liu, Y., Brimble, S., Noaksson, K., Hyllner, J., Schulz, T., Zeng, X., Freed, W., Crook, J., Abraham, S., Colman, A., Sartipy, P., Matsui, S., Carpenter, M., Gazdar, A., Rao, M., and Chakravarti, A. (2005). Genomic alterations in cultured human embryonic stem cells. Nat. Genet. *37*, 1099-1103.

Mak, A.N., Bradley, P., Cernadas, R.A., Bogdanove, A.J., and Stoddard, B.L. (2012). The crystal structure of TAL effector PthXo1 bound to its DNA target. Science *335*, 716-719.

Mali, P., Yang, L., Esvelt, K.M., Aach, J., Guell, M., DiCarlo, J.E., Norville, J.E., and Church, G.M. (2013). RNA-guided human genome engineering via Cas9. Science *339*, 823-826.

Mansour, S.L., Thomas, K.R., and Capecchi, M.R. (1988). Disruption of the proto-oncogene int-2 in mouse embryo-derived stem cells: a general strategy for targeting mutations to non-selectable genes. Nature *336*, 348-352.

Mareš, P. (2010). Anticonvulsant action of 2-chloroadenosine against pentetrazol-induced seizures in immature rats is due to activation of A1 adenosine receptors. J. Neural. Transm. *117*, 1269-1277.

Markossian, K.A., and Kurganov, B.I. (2004). Protein folding, misfolding, and aggregation. Formation of inclusion bodies and aggresomes. Biochemistry (Mosc.) *69*, 971-984.

Marteyn, A., Maury, Y., Gauthier, M., Lecuyer, C., Vernet, R., Denis, J., Pietu, G., Peschanski, M., and Martinat, C. (2011). Mutant Human Embryonic Stem Cells Reveal Neurite and Synapse Formation Defects in Type 1 Myotonic Dystrophy. Stem Cell *8*, 434-444.

Masino, L., Musi, V., Menon, R.P., Fusi, P., Kelly, G., Frenkiel, T.A., Trottier, Y., and Pastore, A. (2003). Domain architecture of the polyglutamine protein ataxin-3: a globular domain followed by a flexible tail. FEBS Lett. *549*, 21-25.

Masino, L., Nicastro, G., Menon, R.P., Dal Piaz, F., Calder, L., and Pastore, A. (2004). Characterization of the structure and the amyloidogenic properties of the Josephin domain of the polyglutamine-containing protein ataxin-3. J. Mol. Biol. *344*, 1021-1035.

Mason, I. (1996). Neural induction: do fibroblast growth factors strike a cord? Curr. Biol. *6*, 672-675.

Matilla, T., McCall, A., Subramony, S.H., and Zoghbi, H.Y. (1995). Molecular and clinical correlations in spinocerebellar ataxia type 3 and Machado-Joseph disease. Ann. Neurol. *38*, 68-72.

Matos, C.A., de Macedo-Ribeiro, S., and Carvalho, A.L. (2011). Polyglutamine diseases: the special case of ataxin-3 and Machado-Joseph disease. Prog. Neurobiol. *95*, 26-48.

Mazzucchelli, S., De Palma, A., Riva, M., D'Urzo, A., Pozzi, C., Pastori, V., Comelli, F., Fusi, P., Vanoni, M., Tortora, P., Mauri, P., and Regonesi, M.E. (2009). Proteomic and biochemical analyses unveil tight interaction of ataxin-3 with tubulin. Int. J. Biochem. Cell. Biol. *41*, 2485-2492.

McCampbell, A., Taylor, J.P., Taye, A.A., Robitschek, J., Li, M., Walcott, J., Merry, D., Chai, Y., Paulson, H., Sobue, G., and Fischbeck, K.H. (2000). CREB-binding protein sequestration by expanded polyglutamine. Hum. Mol. Genet. *9*, 2197-2202.

Miller, D.G., Rutledge, E., and Russell, D.W. (2002). Chromosomal effects of adeno-associated virus vector integration. Nat. Genet. *30*, 147-148.

Miller, D.G., Wang, P.R., Petek, L., Hirata, R.K., Sands, M., and Russell, D.W. (2006). Gene targeting in vivo by adeno-associated virus vectors. Nat. Biotechnol. *24*, 1022-1026.

Mitani, K., Wakamiya, M., Hasty, P., Graham, F.L., Bradley, A., and Caskey, C.T. (1995). Gene targeting in mouse embryonic stem cells with an adenoviral vector. Somat. Cell Mol. Genet. *21*, 221-231.

Miyoshi, N., Ishii, H., Nagano, H., Haraguchi, N., Dewi, D.L., Kano, Y., Nishikawa, S., Tanemura, M., Mimori, K., Tanaka, F., Saito, T., Nishimura, J., Takemasa, I., Mizushima, T., Ikeda, M., Yamamoto, H., Sekimoto, M., Doki, Y., and Mori, M. (2011). Reprogramming of mouse and human cells to pluripotency using mature microRNAs. Cell Stem Cell *8*, 633-638.

Moehle, E.A., Moehle, E.A., Rock, J.M., Rock, J.M., Lee, Y.L., Lee, Y.L., Jouvenot, Y., Jouvenot, Y., DeKelver, R.C., Dekelver, R.C., Gregory, P.D., Gregory, P.D., Urnov, F.D., Urnov, F.D., Holmes, M.C., and Holmes, M.C. (2007). Targeted gene addition into a specified location in the human genome using designed zinc finger nucleases. Proc. Natl. Acad. Sci. USA *104*, 3055-3060.

Montgomery, S.B., Sammeth, M., Gutierrez-Arcelus, M., Lach, R., Ingle, C., Nisbett, J., Guigo, R., and Dermitzakis, E.T. (2010). Transcriptome genetics using second generation sequencing in a Caucasian population. Nature *464*, 773-777.

Moscou, M.J., and Bogdanove, A.J. (2009). A simple cipher governs DNA recognition by TAL effectors. Science *326*, 1501.

Müller, F., Laurent, L.C., Kostka, D., Ulitsky, I., Williams, R., Lu, C., Park, I., Rao, M., Shamir, R., Schwartz, P., Schmidt, N., and Loring, J.F. (2008). Regulatory networks define phenotypic classes of human stem cell lines. Nature *455*, 401-405.

Müller, F., Schuldt, B., Williams, R., Mason, D., Altun, G., Papapetrou, E., Danner, S., Goldmann, J., Herbst, A., Schmidt, N., Aldenhoff, J., Laurent, L., and Loring, J. (2011). A bioinformatic assay for pluripotency in human cells. Nat. Methods *8*, 315-317.

Muotri, A.R., Nakashima, K., Toni, N., Sandler, V.M., and Gage, F.H. (2005). Development of functional human embryonic stem cell-derived neurons in mouse brain. Proc. Natl. Acad. Sci. USA *102*, 18644-18648.

Mussolino, C., Morbitzer, R., Lütge, F., Dannemann, N., Lahaye, T., and Cathomen, T. (2011). A novel TALE nuclease scaffold enables high genome editing activity in combination with low toxicity. Nucleic Acids Res. *39*, 9283-9293.

Nag, D.K., Suri, M., and Stenson, E.K. (2004). Both CAG repeats and inverted DNA repeats stimulate spontaneous unequal sister-chromatid exchange in Saccharomyces cerevisiae. Nucleic Acids Res. *32*, 5677-5684.

Nakagawa, M., Koyanagi, M., Tanabe, K., Takahashi, K., Ichisaka, T., Aoi, T., Okita, K., Mochiduki, Y., Takizawa, N., and Yamanaka, S. (2008). Generation of induced pluripotent stem cells without Myc from mouse and human fibroblasts. Nat Biotechnol. *26*, 101-106.

Nakai, H., Montini, E., Fuess, S., Storm, T., Grompe, M., and Kay, M.A. (2003). AAV serotype 2 vectors preferentially integrate into active genes in mice. Nat. Genet. *34*, 297-302.

Nakano, K.K., Dawson, D.M., and Spence, A. (1972). Machado disease. A hereditary ataxia in Portuguese emigrants to Massachusetts. Neurology *22*, 49-55.

Navarro, V., Varnous, S., Galanaud, D., Vaissier, E., Granger, B., Gandjbakhch, I., and Baulac, M. (2010). Incidence and risk factors for seizures after heart transplantation. J. Neurol. *257*, 563-568.

Nemati, S., Hatami, M., Kiani, S., Hemmesi, K., Gourabi, H., Masoudi, N., Alaie, S., and Baharvand, H. (2010). Long-term Self-Renewable Feeder-Free Human Induced Pluripotent Stem Cell-derived Neural Progenitors. Stem Cells Dev. *20*, 503-514.

Niwa, H., Burdon, T., Chambers, I., and Smith, A. (1998). Self-renewal of pluripotent embryonic stem cells is mediated via activation of STAT3. Genes Dev. *12*, 2048-2060.

Noctor, S.C., Flint, A.C., Weissman, T.A., Dammerman, R.S., and Kriegstein, A.R. (2001). Neurons derived from radial glial cells establish radial units in neocortex. Nature *409*, 714-720.

Noda, T., Satake, M., Robins, T., and Ito, Y. (1986). Isolation and characterization of NIH 3T3 cells expressing polyomavirus small T antigen. J. Virol. *60*, 105-113.

Notarangelo, L.D., Giliani, S., Mazza, C., Mella, P., Savoldi, G., Rodriguez-Pérez, C., Mazzolari, E., Fiorini, M., Duse, M., Plebani, A., Ugazio, A.G., Vihinen, M., Candotti, F., and Schumacher, R.F. (2000). Of genes and phenotypes: the immunological and molecular spectrum of combined immune deficiency. Defects of the gamma(c)-JAK3 signaling pathway as a model. Immunol. Rev. *178*, 39-48.

Nunes, F.A., Furth, E.E., Wilson, J.M., and Raper, S.E. (1999). Gene transfer into the liver of nonhuman primates with E1-deleted recombinant adenoviral vectors: safety of readministration. Hum. Gene. Ther. *10*, 2515-2526.

Okita, K., Ichisaka, T., and Yamanaka, S. (2007). Generation of germline-competent induced pluripotent stem cells. Nature *448*, 313-317.

Pabo, C.O., Peisach, E., and Grant, R.A. (2001). Design and selection of novel Cys2His2 zinc finger proteins. Annu. Rev. Biochem. *70*, 313-340.

Padiath, Q.S., Srivastava, A.K., Roy, S., Jain, S., and Brahmachari, S.K. (2005). Identification of a novel 45 repeat unstable allele associated with a disease phenotype at the MJD1/SCA3 locus. Am. J. Med. Genet. B. Neuropsychiatr. Genet. *133(B)*, 124-126.

Parkinson, F.E., Sinclair, C.J., Othman, T., Haughey, N.J., and Geiger, J.D. (2002). Differences between rat primary cortical neurons and astrocytes in purine release evoked by ischemic conditions. Neuropharmacology *43*, 836-846.

Pattanayak, V., Ramirez, C., Joung, J., and Liu, D. (2011). Revealing off-target cleavage specificities of zinc-finger nucleases by in vitro selection. Nat. Methods *8*, 765-770.

Pavletich, N.P., and Pabo, C.O. (1991). Zinc finger-DNA recognition: crystal structure of a Zif268-DNA complex at 2.1 A. Science *252*, 809-817.

Pickrell, J., Marioni, J., Pai, A., Degner, J., Engelhardt, B., Nkadori, E., Veyrieras, J., Stephens, M., Gilad, Y., and Pritchard, J. (2010). Understanding mechanisms underlying human gene expression variation with RNA sequencing. Nature *464*, 768-772.

Porteus, M., and Baltimore, D. (2003). Chimeric nucleases stimulate gene targeting in human cells. Science *300*, 763.

Potschka, H., Löscher, W., Wlaź, P., Behl, B., Hofmann, H.P., Treiber, H.J., and Szabo, L. (1998). LU 73068, a new non-NMDA and glycine/NMDA receptor antagonist: pharmacological characterization and comparison with NBQX and L-701,324 in the kindling model of epilepsy. Br. J Pharmacol. *125*, 1258-1266.

Prince, D., Parada, I., and Graber, K. (2012). Traumatic Brain injury and Posttraumatic Epilepsy. Jasper's Basic Mechanisms of the Epilepsies *4th Edition*, National Center for Biotechnology information (US).

Pruett-Miller, S., Connelly, J., Maeder, M., Joung, J.K., and Porteus, M. (2008). Comparison of zinc finger nucleases for use in gene targeting in mammalian cells. Mol. Ther. *16*, 707-717.

Qing, K., Mah, C., Hansen, J., Zhou, S., Dwarki, V., and Srivastava, A. (1999). Human fibroblast growth factor receptor 1 is a co-receptor for infection by adeno-associated virus 2. Nat. Med. *5*, 71-77.

Racine, R.J. (1972). Modification of seizure activity by electrical stimulation. II. Motor seizure. Electroencephalogr. Clin. Neurophysiol. *32*, 281-294.

Radecke, S., Radecke, F., Cathomen, T., and Schwarz, K. (2010). Zinc-finger nuclease-induced gene repair with oligodeoxynucleotides: wanted and unwanted target locus modifications. Mol. Ther. *18*, 743-753.

Rakic, P. (1988). Specification of cerebral cortical areas. Science *241*, 170-176.

Rebola, N., Porciúncula, L.O., Lopes, L.V., Oliveira, C.R., Soares-da-Silva, P., and Cunha, R.A. (2005). Long-term effect of convulsive behavior on the density of adenosine A1 and A 2A receptors in the rat cerebral cortex. Epilepsia *46 Suppl 5*, 159-165.

Reubinoff, B.E., Itsykson, P., Turetsky, T., Pera, M.F., Reinhartz, E., Itzik, A., and Ben-Hur, T. (2001). Neural progenitors from human embryonic stem cells. Nat. Biotechnol. *19*, 1134-1140.

Reynolds, B.A., and Weiss, S. (1992). Generation of neurons and astrocytes from isolated cells of the adult mammalian central nervous system. Science *255*, 1707-1710.

Reyon, D., Tsai, S.Q., Khayter, C., Foden, J.A., Sander, J., and Joung, J.K. (2012). FLASH assembly of TALENs for high-throughput genome editing. Nat. Biotechnol. *30*, 460-465.

Richardson, W.D., and Westphal, H. (1981). A cascade of adenovirus early functions is required for expression of adeno-associated virus. Cell *27*, 133-141.

Riess, O., Rüb, U., Pastore, A., Bauer, P., and Schöls, L. (2008). SCA3: neurological features, pathogenesis and animal models. Cerebellum *7*, 125-137.

Roberts, R.G., Gardner, R.J., and Bobrow, M. (1994). Searching for the 1 in 2,400,000: a review of dystrophin gene point mutations. Hum. Mutat. *4*, 1-11.

Rodda, D.J., Chew, J.L., Lim, L.H., Loh, Y.H., Wang, B., Ng, H.H., and Robson, P. (2005). Transcriptional regulation of nanog by OCT4 and SOX2. J. Biol. Chem. *280*, 24731-24737.

Rodin, S., Domogatskaya, A., Ström, S., Hansson, E.M., Chien, K.R., Inzunza, J., Hovatta, O., and Tryggvason, K. (2010). Long-term self-renewal of human pluripotent stem cells on human recombinant laminin-511. Nat. Biotech. *28*, 611-615.

Rodrigues, A., do Carmo Costa, M., Silva, T., Ferreira, D., Bajanca, F., Logarinho, E., and Maciel, P. (2010). Absence of ataxin-3 leads to cytoskeletal disorganization and increased cell death. Biochim. Biophys. Acta *1803*, 1154-1163.

Rosenberg, R.N. (1992). Machado-Joseph disease: an autosomal dominant motor system degeneration. Mov. Disord. *7*, 193-203.

Rosenberg, R.N., Nyhan, W.L., Bay, C., and Shore, P. (1976). Autosomal dominant striatonigral degeneration. A clinical, pathologic, and biochemical study of a new genetic disorder. Neurology *26*, 703-714.

Ross, C.A., and Poirier, M.A. (2004). Protein aggregation and neurodegenerative disease. Nat. Med. *10 Suppl*, S10-17.

Rozen, S., and Skaletsky, H. (2000). Primer3 on the WWW for general users and for biologist programmers. Methods Mol. Biol. *132*, 365-386.

Rubnitz, J., and Subramani, S. (1984). The minimum amount of homology required for homologous recombination in mammalian cells. Mol. Cell Biol. *4*, 2253-2258.

Russell, D.W., and Hirata, R.K. (1998). Human gene targeting by viral vectors. Nat. Genet. *18*, 325-330.

Ryu, K.S., Lee, K.J., Bae, S.H., Kim, B.K., Kim, K.A., and Choi, B.S. (2003). Binding surface mapping of intra- and interdomain interactions among hHR23B, ubiquitin, and polyubiquitin binding site 2 of S5a. J. Biol. Chem. *278*, 36621-36627.

Saner, F., Gensicke, J., Olde Damink, S.W., Pavlaković, G., Treckmann, J., Dammann, M., Kaiser, G., Sotiropoulos, G., Radtke, A., Koeppen, S., Beckebaum, S., Cicinnati, V., Nadalin, S., Malagó, M., Paul, A., and Broelsch, C. (2010). Neurologic complications in adult living donor liver transplant patients: an underestimated factor? J. Neurol. *257*, 253-258.

Sartore, R., Campos, P., Trujillo, C., Ramalho, B., Negraes, P., Paulsen, B., Meletti, T., Costa, E., Chicaybam, L., Bonamino, M., Ulrich, H., and Rehen, S. (2011). Retinoic acid-treated pluripotent stem cells undergoing neurogenesis present increased aneuploidy and micronuclei formation. PLoS ONE *6*, e20667.

Schöls, L., Bauer, P., Schmidt, T., Schulte, T., and Riess, O. (2004). Autosomal dominant cerebellar ataxias: clinical features, genetics, and pathogenesis. Lancet Neurol. *3*, 291-304.

Schöls, L., Vieira-Saecker, A.M., Schöls, S., Przuntek, H., Epplen, J.T., and Riess, O. (1995). Trinucleotide expansion within the MJD1 gene presents clinically as spinocerebellar ataxia and occurs most frequently in German SCA patients. Hum. Mol. Genet. *4*, 1001-1005.

Schumacher, M.A., Scott, D.M., Mathews, I.I., Ealick, S.E., Roos, D.S., Ullman, B., and Brennan, R.G. (2000). Crystal structures of Toxoplasma gondii adenosine kinase reveal a novel catalytic mechanism and prodrug binding. J. Mol. Biol. *296*, 549-567.

Sebastião, A.M., and Ribeiro, J.A. (2009). Tuning and fine-tuning of synapses with adenosine. Curr. Neuropharmacol. *7*, 180-194.

Sedivy, J.M., and Sharp, P.A. (1989). Positive genetic selection for gene disruption in mammalian cells by homologous recombination. Proc. Natl. Acad. Sci. USA *86*, 227-231.

Segal, D.J., and Barbas, C.F. (2001). Custom DNA-binding proteins come of age: polydactyl zinc-finger proteins. Curr. Opin. Biotechnol. *12*, 632-637.

Segal, D.J., Beerli, R.R., Blancafort, P., Dreier, B., Effertz, K., Huber, A., Koksch, B., Lund, C.V., Magnenat, L., Valente, D., and Barbas, C.F. (2003). Evaluation of a modular strategy for the construction of novel polydactyl zinc finger DNA-binding proteins. Biochemistry *42*, 2137-2148.

Shalem, O., Sanjana, N.E., Hartenian, E., Shi, X., Scott, D.A., Mikkelsen, T.S., Heckl, D., Ebert, B.L., Root, D.E., Doench, J.G., and Zhang, F. (2014). Genome-scale CRISPR-Cas9 knockout screening in human cells. Science *343*, 84-87.

Shao, J., and Diamond, M.I. (2007). Polyglutamine diseases: emerging concepts in pathogenesis and therapy. Hum. Mol. Genet. *16 Spec No. 2*, R115-123.

Shindo, A., Nakamura, T., Matsumoto, Y., Kawai, N., Okano, H., Nagao, S., Itano, T., and Tamiya, T. (2010). Seizure suppression in amygdala-kindled mice by transplantation of neural stem/progenitor cells derived from mouse embryonic stem cells. Neurol. Med. Chir. (Tokyo) *50*, 98-105.

Slow, E.J., Graham, R.K., Osmand, A.P., Devon, R.S., Lu, G., Deng, Y., Pearson, J., Vaid, K., Bissada, N., Wetzel, R., Leavitt, B.R., and Hayden, M.R. (2005). Absence of behavioral abnormalities and neurodegeneration in vivo despite widespread neuronal huntingtin inclusions. Proc. Natl. Acad. Sci. USA *102*, 11402-11407.

Smith, A.G. (2001). Embryo-derived stem cells: of mice and men. Annu. Rev. Cell Dev. Biol. *17*, 435-462.

Song, H., Chung, S., and Xu, Y. (2010). Modeling disease in human ESCs using an efficient BAC-based homologous recombination system. Cell Stem Cell *6*, 80-89.

Sonoda, E., Sasaki, M.S., Morrison, C., Yamaguchi-Iwai, Y., Takata, M., and Takeda, S. (1999). Sister chromatid exchanges are mediated by homologous recombination in vertebrate cells. Mol. Cell Biol. *19*, 5166-5169.

Spits, C., Mateizel, I., Geens, M., Mertzanidou, A., Staessen, C., Vandeskelde, Y., Van Der Elst, J., Liebaers, I., and Sermon, K. (2008). Recurrent chromosomal abnormalities in human embryonic stem cells. Nat. Biotechnol. *26*, 1361-1363.

Srivastava, A., Lusby, E.W., and Berns, K.I. (1983). Nucleotide sequence and organization of the adeno-associated virus 2 genome. J. Virol. *45*, 555-564.

Steinbeck, J.A., Koch, P., Derouiche, A., and Brüstle, O. (2011). Human embryonic stem cell-derived neurons establish region-specific, long-range projections in the adult brain. Cell. Mol. Life Sci.*69*, 461-470.

Stender, S., Murphy, M., O'Brien, T., Stengaard, C., Ulrich-Vinther, M., Søballe, K., and Barry, F. (2007). Adeno-associated viral vector transduction of human mesenchymal stem cells. Eur. Cell Mater. *13*, 93-99; discussion 99.

Strelchenko, N., Verlinsky, O., Kukharenko, V., and Verlinsky, Y. (2004). Morula-derived human embryonic stem cells. Reprod. Biomed. Online *9*, 623-629.

Summerford, C., Bartlett, J.S., and Samulski, R.J. (1999). AlphaVbeta5 integrin: a co-receptor for adeno-associated virus type 2 infection. Nat. Med. *5*, 78-82.

Summerford, C., and Samulski, R.J. (1998). Membrane-associated heparan sulfate proteoglycan is a receptor for adeno-associated virus type 2 virions. J. Virol. *72*, 1438-1445.

Suzuki, K., Mitsui, K., Aizawa, E., Hasegawa, K., Kawase, E., Yamagishi, T., Shimizu, Y., Suemori, H., Nakatsuji, N., and Mitani, K. (2008). Highly efficient transient gene expression and gene targeting in primate embryonic stem cells with helper-dependent adenoviral vectors. Proc. Natl. Acad. Sci. USA *105*, 13781-13786.

Szybala, C., Pritchard, E.M., Lusardi, T.A., Li, T., Wilz, A., Kaplan, D.L., and Boison, D. (2009). Antiepileptic effects of silk-polymer based adenosine release in kindled rats. Exp. Neurol. *219*, 126-135.

Takahashi, K., Okita, K., Nakagawa, M., and Yamanaka, S. (2007). Induction of pluripotent stem cells from fibroblast cultures. Nat. Protoc. *2*, 3081-3089.

Takahashi, K., and Yamanaka, S. (2006). Induction of pluripotent stem cells from mouse embryonic and adult fibroblast cultures by defined factors. Cell *126*, 663-676.

Takasugi, N., Tomita, T., Hayashi, I., Tsuruoka, M., Niimura, M., Takahashi, Y., Thinakaran, G., and Iwatsubo, T. (2003). The role of presenilin cofactors in the gamma-secretase complex. Nature *422*, 438-441.

Tan, M., Qing, K., Zhou, S., Yoder, M.C., and Srivastava, A. (2001). Adeno-associated virus 2-mediated transduction and erythroid lineage-restricted long-term expression of the human beta-globin gene in hematopoietic cells from homozygous beta-thalassemic mice. Mol. Ther. *3*, 940-946.

Theofilas, P., Brar, S., Stewart, K.A., Shen, H., Sandau, U.S., Poulsen, D., and Boison, D. (2011). Adenosine kinase as a target for therapeutic antisense strategies in epilepsy. Epilepsia *52*, 589-601.

Thomas, K.R., and Capecchi, M.R. (1987). Site-directed mutagenesis by gene targeting in mouse embryo-derived stem cells. Cell *51*, 503-512.

Thompson, J.D., Higgins, D.G., and Gibson, T.J. (1994). CLUSTAL W: improving the sensitivity of progressive multiple sequence alignment through sequence weighting, position-specific gap penalties and weight matrix choice. Nucleic Acids Res. *22*, 4673-4680.

Thomson, J.A., Itskovitz-Eldor, J., Shapiro, S.S., Waknitz, M.A., Swiergiel, J.J., Marshall, V.S., and Jones, J.M. (1998). Embryonic stem cell lines derived from human blastocysts. Science *282*, 1145-1147.

Topaloglu, O., Hurley, P.J., Yildirim, O., Civin, C.I., and Bunz, F. (2005). Improved methods for the generation of human gene knockout and knockin cell lines. Nucleic Acids Res. *33*, e158.

Trono, D. (2000). Lentiviral vectors: turning a deadly foe into a therapeutic agent. Gene Ther. *7*, 20-23.

Tropepe, V., Hitoshi, S., Sirard, C., Mak, T.W., Rossant, J., and van der Kooy, D. (2001). Direct neural fate specification from embryonic stem cells: a primitive mammalian neural stem cell stage acquired through a default mechanism. Neuron *30*, 65-78.

Urbach, A., Schuldiner, M., and Benvenisty, N. (2004). Modeling for Lesch-Nyhan disease by gene targeting in human embryonic stem cells. Stem Cells *22*, 635-641.

van de Warrenburg, B.P., Sinke, R.J., Verschuuren-Bemelmans, C.C., Scheffer, H., Brunt, E.R., Ippel, P.F., Maat-Kievit, J.A., Dooijes, D., Nottermans, N.C., Lindhout, D., Knoers, N.V., and Kremer, H.P. (2002). Spinocerebellar ataxias in the Netherlands: prevalence and age at onset variance analysis. Neurology *58*, 702-708.

Van Dycke, A., Raedt, R., Dauwe, I., Sante, T., Wyckhuys, T., Meurs, A., Vonck, K., Wadman, W., and Boon, P. (2010). Continuous local intrahippocampal delivery of adenosine reduces seizure frequency in rats with spontaneous seizures. Epilepsia *51*, 1721-1728.

Vasileva, A., and Jessberger, R. (2005). Precise hit: adeno-associated virus in gene targeting. Nat. Rev. Micro. *3*, 837-847.

Vasileva, A., Linden, R.M., and Jessberger, R. (2006). Homologous recombination is required for AAV-mediated gene targeting. Nucleic Acids Res. *34*, 3345-3360.

Vignoli, T., Nehlig, A., Massironi, S.G., Coimbra, R.d.C.S., Mazzacoratti, M.d.G.N., Silva, I.R., Neto, E.F.d.C., Persike, D.S., and Fernandes, M.J.d.S. (2012). Consequences of pilocarpine-induced status epilepticus in immunodeficient mice. Brain Res. *1450*, 125-137.

Waldman, A.S. (1992). Targeted homologous recombination in mammalian cells. Crit. Rev. Oncol. Hematol. *12*, 49-64.

Wang, B., Li, J., and Xiao, X. (2000a). Adeno-associated virus vector carrying human minidystrophin genes effectively ameliorates muscular dystrophy in mdx mouse model. Proc. Natl. Acad. Sci. USA *97*, 13714-13719.

Wang, D.G., Fan, J.B., Siao, C.J., Berno, A., Young, P., Sapolsky, R., Ghandour, G., Perkins, N., Winchester, E., Spencer, J., Kruglyak, L., Stein, L., Hsie, L., Topaloglou, T., Hubbell, E., Robinson, E., Mittmann, M., Morris, M.S., Shen, N., Kilburn, D., Rioux, J., Nusbaum, C., Rozen, S., Hudson, T.J., Lipshutz, R., Chee, M., and Lander, E.S. (1998). Large-scale identification, mapping, and genotyping of single-nucleotide polymorphisms in the human genome. Science *280*, 1077-1082.

Wang, G., Sawai, N., Kotliarova, S., Kanazawa, I., and Nukina, N. (2000b). Ataxin-3, the MJD1 gene product, interacts with the two human homologs of yeast DNA repair protein RAD23, HHR23A and HHR23B. Hum. Mol. Genet. *9*, 1795-1803.

Wang, Q., Li, L., and Ye, Y. (2006). Regulation of retrotranslocation by p97-associated deubiquitinating enzyme ataxin-3. J. Cell Biol. *174*, 963-971.

Wang, Q., Li, L., and Ye, Y. (2008). Inhibition of p97-dependent protein degradation by Eeyarestatin I. J. Biol. Chem. *283*, 7445-7454.

Wang, Q., Song, C., and Li, C.C. (2004). Molecular perspectives on p97-VCP: progress in understanding its structure and diverse biological functions. J. Struct. Biol. *146*, 44-57.

Wang, Y.H., Amirhaeri, S., Kang, S., Wells, R.D., and Griffith, J.D. (1994). Preferential nucleosome assembly at DNA triplet repeats from the myotonic dystrophy gene. Science *265*, 669-671.

Warren, L., Manos, P.D., Ahfeldt, T., Loh, Y., Li, H., Lau, F., Ebina, W., Mandal, P.K., Smith, Z.D., Meissner, A., Daley, G.Q., Brack, A.S., Collins, J.J., Cowan, C., Schlaeger, T.M., and Rossi, D.J. (2010). Highly Efficient Reprogramming to Pluripotency and Directed Differentiation of Human Cells with Synthetic Modified mRNA. Stem Cell *7*, 618-630.

Weissman, I.L. (2000). Stem cells: units of development, units of regeneration, and units in evolution. Cell *100*, 157-168.

Williams, A.J., Knutson, T.M., Colomer Gould, V.F., and Paulson, H.L. (2009). In vivo suppression of polyglutamine neurotoxicity by C-terminus of Hsp70-interacting protein (CHIP) supports an aggregation model of pathogenesis. Neurobiol. Dis. *33*, 342-353.

Wilz, A., Pritchard, E.M., Li, T., Lan, J.Q., Kaplan, D.L., and Boison, D. (2008). Silk polymer-based adenosine release: therapeutic potential for epilepsy. Biomaterials *29*, 3609-3616.

Wislet-Gendebien, S., Poulet, C., Neirinckx, V., Hennuy, B., Swingland, J., Laudet, E., Sommer, L., Shakova, O., Bours, V., and Rogister, B. (2012). In vivo tumorigenesis was observed after injection of in vitro expanded neural crest stem cells isolated from adult bone marrow. PLoS ONE *7*, e46425.

Wolfe, S.A., Nekludova, L., and Pabo, C.O. (2000). DNA recognition by Cys2His2 zinc finger proteins. Annu. Rev. Biophys. Biomol. Struct. *29*, 183-212.

Yan, L., Burbiel, J.C., Maass, A., and Müller, C.E. (2003). Adenosine receptor agonists: from basic medicinal chemistry to clinical development. Expert Opin. Emerg. Drugs *8*, 537-576.

Zhang, F., Cong, L., Lodato, S., Kosuri, S., Church, G.M., and Arlotta, P. (2011). Efficient construction of sequence-specific TAL effectors for modulating mammalian transcription. Nat. Biotechnol. *29*, 149-153.

Zhang, S.C., Wernig, M., Duncan, I.D., Brüstle, O., and Thomson, J.A. (2001). In vitro differentiation of transplantable neural precursors from human embryonic stem cells. Nat. Biotechnol. *19*, 1129-1133.

Zhou, Y., Zhu, S., Cai, C., Yuan, P., Li, C., Huang, Y., and Wei, W. (2014). High-throughput screening of a CRISPR/Cas9 library for functional genomics in human cells. Nature *509*, 487-491.

Zhu, S., Li, W., Zhou, H., Wei, W., Ambasudhan, R., Lin, T., Kim, J., Zhang, K., and Ding, S. (2010). Reprogramming of Human Primary Somatic Cells by OCT4 and Chemical Compounds. Stem Cell *7*, 651-655.

Zoghbi, H.Y., and Orr, H.T. (2000). Glutamine repeats and neurodegeneration. Annu. Rev. Neurosci. *23*, 217-247.

Zou, J., Maeder, M.L., Mali, P., Pruett-Miller, S.M., Thibodeau-Beganny, S., Chou, B., Chen, G., Ye, Z., Park, I., Daley, G.Q., Porteus, M.H., Joung, J.K., and Cheng, L. (2009). Gene targeting of a disease-related gene in human induced pluripotent stem and embryonic stem cells. Cell Stem Cell *5*, 97-110.

Zwaka, T., and Thomson, J. (2003). Homologous recombination in human embryonic stem cells. Nat. Biotechnol. *21*, 319-321.

10 Danksagung

Herrn Prof. Dr. Oliver Brüstle möchte ich für die Bereitstellung des Arbeitsplatzes und die vielen Freiheiten im täglichen Forschungsbetrieb herzlich danken. Herrn PD Dr. Phiipp Koch danke ich für hilfreiche Unterstützung, viele anregende Diskussionen und das große Wissen dass er mir über die Jahre vermittelt hat.

Herrn Dr. Jerome Mertens und Dr. Jonas Doerr danke ich für die vielen Jahre der guten Freundschaft und für das gute Gelingen gemeinsamer Projekte. Anke Leinhaas danke ich für die viele Geduld und ihr Wissen, die sie in die Tierexperimente eingebracht hat. Frau Prof. Dr. Christa Müller und Frau Marion Schneider danke ich für die Adenosinmessungen in Zellkulturüberständen.

Ein ganz besonderer Dank geht an meine Mitdoktoranden Carolin Haubenreich, Kathrin Stüber, Jasmin Jatho-Gröger und Ksenia Vinnikova sowie alle Mitarbeiter und Mitarbeiterinnen des Instituts für die außerordentlich gute Zusammenarbeit. Diese Arbeit wäre ohne die viele Hilfe und Unterstützung die ich erfahren habe nicht möglich gewesen, weshalb ich mich bei allen herzlich bedanken will.

Ich möchte mich weiterhin bei jenen bedanken, die mich außerhalb des Labors unterstützt haben: Ein ganz besonderer Dank geht an meine Eltern, die mir das Studium ermöglichten und mir auch während der Anfertigung der Doktorarbeit immerzu unterstützend und liebevoll zur Seite standen. Ganz besonderen Dank dafür, dass Sie immer das Beste für meine Geschwister und mich tun und alles Erdenkliche bereit sind, dafür zu geben.

Allen meinen lieben Freunden danke ich für die Ausdauer, Ruhe und Geduld, womit sie mir stets zur Seite standen und mich immer wieder aufgemuntert haben.

Meiner Frau Viola danke ich für alles und noch vieles mehr.

11 Erklärung

Hiermit versichere ich, dass diese Dissertation von mir persönlich, selbständig und ohne jede unerlaubte Hilfe angefertigt wurde. Die Daten, die im Rahmen einer Kooperation gewonnen wurden sind ausnahmslos gekennzeichnet. Die aus anderen Quellen übernommenen Daten, Abbildungen und Konzepte sind unter Angabe der jeweiligen Quelle gekennzeichnet.

Ergebnisse dieser Arbeit wurden in Teilen an folgenden Stellen veröffentlicht:
Koch, P., Breuer, P.*, Peitz, M.*, Jungverdorben, J.*, Kesavan, J.,* ***Poppe, D.****, Doerr, J., Ladewig, J., Mertens, J., Evert, B.O., Tüting, T., Wüllner, U., Klockgether, T., Brüstle, O.*
“Excitation-induced ataxin-3 aggregation in neurons from patients with Machado-Joseph disease”
(Nature 2011)
Poppe D.*, Doerr J., Schneider M., Steinbeck J., Ladewig J., Reik A., Müller C.E., Koch P., Brüstle O.*;
"Gene targeting in neuroepithelial stem cells to generate adenosine-releasing human neurons", *submitted*

Zusätzlich entstanden im Zeitraum der vorliegenden Dissertation weitere Arbeiten, die nicht im Zusammenhang mit der Dissertationsschrift vorgestellt wurden:
Ladewig, J., Mertens, J., Kesavan, J., Doerr, J., ***Poppe, D.****, Glaue, F., Herms, S., Wernet, P., Kögler, G., Müller, F.J., Koch, P., Brüstle, O.*
“Small molecules enable highly efficient neuronal conversion of human fibroblasts”
(Nature Methods 2012)
Mertens, J., Stüber, K., ***Poppe, D.****, Doerr J., Ladewig, J., Brüstle, O., Koch, P.*
“Embryonic stem cell-based modeling of tau pathology in human neurons.”
(American Journal of Pathology 2013)

** equal contribution; # corresponding author*

Die vorliegende Arbeit wurde an keiner anderen Hochschule als Dissertation eingereicht. Ich habe früher noch keinen Promotionsversuch unternommen.

_____

Daniel Poppe,

Bonn, den 11.05.2015